Dynamic Topology Estimation and Resource Allocation for Power Line Communication Networks

Thesis submitted in accordance with the requirements of the University of Liverpool for the degree of Doctor in Philosophy

by

Chao Zhang

January 2016

Declaration

The work in this thesis is based on research carried out at the University of Liverpool.

No part of this thesis has been submitted elsewhere for any other degree or qualification and it is all my own work unless referenced to the contrary in the text.

Chao Zhang

Liverpool, United Kingdom

Abstract

Power line communication (PLC), which uses existing infrastructure of power delivery for data transfer, is regarded as an economical, pervasive and extensive communication solution for smart grid and home broadband applications. One of the challenges of applying communication technologies to power line network lies in acquirement of channel state information (CSI), which is dependent on network topology. Moreover, the knowledge of topology provides a basis for the design of routing protocols and power flow optimization. Therefore, efficient approaches for dynamic topology estimation are highly demanded. While dynamic routing and resource allocation enable high-speed and multi-tasking communication services over power lines. In this thesis, a dynamic topology estimation scheme for PLC is investigated, and a cross-layer routing and resource allocation scheme assisted by dynamic topology estimation is developed to improve the system performance.

In the first contribution, a high-resolution and low-complexity dynamic topology estimation scheme for time-varying indoor PLC networks is proposed. The scheme consists of three parts: a) a time-frequency domain reflectometry (TFDR) based path length estimation method, which requires measurement at a single PLC modem and

achieves a much higher resolution than the frequency domain reflectometry (FDR) based method; b) a node-by-node greedy algorithm for topology reconstruction, which is much more computationally efficient than the existing peak-by-peak searching algorithm; c) an impulsive noise assisted dynamic topology re-estimation method, which results in a significant complexity reduction over fixed-frequency re-estimation.

In the second contribution, a cross-layer routing and resource allocation (RA) scheme assisted by dynamic topology estimation is proposed to optimize the system throughput of indoor PLC network with heterogeneous delay requirements. The proposed scheme provides a multi-layer solution, which conducts the network layer routing based on the result of PHY layer resource allocation which is constrained by the MAC layer queuing delay. With the dynamic topology estimation proposed in the first contribution, the routing can be solved centrally at the source, which is more robust against topology changes compared to distributed solutions. The proposed cross-layer RA scheme consists of subcarrier allocation (SA) to multiple users and power allocation (PA) to subcarriers satisfying heterogeneous delay requirements. It is demonstrated that the proposed centralized routing strategy achieves a much lower packet loss rate (PLR) than a distributed routing scheme; while with optimal RA, the system throughput is significantly improved compared to the routing schemes without considering RA.

Acknowledgment

I would like to express my deepest gratitude to my supervisor Dr. Xu Zhu for her kindly help and patient guidance throughout this research. My research under the supervisor of such a responsible and patient supervisor has been a great gift that I will never forget. This thesis would not have been finished without her constructive advice, constant encouragement and invaluable support. I would also appreciate the help from my supervisor Prof. Yi Huang for his valuable suggestions on my research.

I would like to thank the University of Liverpool, as well as the Department of Electrical Engineering and Electronics, for providing outstanding training and facilities to research students.

Warm thanks to my friends and colleagues in the Wireless Communication and Smart Grid group: Mr. Wenfei Zhu and Kainan Zhu and Mr. Jun Yin for discussions in channel and noise modeling in PLC for Smart Grid, Dr. Linhao Dong and Mr. Zhongxiang Wei for inspiring discussions in resource allocation schemes, Mr. Teng Ma for the tutorials in channel measurement, and Mr. Yanghao Wang for sharing the experience in auto home power control. I am proud of being a member of the group which shares a family-like atmosphere.

Finally, my gratitude is dedicated to my parents. I would had no chance to pursue

any goals in life without their support and encouragement. This thesis is dedicated to them.

Contents

Bibliography **100**

List of Figures

List of Tables

Abbreviations and Acronyms

3G   3rd generation of mobile telecommunications technology

AWGN   additive white Gaussian noise

AMI   automatic metering infrastructure

BB   broadband

BBR   beacon based routing

BER   bit error rate

BLR   beacon less routing

CENELEC   European Committee for Electrotechnical Standardization

CP   cyclic prefix

CIR   channel impulse response

CNR   channel-to-noise ratio

CSI   channel state information

CTS   clear-to-send

DTE-RRA   dynamic topology estimation assisted routing and resource
allocation

FDR   frequency domain reflectometry

FFT   fast Fourier transform

HAN	home area network
HDR	high data rate
HV	high voltage
IEEE	Institute of Electrical and Electronics Engineers
IFFT	inverse fast Fourier transform
IGF	implicit geographic forwarding
ISI	inter-symbol interference
LDR	low data rate
LTV	linear time-variant
LV	low voltage
MAC	medium access control
MIMO	multiple-input and multiple-output
MV	medium voltage
NAN	neighborhood area network
NB	narrowband
OFDM	orthogonal frequency division modulation
OPERA	Open PLC European Research Alliance
p.u.l	per-unit-length
PA	power allocation
pdf	probability density function

PHY	physical
PLC	power line communication
PLR	packet loss rate
PSD	power spectral density
QoS	quality of service
RA	resource allocation
RTS	request-to-send
SA	subcarrier allocation
SG	smart grid
SNR	signal-to-noise ratio
SPR	shortest path routing
TDOA	time difference of arrival
TDR	time domain reflectometry
TFDR	time-frequency domain reflectometry
UNB	ultra narrowband
WAN	wide area network

Chapter 1

Introduction

1.1 Background and Motivation

The idea of communications over power lines [1] was firstly proposed in early 1900s, as it required very low development cost and was easy to implement. However, due to harsh channel condition and immature technology, it was only used by power companies for remote metering [2] and load control [3] with achievable data rates no more than a few kilo-bits per second [4]. The first solutions for communication over power lines all used single carrier and narrowband techonologies operating in low frequency bands [5]. As techonology matured and application space widened, power line communication (PLC) systems operating in high frequency band, i.e. 2-30 MHz, have appeared in the market, which are called broadband PLC [6]. They are used to

provide broadband Internet access to residenttial customers, LAN connectivity within home/office/veihicles, and control capabilities for automation and remote metering [6-9]. In the last decade, by utilizing multicarrier schemes, a so-called "high data rate" narrowband PLC has also drawn a lot of industry interest [4]. In spite of being considered as a promising solution to a multitude of future applications, PLC has not yet taken a mass share of market as wireless solutions do [4]. However, it has become a hot topic and attracted a great amount of research interest recently, due to the development of next-generation power grid--smart grid.

Originated in 1880s for the objective of keeping the lights on, power grid has played a crucial role in the development of human civilization [10]. However, over the past few decades, the aging grid has faced severe challenges from the increasing demand of energy and the resulting environmental problems. Realizing the necessity of modernizing the power grid, government agencies around the world are deploying ubiquitous projects on smart grid, which has great advantages in reliability, safety and efficiency [11]. Unlike traditional power grid which transmits power from central generators to consumers only, the smart grid applies two-way flows of both electricity and information to create an automated and distributed energy delivery network [12]. Moreover, key factors of smart grid, two-way communication, wide-area monitoring and enhanced control functionalists, all rely on a reliable and efficient communication system [13]. The main design requirements of communication over smart grid are low latency, high reliability and high throughput [14]. Since no single wireless or wired solution fits all scenarios, it is commonly recognized that the smart grid will be supported by heterogeneous networking technologies [15].

Utilizing existing infrastructure of power delivery for data transfer, PLC is considered to be more economical, pervasive and extensive than wireless solutions for smart grid and smart home applications [16]. Furthermore, since it can be easily controlled and maintained by the power company itself other than a third party service provider, it is a more efficient solution than other telecommunication technologies using wires [17]. Among the wired alternatives, PLC is the only technology that has deployment cost that can be considered comparable to wireless since there is no need to install extra cables [18]. However, communication in a network initially designed for power distribution is challenging due to a variety of channel impairments [4].

Applying communication technologies to power line networks lies in acquirement of channel state information (CSI), which is dependent on network topology [19]. The knowledge of topology also provides a basis for designing routing protocols [20] [21] and power flow optimization [22]. Initially constructed for power distribution, most power line cables are placed underground or inside walls of buildings [23]. Thus, the topology of a PLC network is usually hard to obtain. Moreover, due to random appliance switchings which cause changes in connectivity of loads, the PLC network topology is considered to be time-varying [24-26]. Routing strategies designed for PLC networks deal with the dynamic topology by either updating the connectivity information periodically [27] [28] or attempting repeatedly when transmission fails [27], which is computational inefficiency. In [29] and [30], the benefits of using topology information for routing were further demonstrated. Efficient approaches for dynamic topology estimation are therefore highly demanded.

With the increasing demand for high speed and multi-tasking communication services, PLC systems for smart grid are expected to provide data transmission for multiple users with heterogeneous delay requirements. For example, users sharing a network can watch internet video clip and download files at the same time while the smart meters sending data to the substations. Since the communication channel of an indoor PLC network suffers various noise and has limited bandwidth [31], adaptive resource allocation is crucial for achieving a high channel capacity for multiuser multi-tasking services. As a multi-level connection network [19], the data transmission between different clusters always goes through multiple hops. Moreover, channel and network topology vary abruptly over time, the exact route may change for every transmitting. To provide reliable and efficient delivery of data packets through the grid, appropriate routing and resource allocation schemes are demanded.

1.2   Research Contributions

The research conducted during this PhD study is aimed to investigate efficient communication solutions to aid the development of reliable and high-speed indoor PLC networks for smart grid applications. In this PhD research, a high-resolution and low-complexity dynamic PLC network topology estimation scheme assisted by impulsive noise source detection is proposed, and a cross-layer routing and resource allocation scheme assisted by dynamic topology estimation is developed for indoor PLC networks.

The main contributions are summarized as follows:

- A time-frequency domain reflectometry (TFDR) based high-resolution and low-complexity dynamic PLC network topology estimation scheme with the assistance of impulsive noise source detection is proposed. This work is different in the following aspects. First, to the best of our knowledge, this is the first work to utilize the TFDR for topology inference, which significantly improves the resolution and accuracy of the estimation with a single measurement point (PLC modem). The TFDR approach investigates signals in both time and frequency domains, and therefore the resolution and accuracy loss caused by frequency-time domain transformation can be avoided. Second, the proposed node-by-node greedy algorithm achieves a much higher computational efficiency over the peak-by-peak searching algorithm in [32]. Third, a novel impulsive noise source detection method is proposed to detect dynamic topology changes, by utilizing the time difference of arrival (TDOA) of the first noise impulses. Topology re-estimations are triggered only by impulsive noise detected, and therefore much less full-topology estimations are required than the previous fixed-frequency re-estimation methods.

- A cross-layer routing and resource allocation scheme assisted by dynamic topology estimation for power line networks is proposed to improve the system throughput. This work is different in the following aspects. First, this is the first work solving the multiuser network layer routing problem based on the result of PHY layer resource allocation for indoor PLC networks. As a result, the system throughput and packet loss performance are greatly improved compared to conventional routing strategies. Second, the proposed

joint power and subcarrier allocation approach obtains the maximal PHY layer throughput satisfying heterogeneous delay requirements with the minimum required power. Moreover, with the assistance of the dynamic topology estimation presented in the first contribution, routing is done with a centralized solution. Simulation result shows that the proposed scheme has a much lower packet loss rate than the distributed solutions in a time-varying network.

1.3   Thesis Organization

The rest of this thesis is organized as follows. In Chapter 2, some background knowledge and research challenges about PLC are provided. The channel and noise modeling is also introduced in this chapter. The network topology of PLC and the related research are demonstrated in Chapter 3. Some basics of time-frequency domain analysis and physical layer resource allocation are reviewed in this chapter as well. Chapter 4 presents a time-frequency domain reflectometry based high-resolution and low-complexity dynamic PLC network topology estimation scheme with the assistance of impulsive noise source detection. In Chapter 5, a cross-layer routing and resource allocation scheme assisted by dynamic topology estimation for power line networks is proposed, and comparisons has been done with other centralized and distributed solutions. Conclusions and future work are presented in the final chapter.

1.4   Publications

1. C. Zhang, X. Zhu, Y. Huang and G. Liu, "High-Resolution and Low-Complexity Topology Estimation for Power Line Communication Networks," in Proc. *IEEE International Conference on Communications (ICC),* London, UK, Jun. 2015.

2. C. Zhang, X. Zhu, Y. Huang and G. Liu, "High-Resolution and Low-Complexity Dynamic Topology Estimation for PLC Networks assisted by Impulsive Noise Source Detection," *in IET Communications，* vol.10, pp. 443-451, Mar.2016

3. C. Zhang, X. Zhu, Y. Huang and Z. Wei, "Cross-Layer Routing and Resource Allocation assisted by Dynamic Topology Estimation for Indoor PLC Networks," to be submitted to *IEEE Transactions on Power Delivery*.

Chapter 2

Power Line Communication Systems and Channel Modeling

2.1 Power Line Communication for Smart Grid

2.1.1 Communication Technologies for Smart Grid

Combining advanced communication and information technologies with distributed green energy generations and intelligent management systems, smart grid is proposed as the next-generation power grid. With smart grid, new applications such as automatic fault detection and recovery, marketization of user-generated electricity, home energy management, and automatic meter reading can be achieved [33]. All of the above applications rely on an efficient and reliable communication infrastructure.

Smart grid consists of different types of networks: home area networks (HANs) which connect the electrical devices, building area networks (BANs) which contain a number of apartments having HANs, and wide area networks (WANs) which provide communications across multiple sites [34-36]. As a result, there is still much debate on what specific communication technology should be used for each smart grid application [37]. Since the applications of smart grid detect, measure and act in real-time, which requires accurate and efficient information exchange, the communication systems for smart grid must: support quality of service (QoS) of data, be highly reliable, have high throughput and guarantee security [33].

There are a number of wireless and wired technologies applicable in smart grid, and they are suitable for different operating environments. For example, wireless Mesh network (WMN) is a cost effective solution with high reliability and large coverage, which is most suitable for WANs [38] [39]. A cellular communication system, such as 3G and 4G is a good option for communicating between far nodes [33]. However, the channel of cellular networks are shared by customer market, which results in network congestion and decreased performance [40]. PLC and ZigBee are commonly recognized as two promising candidates for smart grid in HANs and BANs. ZigBee is commonly used for metering and energy management with low bandwidth requirement and operates within an unlicensed spectrum [41]. However, the low prepossessing capacity and the interference with other appliances sharing the license-free frequency band limit its performance. The most important advantage of PLC is using the existing infrastructure to transmit high-speed data from one device to another, which significantly reduces the development cost. PLC has also been the first choice for communication with smart meters due to direct connections with the meters [42]. Moreover, various studies have shown that PLC

can provide a good system performance, especially when OFDM is applied [43] [44]. Comparing to the mature wireless technologies, PLC has a large research potential and has been chosen to be investigated in this PhD research.

2.1.2   Power Line Communications

2.1.2.1   History and Background

In 1920s, power utilities started using high voltage power lines as the communication medium for voice [1]. The initial system was used only by power utilities as an alternative to telephone to enable communication between transformer stations. The Ripple Control systems were designed and then deployed over medium- and low-voltage electrical networks, which are considered to be the first PLC systems [45]. As the most common form of load control, the Ripple Control system is used in many countries including the UK [46]. It superimposes a higher-frequency signal onto the standard 50 Hz main power grid. By this way, the power utilities are able to transmit electricity to customers together with the commands related to tariff switching and load control[47]. Besides the load control, remote metering was another main driver for the interest of utilities in PLC [4]. However both of applications required very low data rates and used single carrier narrowband (NB) solutions in low frequency bands. With the development of technology and the increasing demand for broadband (BB) Internet access, PLC systems operating in high frequency band and achieving high data rates have appeared in market and drawn a lot of research interest.

According to different operating bandwidths, PLC technologies can be divided into three classes: ultra narrowband (UNB), NB and BB. Table 2.1 shows the bandwidth of the three classes and the corresponding achievable data rates.

Table 2.1 Bandwidths and achievable data rates of PLC technologies

Class	Bandwidth	Achievable Data Rate
UNB	0.3 – 3 kHz	~100 bps
NB	3 – 500 kHz	Low Data Rate (LDR): a few kbps High Data Rate (HDR): ~500 kbps
BB	1.8 – 250 MHz	Several hundred Mbps

UNB-PLC is a very mature technology that has been widely used in Advanced Meter Reading (AMR) and load control applications. Although the data rate is low, the very large operational range (more than 150 km) has attracted the interest of hundreds of utilities. There are two kinds of NB solutions: LDR which uses single carrier technologies and HDR which based on multicarrier technologies. NB-PLC technologies are gaining interest for AMR applications [4]. BB-PLC achieves a high data rate which is suitable for supporting Internet access for HANs. Considered as an excellent home networking technology for complementing WiFi [4], BB-PLC has attracted a great amount of research interest.

2.1.2.2 Network Architecture

The power line networks are classified according to their voltage levels as shown in Fig. 2.1. Table 2.2 shows some common voltage levels of power networks in Europe [45]. The power plants deliver the generated power to urban area through the High Voltage (HV) transmission networks. PLC of HV enables several applications such as state estimation and power system control [48]. Medium Voltage (MV) networks distribute power to substations in different areas. Substation automation functions require information exchange with other substations. For example, voltage dispatch

on the distribution system requires communication between intelligent electronic devices (IEDs) of substations. Thus, MV PLC is critical for the applications of MV level power grid. In charge of power distribution to residential network, Low Voltage (LV) has the most communication demand [48]. Important smart grid applications such as AMR, vehicle-to-grid communications, demand side management (DSM), and in-home energy management all rely on the LV PLC [4].
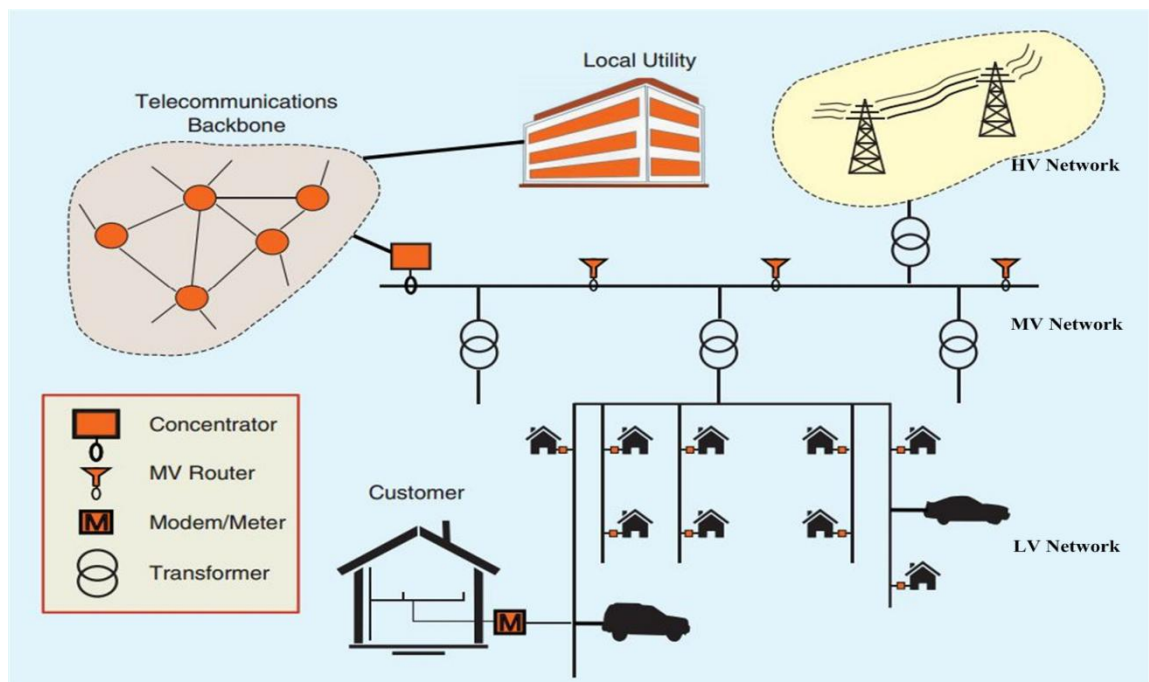
Fig. 2.1 The architecture of PLC network [48]

Table 2.2 Common levels of electrical voltage in Europe

Network	Name of the network	Common voltage levels
HV	Ultra High Voltage	225 kV / 400 kV
	High Voltage	65 kV / 65 kV
MV	Medium Voltage	20 kV / 11kV (UK)
LV	Low Voltage	380 V (three phase)
		220 V (single phase)

Since we are more interested in improving users' experience of daily life with PLC, this thesis focuses on investigating the communication over a LV network. The indoor PLC network has a two-level connection structure with a time-varying characteristic [19]. The first connection level is between the appliances and the associated derivation box (also known as "junction box") which is used in a cluster as the coordinator of the appliance connected to it , while the second level refers to the connections between derivation boxes. Fig. 2.2 demonstrates a typical indoor PLC network. Several challenges have been identified regarding the research of indoor PLC. First of all, the channel modeling is complex and there is still no universally recognized model yet [49]. Second, the communication environment is harsh with complex noise and interference scenario. Finally, random user activities change the connectivity of appliances, which makes the topology of the network time-varying and unpredictable. In the rest of this thesis, the above challenges are discussed in detail.
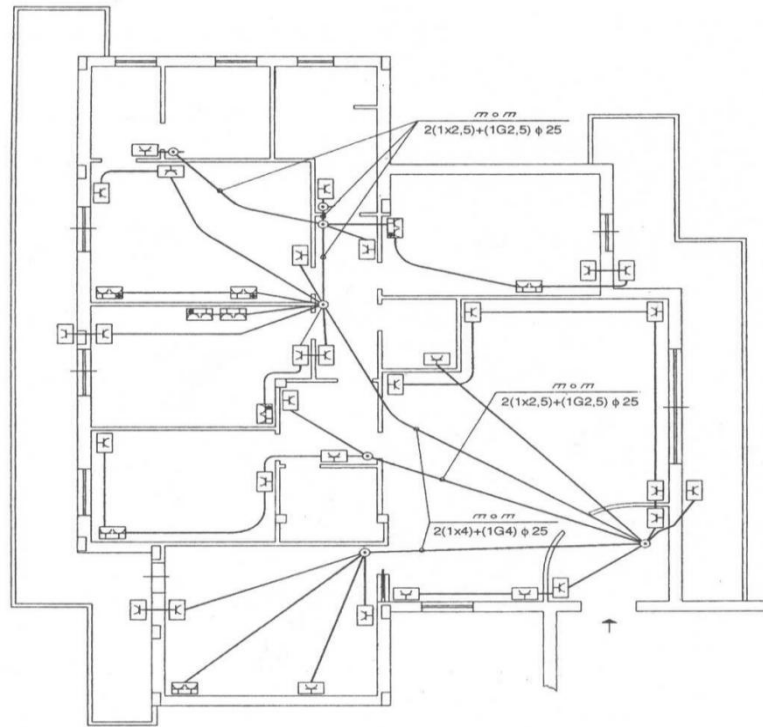
Fig. 2.2 A typical indoor PLC structure showing derivation boxes and connections with appliances [19]

2.2   Channel and Noise Modeling for PLC

2.2.1   PLC Channel Modeling

Built for delivery of power, the power line channel is very harsh and noisy for communication and is difficult to model [49]. First, signal reflections and transmissions caused by impedance mismatches at branch and end nodes make the channel frequency selective. Second, various network changes such as variations of topology and fluctuation of cable parameters make the channel time-varying. Moreover, the structure of the grid differs from country to country. For instance, three-phase configuration is commonly used in Europe while two-phase dominates in the US [50]. Finally, the channel characteristics of each section of the grid are not constant. The path loss is small at the transmission side (HV), but it grows dramatically at the distribution side (MV/LV) especially at higher frequencies [51]. As can be derived from Joule's law, the path loss increase with the decrease of the transmission voltage. It is also clear that due to skin effect, a higher freqeuncy makes a higher effective resistance which leads to a higher path loss. Table 2.3 shows some typical path loss values of different PLC networks. Extensive studies on channel modeling are highly demanded since any communication system must be designed to match the characteristics of channel.

Table 2.3 Typical path loss values (in dB/km) for PLC [4]

	$f = 100$ kHz	$f = 10$ MHz
HV (Overhead)	0.01 - 0.09	2- 4
MV(Overhead)	0.5 - 1	30 - 50
MV(Underground)	1 - 2	50 - 80
LV	1.5 - 3	160 - 200

In recent years, a great amount of work has been conducted to model the channel of power line network. The modeling approaches can be classified into bottom-up approaches [19, 52-58] and top-down approaches [59-62]. A bottom-up approach attempts to derive a deterministic model based on the transmission line theory. The channel transfer function can be deterministically calculated once the network topology is obtained. On the other hand, a top-down approach tries to find the most fitted statistical model according to measurement results.

2.2.1.1 Bottom-Up Approaches

As described in previous subsection, the fundamental of bottom-up approaches is the transmission line theory. For a better understanding of the approach, the basics of transmission line theory are reviewed first. Fig. 2.3 represents a typical two-conductor transmission line model. The transmission line equations can be derived from either the integral form of Maxwell's equation or the per-unit-length distributed parameter equivalent circuit. In this subsection, the latter has been chosen for simpler demonstration.

Since the voltage and current at a point of the line varies with the distant from source z, the Ohm's law is not suitable for the system [63]. To solve this problem, the transmission is divided into an infinite number of segments with a unit distance $\Delta z \to 0$. Thus, the voltage and current with a segment can be seen as constant. Fig. 2.4 shows an equivalent circuit of a segment of the transmission line. The per-unit-length resistance, inductance, conductance and capacity of the line are represented as *r, l, g and c* respectively. Applying Kirchhoff's voltage law (KVL) to the loop gives:

$$V(z+\Delta z,t)-V(z,t)=-r\Delta zI(z,t)-l\Delta z\frac{\partial I(z,t)}{\partial t} \qquad (2.1)$$

Divide both sides by Δz. Since we have $\Delta z \to 0$, the first transmission line equation can be obtained as：

$$\frac{\partial V(z,t)}{\partial z} = -rI(z,t) - l\frac{\partial I(z,t)}{\partial t} \qquad (2.2)$$

Similarly, the transmission line equation for current can be obtained by applying Kirchhoff's current law (KCL):

$$\frac{\partial I(z,t)}{\partial z} = -gV(z,t) - c\frac{\partial V(z,t)}{\partial t} \qquad (2.3)$$
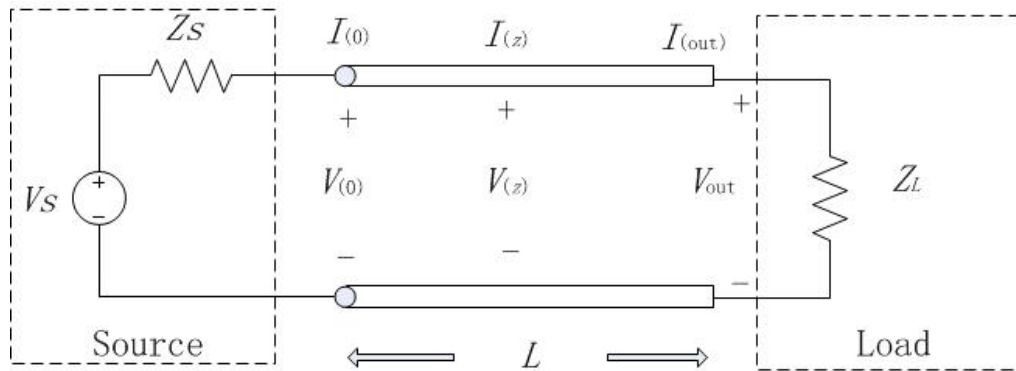
Fig. 2.3 A typical two-conductor transmission line network (e.g. tinned copper twincore cable)
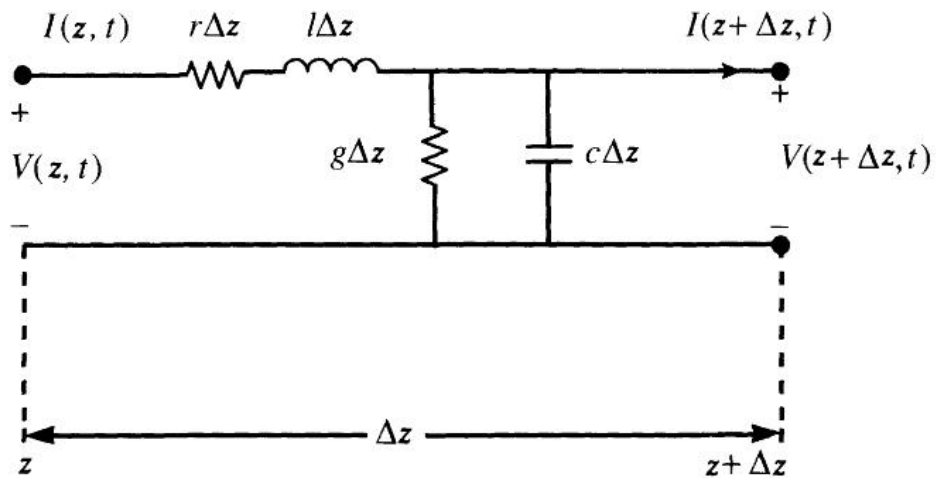
Fig. 2.4 The per-unit-length equivalent circuit for derivation of the transmission-line equations [63]

Replacing the time derivatives $\dfrac{\partial}{\partial t}$ in (2.2) and (2.3) with $j\omega$, where $\omega = 2\pi f$.

Thus, the frequency domain transmission line equations can be obtained:

$$\frac{d}{dz}V(z) = \underbrace{-(r + j\omega l)}_{Z_u}I(z) \tag{2.4}$$

$$\frac{d}{dz}I(z) = \underbrace{-(g + j\omega c)}_{Y_u}V(z) \tag{2.5}$$

where Z_u and Y_u are the per-unit-length impedance and admittance of the line, respectively. By solving (2. 4) and (2. 5), we can get [63]:

$$V(z) = V^+ e^{-j\gamma z} + V^- e^{j\gamma z} \tag{2.6}$$

$$I(z) = \frac{V^+ e^{-j\gamma z} + V^- e^{j\gamma z}}{Z_C} \tag{2.7}$$

Where $\gamma = \alpha + j\beta$ is the complex propagation constant which is frequency dependent, and α, β are the attenuation and phase constant respectively. V^+ and V^- represent the voltage of forward-traveling and backward-traveling direction respectively. $Z_C = \sqrt{Z_u / Y_u}$ is the characteristic impedance of the line.

The reflection coefficient at node z, $\Gamma(z)$ can be calculated as the voltage ratio of the backward-traveling and forward-traveling waves:

$$\Gamma(z) = \frac{V^- e^{j\gamma z}}{V^+ e^{-j\gamma z}} = \frac{V^-}{V^+} e^{j2\gamma z} \tag{2.8}$$

Substituting (2.8) into (2.6) and (2.7) yields:

$$V(z) = V^+ e^{-j\gamma z}[1 + \Gamma(z)] \tag{2.9}$$

$$I(z) = \frac{V^+}{Z_C} e^{-j\gamma z} [1 - \Gamma(z)] \tag{2.10}$$

Since at the load we have $Z_L = V(L)/I(L)$, we have:

$$Z_L = Z_C \frac{1 + \Gamma(L)}{1 - \Gamma(L)} \tag{2.11}$$

$$\Gamma(L) = \frac{Z_L - Z_C}{Z_L + Z_C} \tag{2.12}$$

As can be derived from Fig. 2.3, $V_S = I(0)Z_s + V(0)$. The transfer function of a transmission line is defined as the ratio of $V(L)$ to V_s:

$$H(f) = \frac{V(L)}{V_s} = \frac{1 + \Gamma(L)}{1 - \Gamma_s \Gamma(L) e^{-2\gamma L}} \frac{Z_C}{Z_C + Z_s} e^{-\gamma L} \tag{2.13}$$

The transfer function is frequency dependent since all per-unit-length parameters and the propagation constant of a power line are frequency dependent.

In order to calculate the transfer function of a PLC network with multiple branch and end nodes, an impedance carry back method was proposed by Tonnello [19]. The approach divides a large network into a number of small parts and the impedance of branch nodes is carried back to the backbone. The transfer function of each part can then be calculated by using (2.13). The overall transfer function of the network is the product of transfer functions of all parts.

2.2.1.2 Top-Down Approaches

As introduced in previous subsection, the deterministic channel transfer function can be obtained via the bottom-up approaches. However, this kind of approaches has very high computational complexity when the numbers of nodes are large. Moreover, it requires the knowledge of all components (cable parameters, joints, connected

devices) which are difficult to obtain [64]. Therefore, the top-down approaches with much lower complex have been investigated by many researchers [59-62]. These approaches consider the communication channel as a black box and describe its transfer characteristics by corresponding frequency response with very few relevant parameters [59]. Different from the bottom-up approaches which derive the relevant parameters from component properties, by analyzing a great number of measurements, the models are formed based on fundamental physical effects. The most well known top-down model was proposed in [59], and details about this model are described in the following paragraph and Chapter 4 of this thesis.

The signal propagation along a PLC network does not go a direct line-of-sight only. The additional paths caused by echoes between adjacent nodes must also be considered. Fig. 2.5 illustrates the multipath signal propagation with a simple example topology. The idea of a top-down approach is to model the channel transfer function as a sum of multiple signal paths. Signal propagates along each path independently with different amplitudes, phases and delays. According to this model, the transfer function is expressed as [64]:

$$H(f) = \sum_{i=1}^{N} g_i(f) e^{-(a_0 + a_1 f^k) d_i} e^{-j 2\pi f (d_i / v)} \tag{2.14}$$

Where $g_i(f)$ is the weighing factor of path i which is determined by the transmission and reflection coefficients of the path. The length of path i is represented by d_i, and v is the propagation speed along the line. a_0, and a_1 are attenuation parameters of power line, while k is the dependency of attenuation on frequency which reflects the attenuation caused by skin effect [4]. These parameters are usually derived from measured transfer functions since it is difficult to obtain all necessary cable and geometry data for real networks. The typical values of the exponent of the

attenuation factor k are between 0.5 and 1. As can be seen, the attenuation increases with the frequency and distance. More detailed derivation of (2.14) will be shown in Chapter 4.
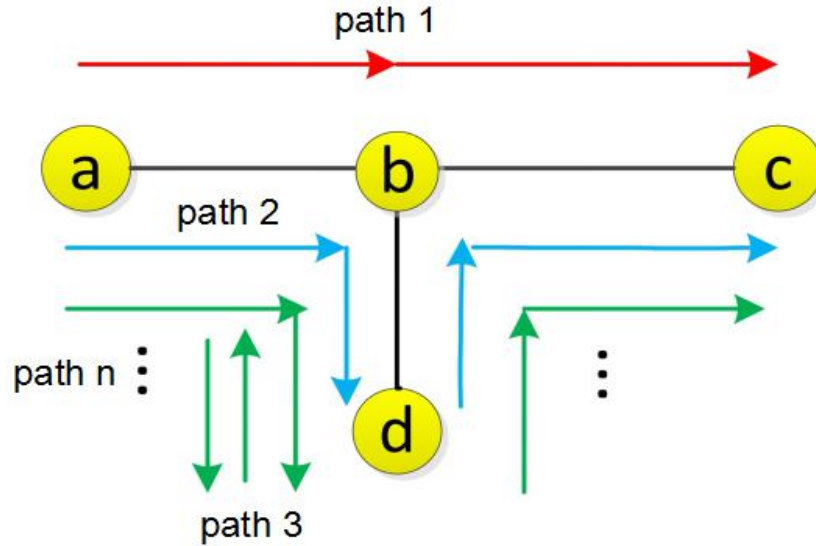
Fig. 2.5 Multipath signal propagation in a simple network

The model is realized by assigning proper values to parameters involved in (2.14). Intensive researches have been done in determining the parameters of (2.14) base on channel measurements. [58] first proposed a general fitting procedure that enables the model to reproduce the statistics of a given set of measured channels. In the Open PLC European Research Alliance (OPERA) project [65], nine classes of reference channels for LV/MV networks have been introduced as suitable representatives of real channels. A random channel generator based on Zimmermann's model [59] was developed in [53], and the frequency bandwidth was extended to (2-100 MHz) recently in [66] by including more statistical results. In this thesis, the works are mainly developed based on the top-down models which have lower computational complexity.

2.2.2 Noise Modeling of PLC

The noise scenario is rather complicated for a power line network since different sources of disturbance exist at the same time. Therefore, the noise cannot be modeled as additive white Gaussian noise (AWGN) which is employed by a lot of other communication channels. Noise generated by multiple sources superimpose at the receiver makes the noise model colored. There are two classes of noise in general: background noise and impulsive noise [67]. For an indoor PLC system, the colored background noise is caused by building and residential electronic devices. While the narrowband interference is generally sourced from external broadcast radio bands. On the other hand, the impulsive noise is generated by the load and connectivity changes of the home appliances such as the switching on/off of a kettle. Three kinds of impulsive noise have been found [67]: periodical impulsive noise synchronous with the mains frequency, periodic impulsive noise asynchronous with the mains frequency and aperiodic impulsive noise. Fig. 2.6 shows the general noise scenario on PLC.
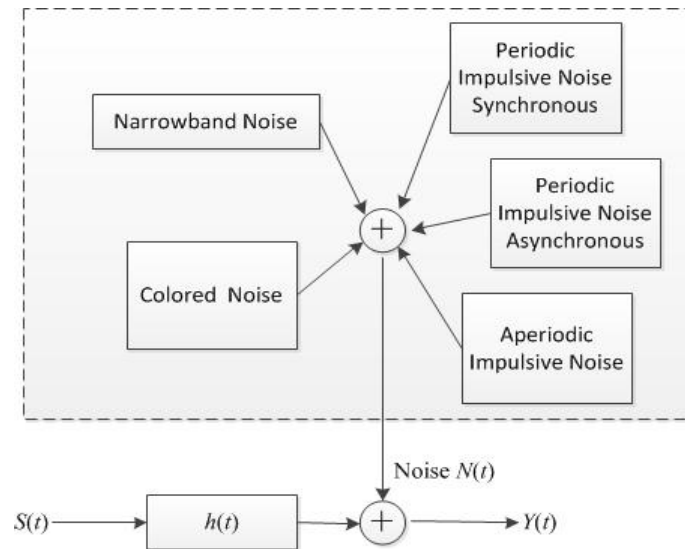
Fig. 2.6 Classification of noise on PLC channels

Colored background noise, narrowband noise and periodic impulsive noise are usually modeled as background noise since they remain stationary for a relatively long period of time [67]. In this subsection, some of the representative models of colored background noise and impulsive noise are further discussed.

2.2.2.1 Colored Background Noise

The multiple measurement results in [65] indicate that the power spectral density (PSD) of the background noise decreases with the increase of frequency. Several similar models are obtained by measurements and data fitting [68][69]. The background noise PSD in [67] is expressed as:

$$N(f) = a + b|f|^c \quad [dBm/Hz] \tag{2.15}$$

Where a, b and c are parameters derived from measurements and f is the frequency in MHz. Another model based on long-term measurements in office and home environment was proposed in [69], which represents the PSD as:

$$N(f) = B_\infty + B_0 e^{-f/f_0} \quad dB/Hz \tag{2.16}$$

Where B_∞ is the PSD when $f \to \infty$, while B_0 is the difference between the maximum PSD and B_∞. And f_0 refers to the decaying exponential rate. The two models are compared using some typical values of parameters obtained from the measurements in [68] and [69], and the simulation results are showed in Fig. 2.7. For the first model the parameters are set as: [a, b, c] = [-145, 53.23, -0.337] for the worst case scenario, and [a, b, c] = [-140, 38.75, -0.72] for the best case [63]. For the second model, B_∞ = -136, B_0 = 38 and f_0 = 0.7 are used as in [65]. As can be seen from the figure, similar trend of the noise is obtained by both models, however the second model has a more reasonable PSD when the frequency is low.
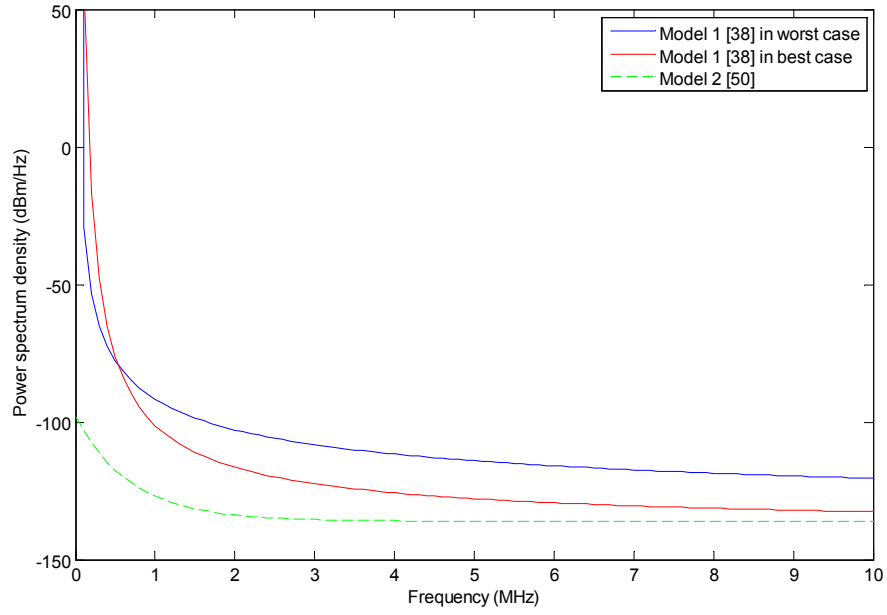
Fig. 2.7　PSD of existing models of background noise

2.2.2.2　Impulsive Noise

As stated in previous section, the periodic impulsive noise is usually modeled as background noise since it remains stationary over a long time. Thus, this subsection focuses on the aperiodic impulsive noise for indoor PLC. Since impulsive noises caused by switching power supplies occur only for a very short time, they are hard to measure. In [70], impulsive noise of 23 different domestic appliances are measured and classified according to activities on different kinds of appliances. Markov chain model [64] describes the impulsive noise behavior accurately, but with high complexity. In [71-73], the impulsive noise are modeled with an arrival process specified by the duration, amplitude and inter-arrival between impulses. The Bernoulli Gaussian model was proposed in [73], which is also known as the two terms Gaussian model. It describes the overall noise at any given time instant as a random value with the probability density function (pdf):

23

$$p(z) = (1-P) \cdot G(0, \sigma_b^2) + P \cdot G(0, \eta \sigma_b^2) \qquad (2.17)$$

where P is the probability of the occurrence of impulsive noise which follows Bernoulli random process, $G(0, \sigma_b^2)$ represents the Gaussian distribution of the background noise with zero mean and variance σ_b^2, while η is the ratio of impulsive noise power to background noise power.

Another commonly accepted model, Middleton's class A [72] is an infinite Gaussian mixture model. It expresses the pdf of the background plus impulsive noise as:

$$p(z) = \sum_{m=0}^{\infty} \frac{e^{-A} A^m}{m!} \frac{1}{\sqrt{2\pi\delta_m^2}} \exp(-\frac{z^2}{2\delta_m^2}) \qquad (2.18)$$

With $\quad \delta_m^2 = (\delta_b^2 + \delta_i^2)((m/A) + \Gamma)/(1+\Gamma) = \delta_b^2(1 + 1/\Gamma)((m/A) + \Gamma)/(1+\Gamma) \quad (2.19)$

Where $\dfrac{1}{\sqrt{2\pi\delta_m^2}} \exp(-\dfrac{z^2}{2\delta_m^2})$ is a Gaussian distribution with zero mean and variance δ_m^2. The expression $\dfrac{e^{-A} A^m}{m!}$ is the Poisson distribution controlling the occurrence of impulsive noise, and A is called impulsive index. $\Gamma = \delta_b^2/\delta_i^2$ is the ratio of background noise power to impulsive noise power. By setting the parameters as the fitted results in [67], the pdf of the two models are simulated as shown in Fig. 2.8. Where $\delta_b^2 = 2.6456 \cdot 10^{-5} V^2$, $P = 0.01$ and $\eta = 100$ for the Bernoulli Gaussian model, and $A = \Gamma = 0.01$ for the Middleton's class A model. As can be seen from the figure, the two models obtain very similar pdf. This is because the Bernoulli Gaussian model is in fact a simplified version of Middleton's class A model [67].
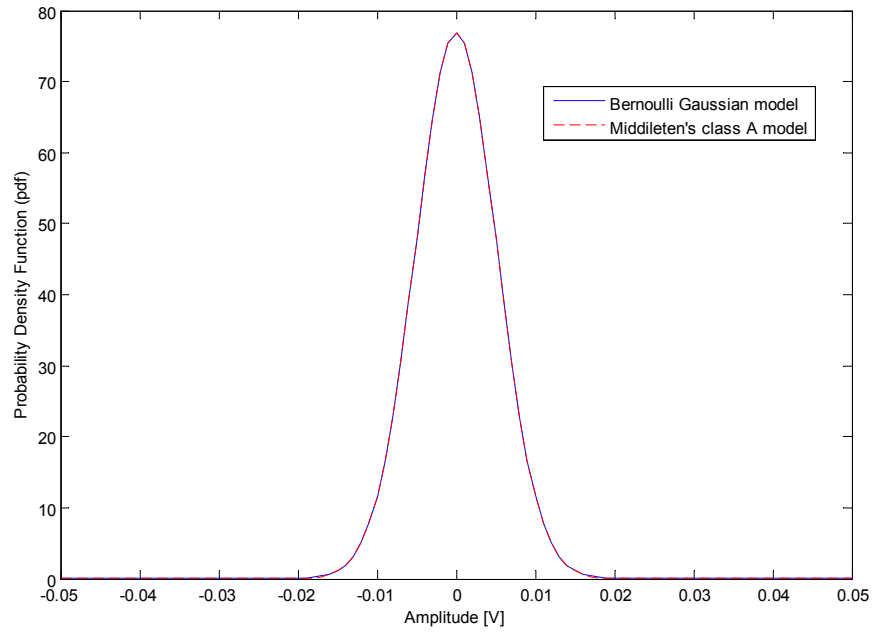
Fig. 2.8 Pdf obtained by Bernoulli Gaussian model [73] and Middleton's class A model [72]

2.3　Summary

In this chapter, the overview of communication technologies for smart grid was provided first. The advantages and drawbacks of PLC applied to smart grid were discussed. In Subsection 2.1.2, detailed introductions of the background, classification and architecture of PLC network were given. The communication applications of the HV, MV and LV networks were discussed. It is also emphasized that the difficulties in channel and noise modeling, and the random topology changes are the main research challenges for PLC. In Section 2.2, the bottom-up and top-down channel modeling approaches were reviewed. The transmission line theory for deriving the transfer function and the well-known multipath channel model were also presented. Finally, the complex noise scenario for PLC and the most commonly accepted models for colored background noise and impulsive noise were reviewed.

Chapter 3

Overview of Topological Analysis and Resource Management for PLC Networks

This chapter presents an overview of the preliminaries for our research topics. In Section 3.1, the recent research on PLC network topology is reviewed. The basis of time-frequency analysis is described in Section 3.2, and the resource allocation for OFDM based systems is introduced in Section 3.3. Finally, the summary is presented in Section 3.4.

3.1 Topological Analysis of PLC

As stated in Chapter 2, the estimation of random and time-varying network topology is one of most important the challenges for the development of PLC. This section first introduces the well-known indoor PLC topology models. And a random topology generation method is presented for the investigation of channel characteristics.

3.1.1 Network Topology

The research on topology of power line network provides a deep understanding of the network dynamics, and it is also crucial for channel modeling [4]. This thesis focuses on topologies LV power distribution networks including the indoor PLC networks. Different physical layouts are found in distribution networks, since they are designed according to different constraints of budget, system reliability and load impedance. Ring and radial (tree) layouts are the most commonly seen topologies for distribution power grid.

With the advantages in construction cost and simplicity, radial topologies [19] are most widely used for distribution networks. In a radial network, power from a substation radiates out into progressively lower voltage lines until the residential and business buildings are reached. Fig. 3.1 shows the physical layout of a typical radiate network. However, this kind of topology has a relatively large communication delay because the number of hops between source and destination grows with the increase of the size of the network. Moreover, in the case of any feeder failure, the associated consumer would not get any power since there is no alternative path to feed power.

A ring or interconnected topology [4] which has multiple connections between points is normally applied in urban areas. The connections are remotely controlled by power utilities by opening and closing the switches between them. In this case, if one feeder is under fault or maintenance, the associated consumer can still be supplied by other feeders connected to it, and only a small part of the network needs to be isolated.

Indoor power line network can be represented by a two-level tree structure as described in [19]. The first level is the connections between appliances and the

associated derivation box while the second level refers to the connections between derivation boxes. In this structure, two types of connection layout between outlets and the associate derivation box are found: star type and bus type [19]. Fig. 3.2 demonstrates a typical indoor power line network topology with both types of connections.
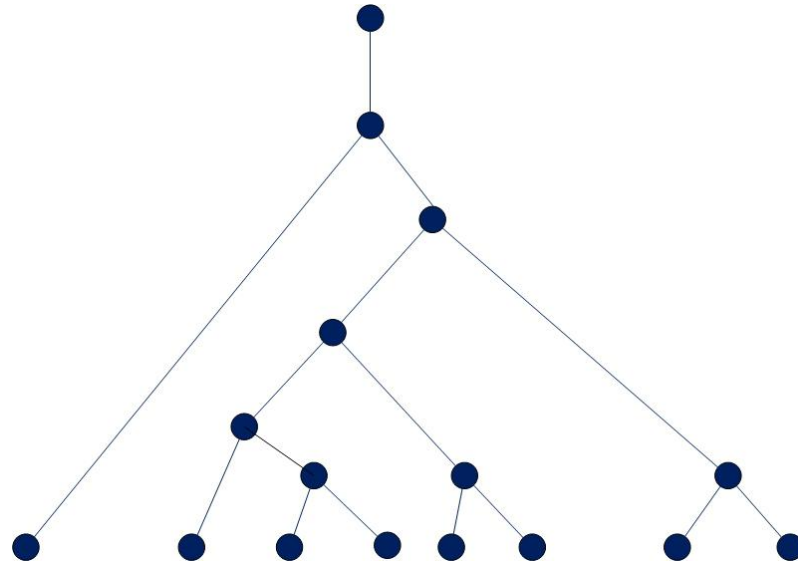
Fig. 3.1 An example tree topology of a distribution network
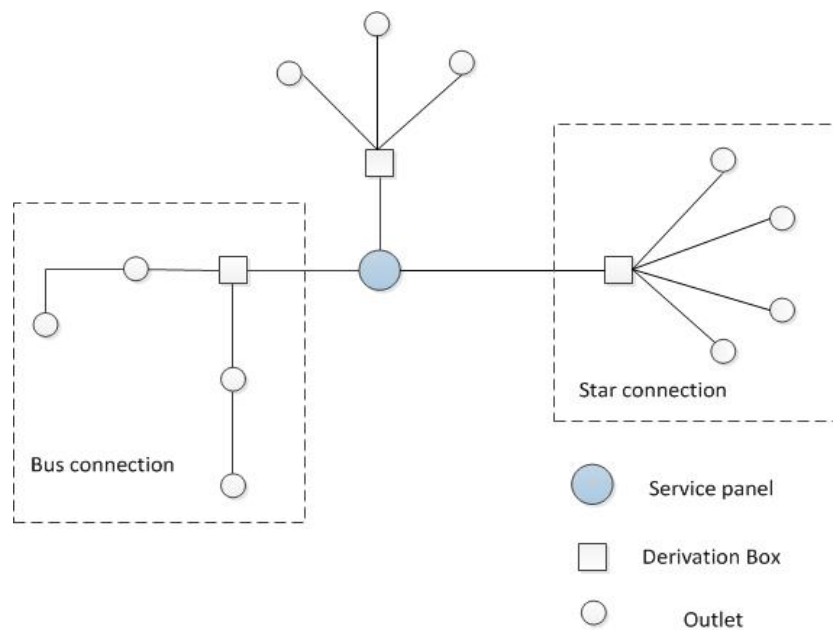
Fig. 3.2 A typical indoor power line network topology

3.1.2 Random Topology Generator

To produce a statistical channel model for indoor PLC, there have been a number of research attempts [4] done to develop algorithms that generate a large number of random topologies for testing cases. According to the characteristic of power grid which is sparsely connected with small-world network properties, a random topology model is proposed in [74]. This model generates a large-scale network in three steps: 1. Construct sub-networks with size limited by connectivity requirements. 2. Connect the sub-networks through lattice connections. 3. Generate the line impedance. This thesis focuses on indoor PLC. More details about this random topology model for large-scale networks can be found in [74].

A well-known random topology generator for indoor power line networks was proposed in [19]. Based on the two-level connection structure, the topology is divided into area elements, each of which contains a derivation box and all the outlets connected to it. An outlet is defined as a connection point between home appliance and the power cable. Each area is referred as a "cluster" and has a rectangular shape [19]. Assume the total area of topology is A_f and each cluster has an identical area A_c, the number of clusters can be calculated as:

$$N_c = \frac{A_f}{A_c} \tag{3.1}$$

A boolean matrix of size $r \times c$ is used to represent the layout of the topology with rc clusters. For example, the matrix:

$$M = \begin{bmatrix} 1 & 1 & 0 \\ 1 & 1 & 1 \end{bmatrix} \tag{3.2}$$

refers to the topology shown in Fig. 3.3, where $M(i,j) = 1$ denotes the presence of cluster at the *i-th* row and *j-th* column, otherwise the cluster is absent. (This model is a well recongnized model proposed in [19], and it has been cited by a lot of papers investigating topology of PLC)
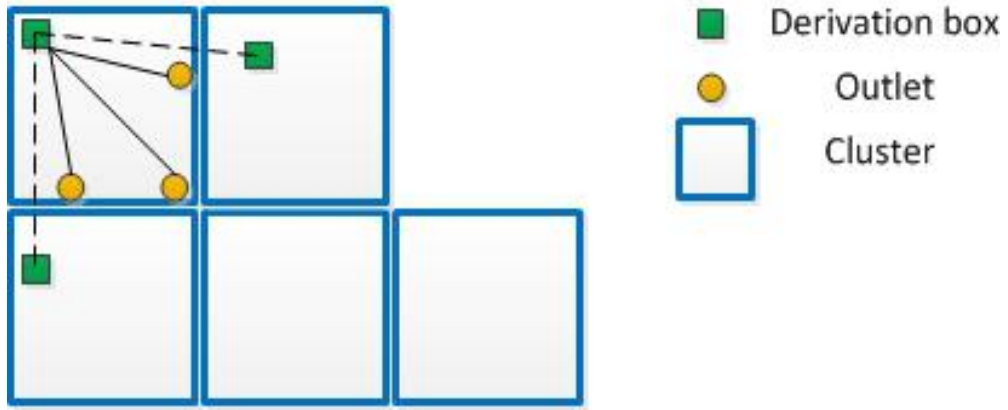
Fig. 3.3 Example cluster arrangement of an indoor PLC network [19]

The first step of the generator is to randomly arrange the layouts of clusters. From experiment evidences in [19], it is found the number of rows can be considered as a uniform distribution over [1, N_c], and the number of columns can be calculated as : $c = \left\lceil \dfrac{N_c}{r} \right\rceil$. Where $\lceil x \rceil$ is the ceiling operator. To maintain randomness, when $rc > N_c$ all elements in the first (*r*-1) rows and (*c*-1) are set to one, while ($rc - N_c$) zeros are randomly assigned to the elements in the *r-th* row and the *c-th* column.

The derivation boxes and outlets should be placed in appropriate location after the clusters are determined. Derivation boxes are assumed to be at the top left corner of the clusters, whose locations are shifted from the corner by a bi-dimensional offset distance over [0, $D = L/4$]. Where L is the side length of cluster. The number of outlets are placed along the cluster edge according to Poisson distribution with mean λA_c, while the distances between outlets follow uniform distribution [19]. Distances

between outlets and the associate derivation box can be calculated by simple geometric calculations according to the type of connection: star or bus. Fig. 3.4 shows a randomly generated topology with the parameters shown in Table 3.1.

The random topology generator has provided a way to statistically model PLC channel and investigate the characteristic of PLC networks. However, since the difference between networks is substantial, the design of communication schemes for a specific network still requires accurate knowledge of the instantaneous topology. Much recent work has focused on developing algorithms to infer topologies for power line networks, and they will be reviewed in detail in Chapter 4.

Table 3.1 Example parameters for the random topology generator

Area of network A_f	150 m^2
Minimum value of cluster area A_{min}	15 m^2
Maximum value of cluster area A_{max}	50 m^2
Outlet density λ	0.2 outlets/m^2
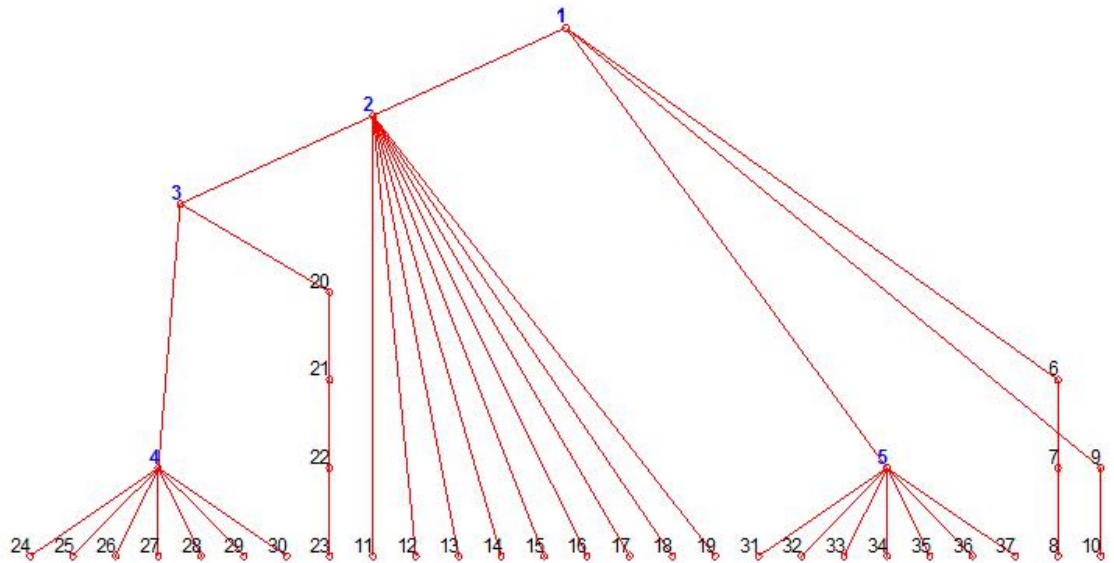
Fig. 3.4 An example topology generated with the parameters in Table 3.1 (not to scale)

3.2 Time-Frequency Domain Analysis

In order to provide a high resolution and low complexity solution for topology estimation, a time-frequency domain reflectometry based scheme is proposed in Chapter 4. For a better understanding of the proposed scheme, some basic knowledge of the time-frequency domain analysis is introduced in this section.

Time-frequency analysis was first proposed to analyze non-stationary signals whose spectrum change with time [75]. The Conhen's class [75] including Wigner distribution, Cone-shape distribution and Choi-Williams distribution is considered to be a high resolution and low interference model. By this bilinear transformation, a non-stationary time series can be expressed as a distribution function of time, frequency and kernel. The mathematical definition of the Conhen's class distribution can be expressed as [75]:

$$C_x(t,\omega) = \frac{1}{2\pi} \int\int A_x(\theta,\tau)\phi(\theta,\tau)e^{-j(\omega\tau+\theta t)}d\theta d\tau \qquad (3.3)$$

where $\phi(\theta,\tau)$ is the kernel of the time-frequency distribution, which is usually a low-pass function designed to reduce interference, θ and τ are frequency and time dummy variables of integration, and $A_x(\theta,\tau)$ represents the ambiguity function of signal $x(t)$ which is given by [76]:

$$A_x(\theta,\tau) = \frac{1}{2\pi} \int x(t+\frac{\tau}{2})x^*(t-\frac{\tau}{2})e^{j\theta t}dt \qquad (3.4)$$

Note that for $\theta = 0$, $A_x(\theta,\tau)$ reduces to the autocorrelation of $x(t)$ which is defined as follows [77]:

$$R_x(t,\tau) = x(t+\frac{\tau}{2})x^*(t-\frac{\tau}{2}) \qquad (3.5)$$

Different types of distributions are classified according to the kernels $\phi(\theta, \tau)$ as shown in Table 3.2.

Table 3.2 Kernels of Cohen's Class

Distribution	Kernel $\phi(\theta, \tau)$
Wigner-Ville	1
Cone-shape	$\dfrac{\sin(\theta\tau)}{\theta\tau} e^{-\alpha\tau^2}$
Choi-Williams	$e^{-\dfrac{\theta^2\tau^2}{\alpha}}$

Let us take a linear modulated chirp signal with a Gaussian envelope $s(t)$, which is often used as a reference signal for time frequency domain reflectometry [78], as an example.

$$s(t) = (\alpha/\pi)^{1/4} e^{-\alpha(t-t_0)^2/2 + j\beta(t-t_0)^2 + j\omega_0(t-t_0)} \tag{3.6}$$

where α, β, t_0, and ω_0 are the time duration, frequency sweep rate, time center and frequency center respectively. The signal is shaped by a Gaussian envelope in both time and frequency domains, and the frequency of the signal increases linearly with time. $s(t)$ can be transformed into time-frequency domain by the Wigner-Ville distribution [79]:

$$W_s(t, \omega) = \frac{1}{2\pi} \int s(t + \frac{1}{2}\tau) s^*(t - \frac{1}{2}\tau) e^{-j\tau\omega} d\tau \tag{3.7}$$

Thus, we obtain:

$$W_s(t, \omega) = \frac{1}{\pi} e^{-\alpha(t-t_0)^2 - (\omega - \beta(t-t_0) - \omega_0)^2/\alpha} \tag{3.8}$$

By applying a set of example parameters designed for the RG type coaxial cables described in [78] : $\alpha = 50$ ns, $\beta = 2 \times 10^{15} \cdot 2\pi$ Hz/s, $t_0 = 100$ ns, $\omega_0 = 450$ MHz. The time-frequency distribution $W_s(t,\omega)$ over 100 MHz band is shown in Fig. 3.5.
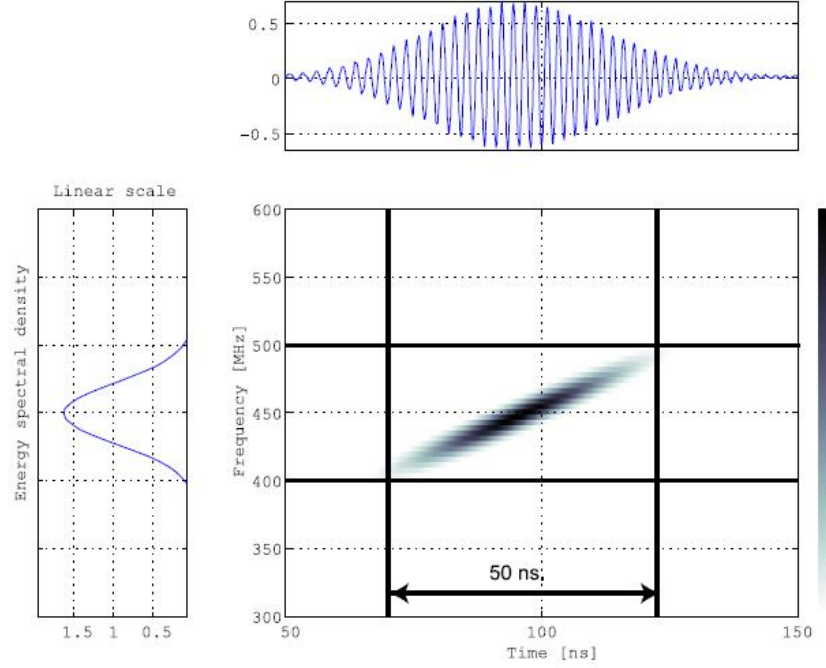
Fig. 3.5 Time-frequency distribution of an example linear modulated chirp signal with a Gaussian envelope [78]

There are a number of desirable properties of the time-frequency distribution, such as realness, nonnegativity, time shift and frequency modulation etc. In this section, we mainly introduce the time shift and frequency modulation properties and the corresponding requirements of kernel which are used in the later chapters. If the kernel $\phi(\theta, \tau)$ does not depend on t, the time shift of signal $s(t)$ can be described as [79]:

$$s_1(t) = s(t - t_0) \rightarrow C_{s_1}(t, \omega; \phi) = C_s(t - t_0, \omega; \phi) \tag{3.9}$$

On the other hand, if the kernel $\phi(\theta,\tau)$ is independent of ω, the frequency modulation is represented by:

$$s_1(t) = s(t)e^{j\omega_0 t} \to C_{s_1}(t,\omega;\phi) = C_s(t,\omega-\omega_0;\phi)$$

(3.10)

As can be seen, the kernel plays a crucial role in determining the properties of time-frequency distribution of a signal. More detailed description of the properties of time-frequency distribution can be found in [79].

3.3   Overview of Resource Management for Broadband PLC Systems

3.3.1   OFDM Technique

As described in Chapter 2, a PLC channel can be seen as a multipath frequency selective fading channel. To combat the frequency selectivity, orthogonal frequency division multiplexing (OFDM) is widely used in PLC standards, with the advantages of full use of spectrum, robustness against narrowband interference, and good performance in multi-path environments. It uses a large number of equi-spaced frequencies, called subcarriers, to carry data [80]. The data is reformed into parallel streams, and each stream is carried by one subcarrier which occupies a narrow bandwidth so that the corresponding subchannel can be seen as frequency-flat.

The procedure of an OFDM system is presented in Fig. 3.6. Assume the total bandwidth of the channel is B, and suppose there are N symbols ($x[0]$,..., $x[N$-1]) to be transmitted. By inverse fast Fourier transform (IFFT), the transmission data can be expressed as:

$$X[n] = \sum_{i=0}^{N-1} x[i] e^{j\frac{2\pi}{N}in} \qquad n \in \{0,...,N-1\} \tag{3.11}$$

A cyclic prefix (CP), which refers to the prefixing of a symbol with a repetition of the end, is inserted to the symbols to eliminate the multipath effect. The received signals are:

$$y[n] = h[n] \otimes X[n] + z[n] \qquad n \in \{0,...,N-1\} \tag{3.12}$$
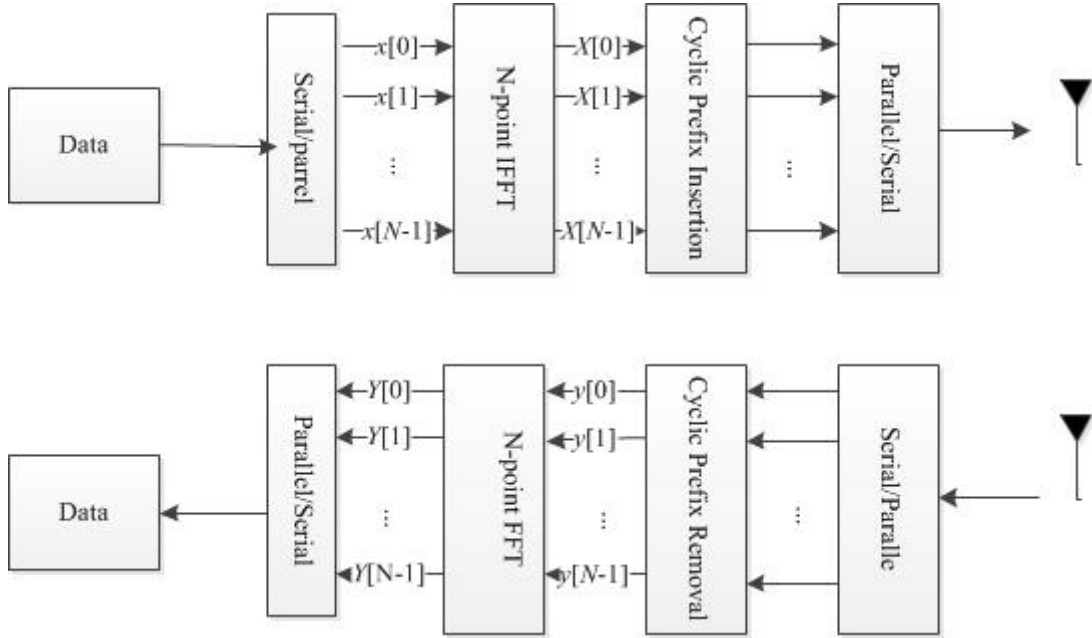
Fig. 3.6 Simplified block diagram of the OFDM system

where $h[n]$ and $z[n]$ are the channel impulse response (CIR) and noise of symbol n. The FFT is applied to the received signals after CP removal, and the recovered signals are obtained:

$$\begin{aligned} Y[n] &= FFT\{h[n] \otimes X[n] + z[n]\} \\ &= H_n x[n] + Z[n] \end{aligned} \tag{3.13}$$

where H_n is the frequency response of the n-th subchannel, and $Z(n)$ is the noise on the n-th subchannel in frequency domain. As can be seen, the frequency range for each symbol is narrowed to B/N so that each transmission data carried on one subcarrier undergoes flat fading and can be processed independently.

3.3.2   Diversity in OFDM based Systems

There are several kinds of diversity for OFDM based system which play crucial role in resource management. In this subsection, the most commonly used diversities, frequency and multiuser diversities, are presented.

3.3.2.1 Frequency Diversity

Since broadband PLC systems suffer from frequency selective fading, some parts of the spectrum are in deep fading while some other parts have a much better channel condition. Therefore, by dividing the signal frequency band into a number of narrowbands, frequency diversity appears in the OFDM system [81]. Fig. 3.7 represents different amplitudes of subcarriers.

The investigation of frequency diversity provides a high degree of freedom for designing transmission schemes to improve system performance. For example, resource allocation for a single user OFDM system can be done according to the frequency diversity [81]. Different amount of power and data can be allocated to different subcarriers according to calculation results of proper optimization algorithms; proper modulation employed in each frequency band can reduce bit error rate (BER) and enhance the system capacity [82].
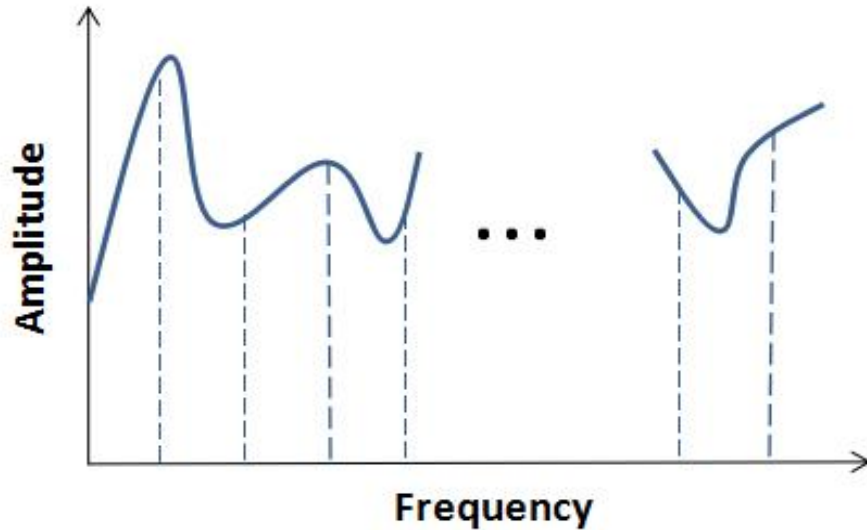
Fig. 3.7 Different amplitude values of subcarriers

3.3.2.2 Multiuser Diversity

From Chapter 2 it is clear that the channel of PLC system is time varying which refers to the fading changes over time. In multiuser PLC systems, the channel frequency response are different across users since the weighing factors and dominate path distances are different as described in Subsection 2.2.1. A lot of research has been done on multiuser diversity [83] [84] [85]. Fig. 3.8 shows an example to represent multiuser diversity, the channel for user 1 is under deep fading while it may be in a good condition for user 2. Therefore, there is a freedom for the system to always transmit data from the user with higher SNR, which obtains a better system capacity than conventional systems. Note that this diversity exists in frequency domain as well.

When the number of users increases, there is more degree of freedom and more choice for data transmission. As a result, the system performance in terms of capacity and spectral efficiency benefits from the multiuser diversity with the increase of the number of users.
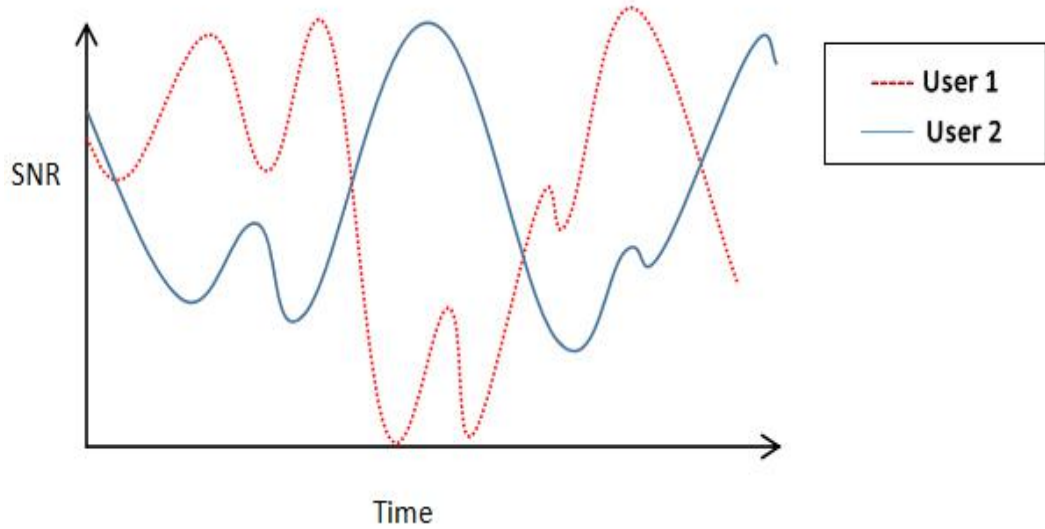
Fig. 3.8 Example SNR of two users

3.3.3 Resource Allocation for Indoor PLC Systems

With the diversities described in Subsection 3.3.2, OFDM based communication systems have more flexibility in data transmission. Allocating communication resources properly can substantially improve system performance. For an indoor PLC system, the resources are usually referred to the following prime elements: bandwidth, carrier frequency, and transmit power. For an OFDM system, the so called subcarrier allocation (SA) is used to allocate the bandwidth and carrier frequency simultaneous.

In a multiuser PLC system, due to the existence of multiuser diversity in frequency domain, allocating a number of subcarriers to different users results in a higher capacity. The CSI of subcarriers for all users are obtained to form the SA map first. Afterwards, each subcarrier is assigned to the user with the highest SNR in one transmission period. Thus, users get different numbers of subcarriers according to their channel condition. As described in Subsection 3.3.2, the system throughput obtained by SA benefits more as the number of users increases. An example of SA is

illustrated in Fig. 3.9, where the numbers in cubes are the relative values of SNR, and the purple color indicates the highest value among users.

Similarly, uniform power allocation (PA) cannot obtain optimized system capacity and BER due to frequency diversity in an indoor PLC network. Since all subcarriers are mutually independent, adaptive power allocation [86] on each subcarrier greatly enhances system performance. The most famous power allocation method is the water-filling algorithm [87]. As the name suggests, the algorithm allocates power to subcarriers to fulfill a unified water level, as demonstrated in Fig. 3.10, where the green bars are the reciprocal of CNR and the blue bars indicate the power required for each subcarrier to reach the water level. Assume the water level is set to be ξ, and the CNR of sub-carrier n is η_n. The allocated power on subcarrier n can be calculated as:

$$p_n = \left[\xi - \frac{1}{\eta_n} \right]^+, \qquad n = 0,..., N \tag{3.14}$$

As can be seen, the allocated power increases with the CNR η_n which means that if the channel condition is good the allocated power is high. For example, the power allocated on subcarrier 3 in Fig. 3.10 is the highest due to its highest CNR among the 8 subcarriers. PA and SA are usually conducted jointly to achieve an optimal system performance [81]. However,if the goal is to achieve the Shannon capacity in practice, capacity-approaching codes such as low-density parity-check (LDPC) codes [88] and turbo codes [89] are required. The turbo codes are the most widely applied forward error correction codes which are also considered as the first practical codes developed to closely approach the Shannon capacity [90]. Since this thesis mainly focus on optimal resource allocation part, if readers are interested in turbo codes, more details can be found in [89-91].
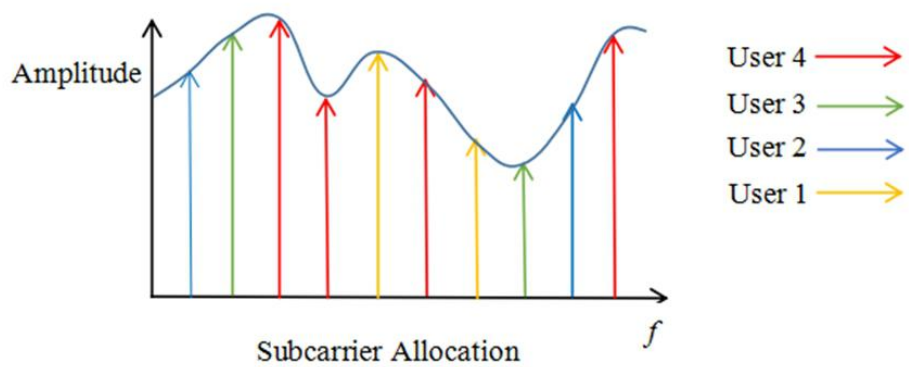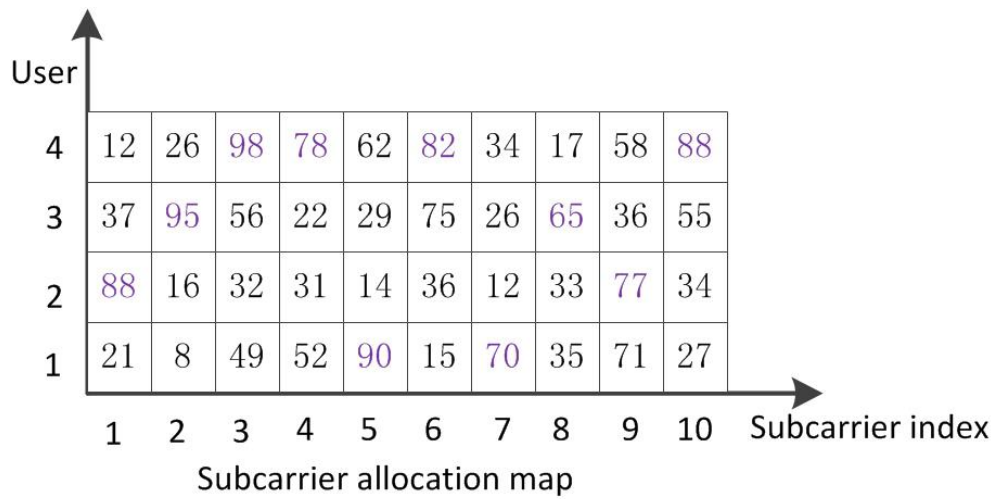
Fig. 3.9 An example of subcarrier allocation
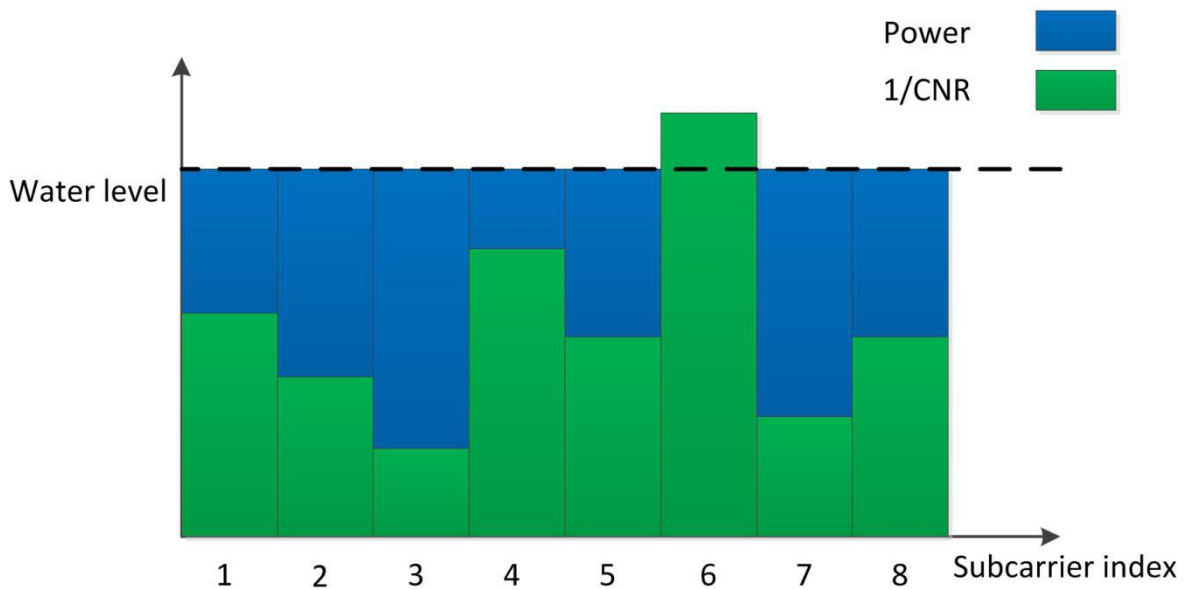
Fig. 3.10 Demonstration of the water-filling algorithm

3.4   Summary

In this chapter, the necessary knowledge required by the research topics covered in this thesis has been reviewed. First, the topological analysis of PLC has been presented, and the properties introduced will be utilized in the research introduced in Chapter 4. Additionally, a random topology generator has been demonstrated, which provides a method to statistically model and analyze PLC channel. Second, some basic knowledge of the time-frequency domain analysis of signal propagation has been reviewed. The Cohen's class distributions provide methods to transform a non-stationary time series to a distribution function of time, frequency and kernel. This is the basis of the time-frequency domain reflectomery based topology estimation method presented in Chapter 4. Finally, a review of resource management for OFDM based indoor PLC systems has been presented. This preliminary helps readers to have a better understanding of the proposed routing and resource allocation scheme in Chapter 5.

Chapter 4

High-Resolution and Low-Complexity Dynamic Topology Estimation for PLC Networks assisted by Impulsive Noise Source Detection

The topology information determines the instantaneous CSI of a PLC network which is crucial for the deployment of communication schemes to power lines [19]. Furthermore, the design of routing protocols [20-21, 27-30] and power flow optimization [22] also rely on the knowledge of topology. However, it is hard to obtain the time-varying topology of an indoor PLC since some parts of the cables are placed inside walls and the changes of connectivity are unpredictable. The development of efficient approaches for dynamic topology estimation are highly demanded and has attracted a lot of research interest.

The topology estimation method in [20] uses two-way handshake for time of flight (TOF) measurement between any two nodes, and tests the hypothesis of two nodes being neighbors according to the TOF. Thus, a PLC modem is required at every branch node and end node in the system. In [92] and [93], signaling between each pair of end nodes was utilized to estimate their distance. Both methods rely on parameter estimation of the channel transfer function between each pair of end nodes, and

therefore require a PLC modem at every end node for data transmission and measurement. In an indoor PLC network, it is not practical to have a PLC modem equipped at every node. In [32], a frequency-domain reflectometry (FDR) based topology inference method was proposed, which requires measurement at a single modem. This kind of reflectometry based method is similar to channel sounding, which obtain the CSI by analyzing the correlation of the received signal and the transmitted signal [94] [95] [96]. However, the FDR based method has a limited resolution, and its computational complexity increases dramatically with the increase of the number of nodes in the PLC network. The approach described in [97] converts path length estimation to a spectral estimation problem of complex damped exponentials. The method requires high accuracy in the measurement of channel transfer function, and has degraded performance when the distances between nodes become large. In summary, the existing PLC topology estimation approaches either require a large number of PLC modems in the network as an essential working condition [20] [92] [93] or have performance limitations [32] [97]. Moreover, these approaches have considered only static network topologies, ignoring the time-varying characteristic of PLC networks in reality. As a result, all the aforementioned methods require a full-topology re-estimation whenever a topology change occurs (how to detect the topology change was not addressed in the previous work), which is computationally inefficient.

In this chapter, a time-frequency domain reflectometry (TFDR) based high-resolution and low-complexity dynamic PLC network topology estimation scheme assisted by impulsive noise source detection is investigated. The scheme consists of three parts: TFDR based path length estimation, node-by-node greedy algorithm based topology reconstruction, and impulsive noise assisted topology

re-estimation. This work contributes in the following aspects. First, to the best of our knowledge, this is the first work to utilize the TFDR for topology inference, although TFDR has been used in solving other problems such as line fault detection [100]. This approach significantly improves the resolution and accuracy of the estimation with a single measurement point (PLC modem). It investigates signals in both time and frequency domains, and therefore the resolution and accuracy loss caused by frequency-time domain transformation in distance calculation can be avoided. Second, the proposed node-by-node greedy algorithm achieves much higher computational efficiency over the peak-by-peak searching algorithm in [32]. Third, a novel impulsive noise source detection method is proposed to detect dynamic topology changes, by utilizing the time difference of arrival (TDOA) of the first noise impulses. Topology re-estimations are triggered only by impulsive noise detected, and therefore much less full-topology estimations are required than the previous fixed-frequency re-estimation methods.

The rest of this chapter is organized as follows. The channel model and the review of the previous estimation methods are presented in Section 4.1. In Section 4.2, the proposed dynamic topology estimation scheme is described. Complexity analysis is presented in Section 4.3 and simulation results are shown in Section 4.4. Finally, a summary is given in Section 4.5.

4.1   Channel Model and Review of the Previous Methods

4.1.1   Multipath Channel Model

A low voltage power line network consists of termination points with loads connected (end nodes), branch nodes connecting the loads, and the power line cables linking

them. Fig. 4.1 illustrates a 4-node network with one branch node and three end nodes. When a signal traveling through the power line reaches a node, part of the signal is reflected back to the previous node due to impedance mismatch, and the remaining part continues propagating. Due to multiple reflections between adjacent nodes during the propagation, multiple replicas of the transmit signal will be received. Therefore, the channel is considered to be a multipath fading channel [59]. For example, in Fig. 4.1, a reference signal is injected to the network from the point of measurement, node *a*. There are in principle an infinite number of replicas of the reference signal with different attenuation and delays received at the measurement point, each of which refers to a propagation path. Example routes are a-b-a, a-b-c-b-a, and a-b-c-b-c-b-a.
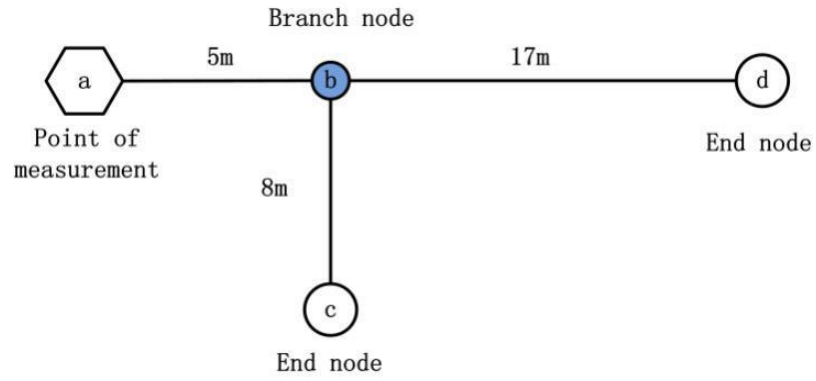
Fig. 4.1 An example 4-node PLC topology

The signal traveling along path *i* is characterized by three factors [59]: the weighing factor g_i, the attenuation factor A_i and the delay factor φ_i . The weighting factor g_i is the product of all transmission and reflection coefficients of path *i* [58]. Assuming that the signal is reflected by N_{i1} discontinuities and passing through N_{i2} discontinuities along path *i*, and $\rho_{i,k1}$ and $\tau_{i,k2}$ are the reflection and transmission coefficients of discontinuity points k_1 and k_2, respectively. Thus, g_i can be calculated as [58]:

$$g_i = \prod_{k_1=1}^{N_{i1}} \rho_{i,k_1} \prod_{k_2=1}^{N_{i2}} \tau_{i,k_2} \qquad (4.1)$$

The attenuation and delay factors are functions of frequency ω (in rad/sec) and related to the path length l_i. The complex propagation constant of the line is defined as $\gamma(\omega) = \alpha(\omega) + j\beta(\omega)$, where $\alpha(\omega)$ is the attenuation constant, and $\beta(\omega) = \omega / v$ is the phase constant with v denoting the propagation speed along the line. A_i and φ_i can then be calculated as:

$$A_i(\omega) = e^{-\alpha(\omega) \cdot l_i} \tag{4.2}$$

$$\varphi_i(\omega) = \frac{l_i}{v} = \frac{l_i \beta(\omega)}{\omega} \tag{4.3}$$

As can be seen, the signal amplitude on each path attenuates with the increase of propagation distance. Counting only the first N_e echoes per branch, we assume that there are N detectable paths. The channel transfer function obtained at the measurement point is expressed as the sum of all path components:

$$H(\omega) = \sum_{i=1}^{N} g_i A_i(\omega) e^{-j\omega \cdot \varphi_i(\omega)} \tag{4.4}$$

Substituting (4.2) and (4.3) into (4.4) yields

$$H(\omega) = \sum_{i=1}^{N} g_i \cdot e^{-\gamma(\omega) \cdot l_i} \tag{4.5}$$

4.1.2 Review of TDR and FDR based Static Topology Estimation Approaches

The general idea of the reflectometry based topology estimation is to inject a reference signal to the network whose reflected signals from the discontinuity points (i.e., nodes) are received at the injection point. By analyzing the cross-correlation of the reference and received signals, the locations of the nodes are estimated. A stand-alone topology estimation process can be divided into two parts: 1) estimation

of the path lengths, and 2) reconstruction of the network via the estimated path lengths.

There are two conventional approaches to locate the discontinuities of a network: time domain reflectometry (TDR) [98] and FDR [99] based approaches. The TDR uses a step pulse as reference signal, whose energy spreads over the whole spectrum. Thus, it is not suitable for analyzing the radio frequency (RF) characteristics of a cable. Also, the resolution of the approach is limited intrinsically.

On the contrary, for the FDR based methods, the sinusoidal reference signal used has its energy spread over a large range of time, which makes the time-domain analysis complicated. It measures the steady state spectral content natively, and has to use Inverse Fourier Transform (IFT) to calculate the path lengths. The results obtained via IFT have a resolution limitation due to the time-frequency uncertainty [97]. Letting $B_{measure}$ denote the bandwidth of measurement, the minimum distinguishable difference between two path lengths can be expressed as: $\Delta l_{\min} \approx \Delta t \cdot v$, where $\Delta t = 1/B_{measure}$ is the time resolution of the FDR based approach. Since the signal propagation speed in power lines is high, an extremely high measurement bandwidth is required for a high resolution of topology estimation. For example, with $v = 2 \times 10^8$ m/s and $B_{measure}$ = 10 MHz, the achievable resolution is 20 m. The FDR based parametric model [97] achieves a higher resolution than the non-parametric method [32]. However, the parametric method requires high accuracy in measuring the amplitude of the channel transfer function, and some of the paths cannot be detected if multiple paths have the same distance. Moreover, as the number of measured path increases, the accuracy of the FDR based methods decreases significantly [32] [97]. Thus, the FDR based methods are not suitable for a small-scale network, such as an indoor PLC network.

4.2 TFDR based and Impulsive Noise Source Assisted Dynamic Topology Estimation

The topology estimation is conducted in three steps. First, we estimate the round trip path lengths from a single measurement point to each node by using the TFDR. Second, the obtained path lengths are used to reconstruct the connections between nodes with a node-by-node greedy algorithm at the measurement point. Third, impulsive noise source detection is employed to trigger topology re-estimation and reduce its complexity in time-varying PLC networks.

4.2.1 Path Length Estimation via TFDR

Time-frequency analysis overcomes the limitation of the classical Fourier transform analysis which cannot provide time-localized information of the non-stationary signals. It has wide applications, such as instantaneous frequency estimation and time-frequency filtering. TFDR, featuring the advantages of both TDR and FDR, was recently used to locate fault on a power line cable [100].

Different from solving a fault detection problem, to estimate a network topology which has many branches and end nodes, the multipath channel model described in Section 2 must be considered. TFDR uses a linearly modulated chirp signal with a Gaussian envelope [78] as the reference signal, where the Gaussian envelope is used to remove the sidelobes in frequency domain. The frequency of the signal increases linearly with time.

Let B_s be the frequency sweep band and T_s be the period of the signal. Define $p = 1/(2T_s{}^2)$ and $q = 2\pi \cdot B_s / T_s$. Also define t_0 and ω_0 as the time center and frequency center, respectively. The chirp signal injected to the network is expressed as:

$$V_t(t) = (p/\pi)^{1/4} e^{-p(t-t_0)^2/2 + jq(t-t_0)^2 + j\omega_0(t-t_0)} \tag{4.6}$$

Since the chirp signal has a pre-determined period of time and the frequency sweep range, it is convenient to analyze the signal in the time-frequency domain. The signal in (6) is transformed into the time-frequency domain by Wigner distribution [101] as:

$$W_{v_t}(t,\omega) = \frac{1}{\pi} e^{-p(t-t_0)^2 - (\omega - q(t-t_0) - \omega_0)^2/p} \tag{4.7}$$

Consider the multipath channel described in Section 4.1.1, as derived in [78], the time-frequency transfer function is :

$$H(t,\omega) = \sum_{i=1}^{N} g_i^2 \, e^{-2\gamma(\omega)\cdot l_i} \tag{4.8}$$

By multiplying the reference signal $W_{v_t}(t,\omega)$ by $H(t,\omega)$, the time-frequency domain received signal can be represented as:

$$W_{v_r}(t,\omega) = \sum_{i=1}^{N} g_i^2 \frac{1}{\pi} e^{-p(t-l_i/v)^2 - (\omega - q(t-l_i/v) - \omega_0)^2/p} \cdot e^{-\gamma(\omega)\cdot l_i} \tag{4.9}$$

Finally, the time-frequency domain cross-correlation function of the reference and reflected signals at the measurement point is:

$$C_{sr}(t) = \frac{2\pi}{E_{v_t} E_{v_r}} \iint W_{v_r}(t',\omega) W_{v_t}(t'-t,\omega) d\omega \cdot dt' \tag{4.10}$$

where $E_{v_t} = \iint W_{v_t}(t,\omega) dt d\omega$ and $E_{v_r} = \iint W_{v_r}(t',\omega) d\omega dt'$ are normalizing factors.

Assuming that the frequency dependent attenuation of the channel is linear, we can write $\gamma(\omega) = B\omega$ [100], where B is a positive-valued constant. Substituting (4.7) and (4.9) into (4.10) yields:
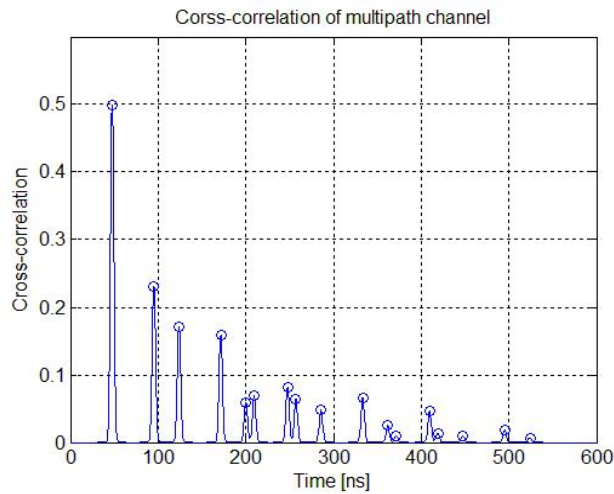
Fig. 4.2 Cross-correlation $C_{sr}(t)$ of the reflected and reference signals of the topology shown in Fig. 4.1

$$C_{sr}(t)=\sum_{i=1}^{N}g_i^2 \cdot e^{-\frac{p^2+q^2}{2p}(Bl_i)^2} \cdot e^{-\frac{p^2+q^2}{2p}(t-l_i/v)^2} \qquad (4.11)$$

Since the values of p and q are both large, the peak values of the cross correlation in (4.11) occur only at $t_i = l_i/v$. Therefore, the length of path can be calculated as:

$$l_i = t_i \cdot v \qquad (4.12)$$

where t_i represents the time of the i-th peak. Since the distances are obtained directly from the time domain information, the resolution is not limited by the measurement bandwidth like the FDR based approach.

Fig. 4.2 shows the cross-correlation function $C_{sr}(t)$ of the sample topology in Fig. 4.1. The parameters used are set with the consideration of the characteristics of indoor PLC which uses the frequency band of up to 30 MHz. The center frequency is chosen to be $\omega_0 = 2\pi \cdot 15$ MHz to avoid significant background noise in lower band [102], and the frequency sweep band B_s is set to 10 MHz. In terms of the rise/fall time limitation of the signal generators, the time duration is chosen as $T_s = 5$ ns. Thus, $p = 2 \times 10^{16}$ s^{-2} and the frequency sweep rate is $q = 4\pi \times 10^{15}$ Hz/s. The maximum time of repeats of each edge $N_e = 4$. The locations of the peaks are marked by circles in Fig. 4.2 and they are used to obtain the path lengths according to (4.12).

As can be seen from (4.12), only the "location" of the peaks matters in the estiamtion of path length, therefore the noise which only has effect on amplitude of the peaks does not change the results. Since the FDR based method obtains the peak of time domain correlation by taking IFT frequency domain 'trace' [32], the resolution is therefore limited by the measurement bandwidth as derived in 4.1.2 and suffers time-frequency uncertainty. On the other hand, the peak locations in TFDR are directly obtained from time domain calculation, thus the frequency-to-time domain IFT is avoided. However, the overlap of adjacent peaks should be avoided. The resolution of the round trip path of the TFDR method is given by:

$$\Delta l_{\min} \approx T_s v \tag{4.13}$$

With $T_s = 5$ ns and $v = 2 \times 10^8$ m/s, the resolution is 1 m (note: in this chapter, 'resolution' refers to the minimum interval between two detected peaks, and it has nothing to do with the precision.), which is 20 times as high as that achieved by the FDR method described in Subsection 4.1.2.

As can be seen from (4.12), the path lengths are determined only by the location of peaks in time domain. Thus, the method does not require high accuracy of the measurement of peak amplitudes. However, if the amplitude of a peak is too low, it is hard to detect. According to (4.11), the decrease in the weighting factor g_i or the increase in the path length l_i causes a decrease in the amplitude of the i-th peak. Since g_i is the product of the transmission coefficient ρ_i and the reflection coefficient τ_i, and $\rho_{i,k1} \leq 1$ and $\tau_{i,k2} \leq 1$ for all nodes, the amplitude of g_i decreases with the increase of the number of nodes. Therefore, some ambiguity may occur in detecting the peaks, which increases the estimation error rate, when the number of nodes and the distances between nodes increase to a certain degree. This will be discussed further in Section 4.4 with numerical results.

4.2.2   Node-by-Node Greedy Algorithm for Topology Reconstruction

With the path lengths estimated, a proper algorithm to reconstruct the connections among nodes is required. The algorithm is performed at the single measurement point. The algorithm used in [32] reconstructs topology by processing individual peaks of the measured correlation function $C_{sr}(t)$. However, with the increase of the number of nodes in a network, the number of measured peaks increases dramatically and it becomes computationally difficult to process the peaks one by one. Moreover, since the same group of edges with different repeating times generates different

groups of peaks, analysis of all the peaks is unnecessary. For example, with the topology shown in Fig. 4.1, analyzing the peaks on paths a-b-c-b-c-b-a and a-b-c-b-a actually detects the same edges a-b and b-c. The method in [32] also repeatedly searches all possible connections for the same group of nodes in processing of every peak, which causes redundancy.

We propose an enhanced greedy searching algorithm with reduced complexity for topology reconstruction, which searches possible topologies node-by-node instead of peak-by-peak. Since in most indoor power line networks, the outlets (end nodes) are visible, we assume that the number of end nodes N_{max} is known. The reconstruction starts with a two-node topology S_1. Let Lp_k be the distance from measurement point to the *k-th* peak of the TFDR correlation, thus the distance between the two nodes in S_1 is $Lp_k/2$. Then we add new connections to a node in the topology with possible distances to form candidate topologies. Unlike the algorithm in [32] which tries to connect a new node to one of the existing nodes in each iteration, in our algorithm, all possible connections to a particular node are generated within one iteration. Then the theoretical path lengths of the new topologies are compared to the results obtained from the measured TFDR correlation. The ones having consistent path lengths with the measurement are kept in the candidate set and are processed in next iteration. The process is repeated until the number of end nodes exceeds N_{max}.

A new approach to determine the set of possible distances for the new nodes to be connected is proposed. As described above, the peak locations are calculated by combinations of different numbers of echoes of edges. Let D_n be the length of the shortest path from the measurement point to node *n*. Then the lengths of the edges that connected to node *n* must be included in $Dif_n = Lp_k - D_n$, ($\forall k \in \{1,...,|L_{pk}|\}$). For

example, edge d-e can be detected by the peak location of path a-b-d-e-d-b-a minus the shortest path from node a to node d: a-b-d-b-a. For comparison with the algorithm in [32], we use the same setup of maximum 2 new branches connected to one branch node, and this can be extended to the cases with more branches. The proposed greedy algorithm is described as follows.

Initialize S, the set of possible topologies, as $S = \{S_1\}$, where $S_1 = [(1, 2)\ Lp_k\ /2]$, where the first and second elements refer to the two nodes and the third element indicates the distance between them. The number of end nodes $N_{end} = 2$.

While $N_{end} \leq N_{max}$

Start the search with node $n = 2$.

1. **For** $i = 1, ..., |S|$:

   1) Load topology S_i, and calculate the set of possible distances Dif_n for the new nodes to connect to node n. Initialize an empty temporary sets T to store the new possible topologies generated.

   2) **For** $j = 1, ..., |Dif_n|$:

   Add a new node connected to node n, with distance of $Dif_{n,j}$ to form a new candidate topology. Compare the theoretical path lengths of the new topology with the measurement. If it is consistent with the measured result, keep it in set T.

   End For

   3) If $|T| > 1$, let $T_{u,v}$ represent the combined topology of element u and v, which has two new nodes connected to node n. Find pairwise combinations of all the elements of T.

   4) Check the theoretical path lengths for each of the topologies, $T_{u,v}$ ($\forall u \in \{1,...,|T|\}, \forall v \in \{1,...,|T|\}, u \neq v$). Keep the ones whose path lengths are consistent with the path lengths obtained via the measured TFDR correlation.

   End For

2. Update S and N_{end} according to the candidate topologies obtained.

$n = n+1$;

End While

Fig. 4.3 shows a sample reconstruction process of the 4-node topology in Fig. 4.1. Dealing with nodes instead of peaks avoids processing repeating information. And the instantaneous update of possible topologies after each iteration ensures that each node is only processed once.
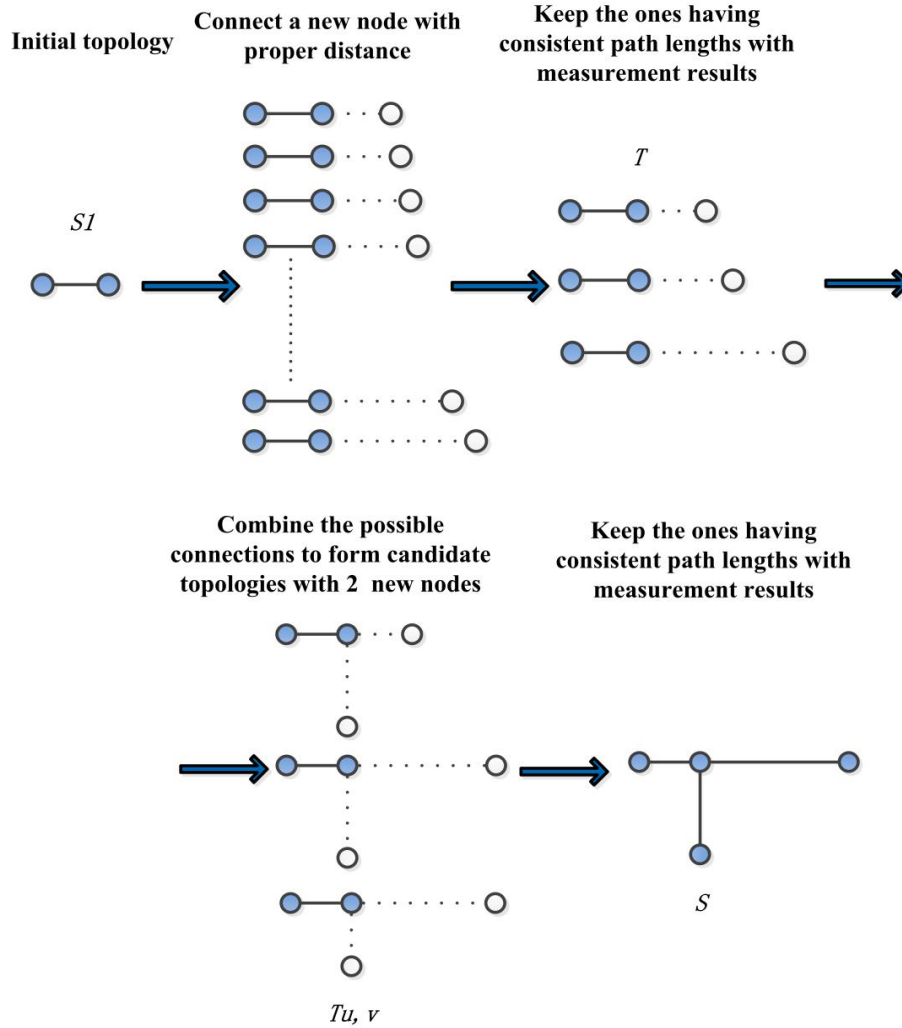
Fig. 4.3 Reconstruction process of the topology shown in Fig. 4.1

4.2.3 Impulsive Noise Source Assisted Dynamic Topology Re-Estimation

PLC network is time-varying. Random activities such as appliance switched on/off and plugged in/out cause changes to topology. Since how to detect the topology

change was not addressed in the previous works, to grasp the instantaneous status of a PLC network, a conventional approach is to estimate the full topology periodically. If the topology estimation frequency is set too high, the computational complexity required is dramatic; if the topology estimation frequency is too low, topology changes in the network may be missed. Hence, the fixed-frequency topology estimation is computationally inefficient.

The activities causing topology changes always generate impulsive noise [103] in PLC networks. Thus, we propose to detect topology change by detecting the source of impulsive noise. Unlike the periodic topology re-estimation, the proposed topology re-estimation is triggered only by detection of impulsive noise, and does not operate at a fixed frequency and a fixed complexity. If the impulsive noise source is uniquely identified, the corresponding end node will simply be added/removed from the network topology. Only if there is ambiguity with the impulsive noise source, *i.e.*, the impulsive noise source is not the only end node connected to a branch node, a full-topology re-estimation needs to be conducted.

To model the impulsive noise，several statistical distributions such as Bernoulli-Gaussian (BG) [71], Middleton Class-A [72] and Gaussian-Mixture [73] have been proposed. In this chapter, we consider the BG model which has been widely recognized as an accurate approximation of impulsive behavior for practical channels including urban PLC systems [104]. The probability density function of the impulsive noise is expressed as a mixture of two Gaussian distributions:

$$p(z) = (1-P) \cdot G(0,\sigma_b^2) + P \cdot G(0,\eta\sigma_b^2) \qquad (4.14)$$

where P is the probability of impulsive noise occurrence, η is the ratio of impulsive noise power to background noise power and $G(0,\sigma_b^2)$ represents the Gaussian distribution of the background noise with zero mean and variance σ_b^2.

As can be seen, the occurrence of the impulsive noise is unpredictable, and therefore it is hard to obtain the round trip propagation time by measuring the received peak locations as we do in path lengths estimation. We propose a time difference of arrival (TDOA) based approach to locate the impulsive noise source. The impulses often occur in bursts, which is difficult to distinguish the echoes of each impulse with other impulses. Therefore, a second measurement node is required, which is the end node with the longest direct path to the current measurement node. We calculate the TDOA of the measured first peaks at the two measurement nodes only. Assume that the initial topology before change is perfectly known via the estimation approach described in previous subsections, the lengths of the direct paths from node n to the two measurement points, $D_{n,1}$ and $D_{n,2}$ can then be obtained. The TDOA of the first peaks of the impulsive noise traveling from node n to the two measurement points, $T_{D,n}$, can be expressed as:

$$T_{D,n} = \frac{D_{n,1} - D_{n,2}}{v}$$

(4.15)

Therefore, a lookup table can be established with $T_{D,n}$ ($n=1,\dots N_{max}$). Appropriate thresholds should be set to detect impulsive noises at both measurement nodes. Whenever the first peaks of an impulsive noise are detected, the corresponding time difference ($t_1 - t_2$) can be calculated. By matching the calculated value of time difference with the values in the lookup table, the impulsive noise source can be located. Since the on/off status of the node before topology change is known, the topology after change can be estimated.

4.3 Complexity Analysis

In this section, we analyze the computational complexity of the proposed TFDR based topology estimation scheme. The reflectometry based approaches (both FDR and TFDR) have the same complexity in path length estimation, as (4.12) is used by both approaches to calculate the path lengths [32]. Hence, the computational complexity of path length estimation is in the order of the number of measured peaks N. Therefore, in the following analysis, we focus on the complexities of topology reconstruction for initial topology estimation and dynamic topology estimation. We first analyze the complexity of topology reconstruction in terms of the number of comparisons required. For dynamic topology estimation, the number of full-topology estimations required is evaluated.

4.3.1 Complexity of Topology Reconstruction

As described in Subsection 4.2.2, to estimate the topology of an N-node network, the proposed algorithm starts with a 2-node topology, where node 1 is the measurement node. Let N_p be the number of measured peaks, there are (N_p–1) possible topologies with one new node connected to node 2. Let M_n denote the number of candidates with one new node connected to node n which generates consistent path lengths with the measurement result. After the first iteration of selection, M_2 candidates are obtained. The number of possible topologies with two new nodes connected to node 2 is $C_{M_2}^2$, where C_n^k represents the k-combination of n elements. If the new topology which is formed by the combination of two candidate topologies has consistent result with the measurement, the two element topologies are removed from the candidate set while the combined one is kept. Therefore, to

obtain all possible connections to node 2, a total of $N_p - 1 + C_{M_2}^2$ comparisons are required. Let $\tilde{M}_n$ represent the number of candidates kept to be processed in next iteration. Since node 1 is the measurement node, there is only one node connected to it, $\tilde{M}_1 = 1$. The total number of comparisons required for the node-by-node greedy algorithm is expressed as:

$$N_{cn} = \tilde{M}_1[(N_p - 1) + C_{M_2}^2] + \tilde{M}_2[(N_p - 2) + C_{M_3}^2] + ... + \tilde{M}_{(N-3)}[N_p - (N-3) + C_{M_{N-2}}^2] + \tilde{M}_{(N-2)}[N_p - (N-2)] \quad (4.16)$$

Since the peak-by-peak searching algorithm in [32] connects a new node to one of the existing nodes in the candidate topology in each iteration, and searches through all peaks, the number of comparisons required is given by:

$$N_{cp} = (N_p - 1)(\tilde{M}_1 + M_2) + (N_p - 2)(M_2 + \tilde{M}_2 + M_3) + (N_p - 3)(\tilde{M}_2 + M_3 + \tilde{M}_3 + M_4) + ...$$
$$+ [N_p - (N-2)](\tilde{M}_{(N-3)} + M_{N-2} + \tilde{M}_{(N-2)} + M_{N-1}) + [N_p - (N-1)](\tilde{M}_{(N-2)} + M_7) \quad (4.17)$$

Subtracting (4.16) from (4.17) yields the difference of the total number of comparisons by the two algorithms:

$$N_{cp} - N_{cn} = [M_2(N_p - 1) - C_{M_2}^2] + \tilde{M}_2(N_p - 3 - C_{M_3}^2) + ... + \tilde{M}_{(N-3)}[N_p - (N-2) - C_{M_{(N-2)}}^2] + (N_p - 2)(M_2 + M_3)$$
$$+ (N_p - 3)(M_3 + M_4) + ... + [N_p - (N-2)](M_{(N-2)} + M_{(N-1)}) \quad (4.18)$$

(4.18) can be rewritten as

$$N_{cp} - N_{cn} = N_A + N_B \quad (4.19)$$

where

$$N_A = [M_2(N_p - 1) - C_{M_2}^2] + \tilde{M}_2(N_p - 3 - C_{M_3}^2) + ... + \tilde{M}_{(N-3)}[N_p - (N-2) - C_{M_{(N-2)}}^2] \quad (4.20)$$

and

$$N_B = (N_p - 2)(M_2 + M_3) + (N_p - 3)(M_3 + M_4) + ... + [N_p - (N-2)](M_{(N-2)} + M_{(N-1)}) \quad (4.21)$$

are defined for the convenience of comparison. As described in Subsection 4.2.2, the candidate toplogogies with one new node connected to node *n* are searched among

$(N_p - n)$ possibilities, and the number of filtered candidates is very small, *i.e.*, $M_n <<$ N_p - n. Since $C_{M_n}^2$ is the combination of the candidate topologies that have consistent path lengths with the measurement selected from $(N_p - n)$ possibilities and the algorithm is applied in a small scale network, it can be derived that $C_{M_n}^2 < N_p$ - n . Thus, $N_A > 0$. It is also obvious that $N_B >> 0$. Thus, it can be shown that $N_{cp} - N_{cn} >> 0$, implying that the proposed node-by-node greedy algorithm greatly reduces the required number of comparisons for topology reconstruction than the peak-by-peak searching algorithm in [32]. For example, during the reconstruction of the topology shown in Fig. 4.4, the number of the filtered candidate topologies for each node is shown in Table 4.1. The nodes *a, b, ..., h* can be numbered as nodes 1, 2, ..., 8, and the number of peaks N_p is obtained to be 52. Using (4.16) and (4.17), the number of comparisons made by the node-by-node greedy algorithm and the peak-by-peak searching algorithm are calculated as 482 and 2516, respectively.
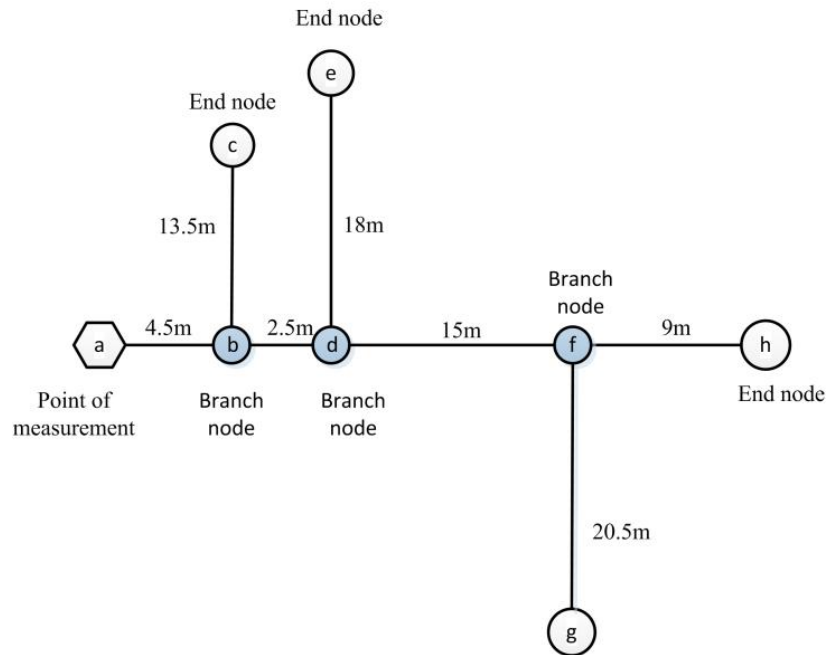
Fig. 4.4 An example 8-node PLC network

Table 4.1. The number of candidate topologies obtained for each node of the topology in Fig. 4.4

Node	a	b	c	d	e	f	g	h
N	1	2	3	4	5	6	7	8
Mn	1	7	1	3	2	7	1	N/A
$\tilde{M}_n$	1	3	1	1	1	3	1	N/A
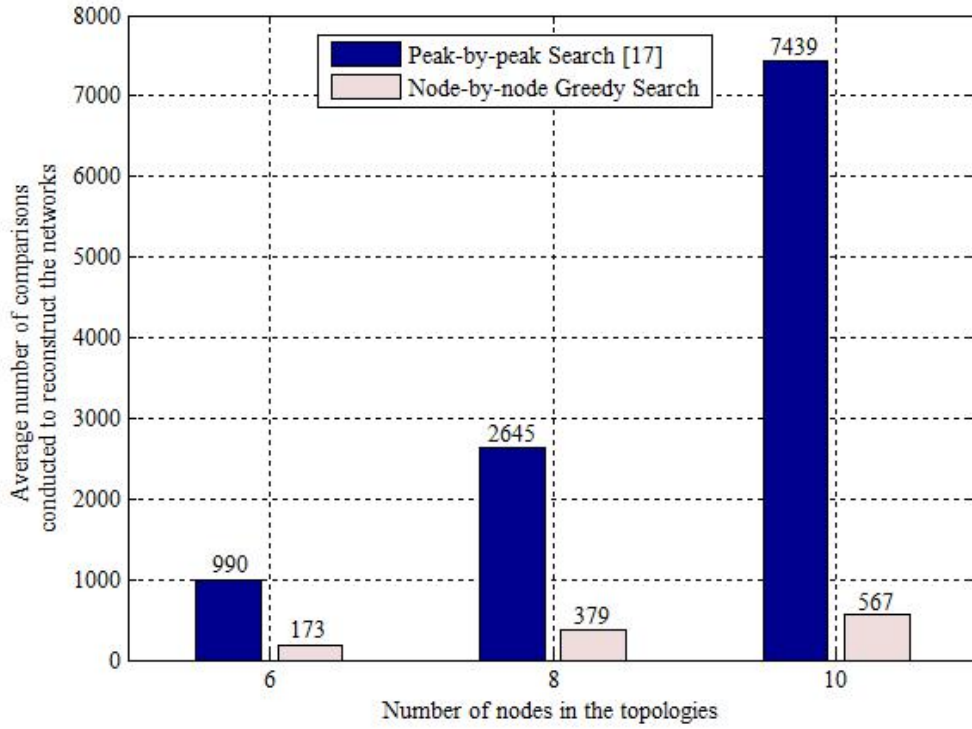
Fig. 4.5. Average number of comparisons conducted to reconstruct the network topology by the node-by-node greedy algorithm and the peak-by-peak algorithm [32]

For a more general comparison, three groups of topologies with 6, 8 and 10 nodes respectively are randomly generated and reconstructed by both searching algorithms. There are 100 topologies generated in each group, and the distances between nodes are randomly generated by uniform distribution over [1, 50] meters. The countable number of echoes per branch is set to be $N_e = 4$. Fig. 4.5 shows the average number of comparisons required by the proposed node-by-node greedy algorithm and the peak-by-peak algorithm [32] to reconstruct the topologies. As can

be seen, the proposed algorithm requires only 17.5%, 14.3% and 7.6% of the complexity of the peak-by-peak algorithm for 6-node, 8-node and 10-node topologies, respectively. With the increase of the number of nodes in the network, the number of measured peaks increases, and therefore more comparisons are required to determine the correct distances between nodes. Moreover, the number of peaks increases much faster than the number of nodes in a network. Therefore, the proposed algorithm is more computationally efficient than the peak-by-peak algorithm, especially in a power line network with more nodes.

4.3.2   Complexity of Dynamic Topology Estimation

In this subsection, we evaluate the complexity of the proposed dynamic topology estimation approach with the assistance of impulsive noise source detection. Assuming perfect detection of the first noise impulse due to topology change, a full-topology re-estimation is conducted only if there is ambiguity about the impulsive noise source detected. Therefore, we use the number of full-topology estimations needed as the complexity metric. Since none of the previous approaches have considered time-varying topology, we assume that a full-topology estimation is conducted periodically with their approaches. Thus, their approaches require a fixed number of full-topology estimations over a certain period of time. We assume that the interval is set to be small enough so that no topology change is missed.

Fig. 4.6 shows the average number of full-topology estimations needed over one hour by the proposed method and the conventional methods. The random topology generator in [19] is used to generate different networks with area 100 m^2. Six groups of networks with 1000 samples each are generated, with the area of clusters ranging from 10 to 35 m^2. The number of outlets per m^2 is set to 0.25 and the probability that an end node is not connected to any loads is 0.3. We consider one household, and set

the impulse rate to 0.0122 impulse/s, which is 1/10 of the mean daytime impulse rate of an apartment building measured in [64]. The BG impulsive noise model [71] is adopted, and the parameters $P = 0.0122$, $\eta = 20$, $\sigma_b^2 = 0.5$ and sampling frequency of 1 Hz are chosen. The simulation results showed that the minimum time interval between the generated noise impulses is about 4.3 s. Thus, to detect all impulses, the minimum frequency of full-topology estimation with fixed interval should be set to no less than $\frac{1}{4.3} \approx 0.23$ Hz. Without losing generality, the frequency used in this experiment is set to be 0.25 Hz to simplify calculations. The average frequency of dynamic topology estimation can be calculated as the number of full estimations divided by time. For example, the average frequency for a 10 m^2 cluster area is calculated as 25.2/ 3600 = 0.07 Hz, which is much lower than a fixed frequency of 0.25 Hz (minimum required) for periodic full-complexity topology estimation. As can be seen from the figure, the average number of full-topology estimations required by the impulsive noise assisted approached is only 2.8~4 % of that required by the methods with fixed full-topology estimation frequency. With the increase of the cluster area, there is a small increase in complexity because the number of outlets connected to the same derivation box increases with the area of cluster [19], causing more ambiguity of the impulsive noise source detection.
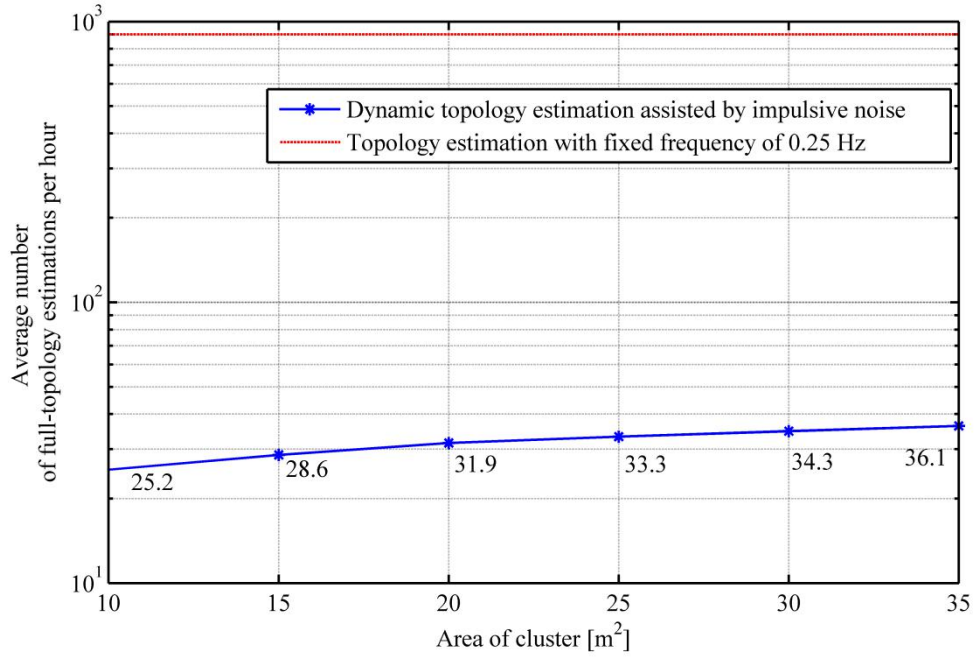
Fig. 4.6 Average number of full-topology estimations required for random topology changes over one hour by the approaches with and without the assistance of impulsive noise source detection

4.4 Simulation Results

We evaluate the performance of the proposed initial topology estimation scheme by comparing it with the FDR based non-parametric method [32] and parametric method [97]. The path lengths of signal traveling in a sample 8-node topology are estimated by both the proposed TFDR based method and the FDR based methods. The results are compared in terms of resolution and accuracy.

4.4.1 Results for a Small-Scale Network

The network topology shown in Fig. 4.4 is estimated by both the TFDR and FDR based approaches. The shortest distance between any two nodes is 2.5 m, which requires high-resolution topology estimation. The load impedance of nodes a, c, e, g, h are chosen to be 1000 Ω, 50 Ω, 150 Ω, 10 Ω, and 150 Ω respectively, which are

typical values of impedance of home appliances. The line parameters of type 0 indoor power line cable [52] are used, and for the parametric FDR method [97], a sampling frequency of $\Delta f = 10$ kHz is chosen to satisfy the maximum detectable distance [97]. We use the same setup of frequency band B_s, central frequency ω_0, and time duration T_s as for Fig. 4.2.

Fig. 4.7 shows the generated cross-correlation of the TFDR based approach. As can be seen, the magnitudes of peaks of the multipath PLC channel do not necessarily decrease with time. The reason is that the reflected signals from different paths may arrive at the measurement point at the same time, so that the magnitudes of the peaks are accumulated.
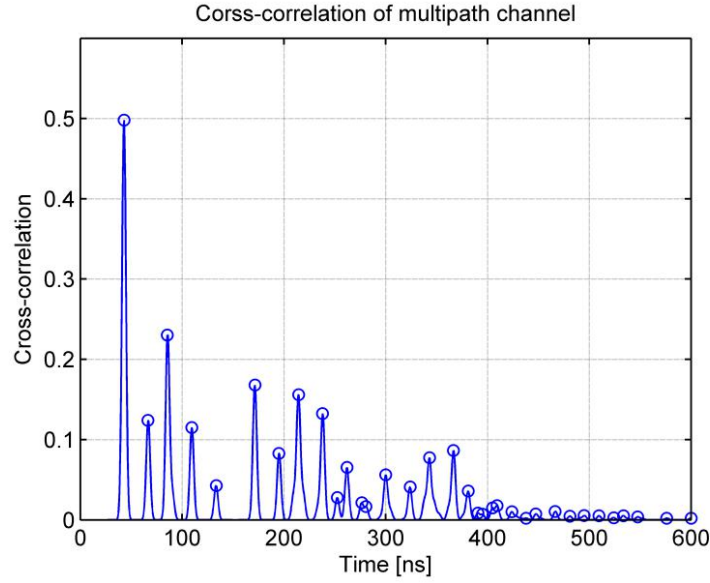
Fig. 4.7 Cross-correlation $C_{sr}(t)$ of the topology shown in Fig. 4.4

The first two columns of Table 4.2 indicate the peak number and the corresponding path lengths of the signal propagation obtained from the measurement point. *e.g.*, peak 1 refers to path a-b-a, peak 2: a-b-d-b-a, peak 3: a-b-a-b-a, peak 4: a-b-d-b-d-b-a, peak 5: a-b-a-b-d-b-a, etc. Due to space limit, we only list the first 10 paths out of a total of 52 in Table 4.2. As can be seen, due to the resolution limitation described in

sub-section 4.1.2, which indicates that the minimum interval of two detectable path of FDR is large, the FDR approaches can only detect a few paths while the TFDR method successfully detects all paths. In terms of accuracy, the average estimation error of all the 52 paths are calculated as: 90.28% for the non-parametric FDR method [32], 61.65% for parametric FDR method [97] (a missed path denoted by ' × ' is counted as 100% error), and only 0.79% for the proposed TFDR method.

According to the path lengths obtained by TFDR based estimation, we use the proposed node-by-node greedy algorithm to reconstruct the network shown in Fig. 4.4, and the topology is estimated with low errors, as shown in Table 4.3.

Table 4.2 Path length estimation of the topology in Fig.4.4 (the missed paths are denoted by ' × ')

Path No.	Actual Path Length (m)	TFDR (m)	Non-parametric FDR [32] (m)	Parametric FDR [97] (m)
1	9	9.03	8.28	8.76
2	14	13.87	×	14.89
3	18	18.07	×	×
4	19	19.26	×	17.98
5	23	22.93	×	×
6	28	27.78	×	×
7	36	36.22	×	34.16
8	41	40.85	41.81	×
9	44	43.57	×	×
10	45	45.25	×	×
...	...	...	...	...
52	126	125.03	×	127.38

Table 4.3 Estimated distances between nodes by the proposed TFDR based topology estimation scheme

Edge	a-b	b-c	b-d	d-e	d-f	f-g	f-h
Distance (m)	4.5	13.5	2.5	18	15	20.5	9
Estimated Dist. (m)	4.52	13.60	2.42	17.76	14.89	20.38	9.17
Error (%)	0.44	0.74	3.20	1.33	0.73	0.59	1.89

4.4.2. Results for a Larger-Scale Network

We also consider a larger-scale network and repeat the simulation above. The topology is the same as that shown in Fig. 4.4, except that the distances between nodes are set to be longer, as shown in Table 4.4. The experimental results are demonstrated in Table 4.5. As can be seen, the TFDR based method still detects all signal propagation paths. Due to the spectral leakage problem [32], which refers to the new spectrum produced by Fourier transform that changes the magnitude and angle of the original frequency domain signal, the FDR based methods miss some of the paths. TFDR yields smaller errors than FDR methods over all paths. The errors by TFDR range from 0.04% to 0.35%, while they are from 0.61% to 3.53% and 0.26% to 1.43% by non-parametric and parametric FDR based methods. The average errors of all path lengths are calculated as 0.17% for the TFDR and 11.28% and 17.34% for the FDR based methods respectively.

Table 4.4 Distances between nodes in a larger-scale network

Edge	a-b	b-c	b-d	d-e	d-f	f-g	f-h
Distance (m)	50	90	40	130	70	120	80

Table 4.5 Path length estimation of a larger-scale network

Path No.	Actual Path Length (m)	TFDR (m)	Non-parametric FDR [32] (m)	Parametric FDR [97] (m)
1	100	99.75	99.39	99.69
2	180	179.55	186.35	177.42
3	200	199.35	197.08	×
4	260	259.10	256.78	257.33
5	280	279.03	273.32	×
6	320	319.20	323.01	316.68
7	360	359.10	361.29	360.94
8	440	438.95	434.83	437.83
9	480	479.15	×	482.66
10	500	499.80	496.95	497.34
...	...	...	...	...
52	880	878.26	875.39	885.91

To evaluate the scalability of the proposed TFDR based method, 5 groups of topologies with the number of nodes ranging from 10 to 50 are randomly generated, and different values of the longest distances between nodes are assigned to each topology. The TFDR based path lengths estimation is conducted for each topology. Table 4.6 shows the occurrence rate of ambiguity in detecting the peaks of each group of topologies, averaged over 100 samples per group. As can be seen, the proposed algorithm works perfectly when the number of nodes is small. As the distances between nodes and the number of nodes increase, the occurrence rate of ambiguity increases gradually, as discussed in Subsection 4.2.1. However, even in the worst case, *i.e.*, a 50-node topology with 300 m maximum distance between nodes, the average occurrence rate of ambiguity is only 5.9%. Since the number of detected peaks is typically above 200 for a 50-node topology, the 5.9% ambiguity

will cause no more than 3% increase in the topology estimation error. Therefore, the proposed TFDR based algorithm can be applied to typical indoor PLC networks.

Table 4.6 Average occurrence rate of ambiguity of each topology group by the TFDR based path lengths estimation

Number of Nodes The Longest distance between nodes	10	20	30	40	50
50 m	0	0	0	2.1%	2.9%
100 m	0	0	0	2.8%	3.6%
150 m	0	0	1.9%	3.1%	4.1%
200 m	0	0	2.2%	3.7%	4.9%
250 m	0	1.1%	2.8%	4.1%	5.3%
300 m	0	1.3%	3.3%	5.2%	5.9%

4.5   Summary

In this chapter, a low-complexity and high-resolution dynamic topology estimation scheme has been proposed for indoor PLC networks, which consists of a TFDR based method for path length estimation, a node-by-node greedy algorithm for topology reconstruction, and an impulsive noise assisted dynamic topology re-estimation method. Simulation results show that the proposed TFDR method significantly outperforms the FDR based methods [32] [97] in terms of both resolution and accuracy for path length estimation, with a resolution of 1 m and an average estimation error of below 1% achieved. Additionally, the proposed node-by-node greedy algorithm can reduce the complexity of the topology reconstruction by as much as 92.4% over the peak-by-peak searching algorithm [32]. The impulsive noise source detection assisted method also effectively reduces the

number of re-estimations by about 97.2% over a topology re-estimation scheme with fixed interval for estimating time-varying topologies. Therefore, the proposed scheme is particularly suitable for in-home power line networks with time-varying topologies, thanks to its low complexity and high resolution and accuracy.

Chapter 5

Cross-Layer Routing and Resource Allocation assisted by Dynamic Topology Estimation

In Chapter 4, an accurate dynamic topology estimation scheme has been proposed, and by utilizing this approach, schemes for improving communication performance of PLC systems can be further developed.

As introduced in Chapter 1, PLC systems for Smart Grid are expected to provide data transmission for multiple users with heterogeneous delay requirements. Adaptive resource allocation algorithm plays a crucial role in achieving a good channel capacity for multiuser multi-tasking services over PLC. Due to the multi-level characteristic and the abruptly varying topology, an appropriate routing scheme is highly demanded to provide reliable and efficient delivery of data packets through the grid.

The previous work has focused on applying the geographic routing algorithms in the wireless communications literature to PLC networks, such as Beacon Less

Routing (BLR) [106], Implicit Geographic Forwarding (IGF) [107], Beacon Based Routing (BBR) [108], flooding [109], etc. However, most of these algorithms based on the concept of 'neighborhood', which determines the 'next hop' distributively at each node. Among these distributed solutions, the BBR, which voids packet duplication and RTS/CTS overhead suffered by the BLR and IGF, is considered as a reliable algorithm for PLC [30]. Flooding [109] refers to the system that every node overhears a message and also retransmits it. By this way, signaling overhead can be greatly reduced [110]. A Shortest Path Routing (SPR) approach was proposed in [29], which provides an energy-efficient solution for packet routing with the knowledge of instantaneous connectivity of devices. However, in [29], resource management was not discussed and the AWGN noise model considered was not suitable for PLC. A routing algorithm based on transporting matrix for PLC was proposed in [111] which is simple to implement. However, this algorithm has limited ability in adapting to dynamic changing toplogies. Paper [112] presented a like-Ant Colony algorithm which has advantage in efficiency of searching, but it costs too much resources at the same time [113]. In [114], a time usage minimization based routing scheme was introduced without consideration of topology change, which is more suitable in a large network with a relatively stable topology. On the other hand, resource management has also been investigated for different optimization objectives in PLC systems [115-118]. In [27], a round robin allocation based algorithm was proposed to maximize the total network rate. In [28], sub-channel ordering was utilized to obtain optimal throughput with the consideration of more practical noise model instead of

AWGN. In [115], a bit-loading lookup table resource allocation algorithm was proposed to solve multiuser and multi-objective problems. The algorithm includes PHY layer constraints, but the different delay requirements of users was not discussed. A cross-layer resource management and scheduling scheme based on utility theory was proposed in [118]. However, the authors only considered subcarrier allocation at the PHY layer, but not power allocation.

In this chapter, a cross-layer routing and resource allocation scheme assisted by dynamic topology estimation is proposed for indoor PLC networks. The scheme is aimed to maximize system throughput subject to transmission power constraint and delay requirements of heterogeneous multi-user indoor PLC networks. This work is different in following aspects. First, to the best of our knowledge, this is the first work solving the multi-user network layer routing problem based on the result of PHY layer resource allocation for indoor PLC network. As a result, the system throughput and packet loss rate (PLR) are greatly improved compared to the approaches without resource allocation. Second, a cross-layer joint power and subcarrier allocation algorithm for indoor PLC communication has been proposed and it obtains the maximal PHY layer throughput satisfying heterogeneous delay requirements with the minimum required power. In this chapter, the "delay" refers to packect queuing delay which is the time a packet waits in the queue before being processed, and the power allocation refers to the process of assigning different amount of power to different subcarriers to optimize the performance of an OFDM system. Finally, with the assistant of dynamic topology estimation, the routing can be

solved with a centralized solution. Simulation results show that the proposed scheme has a much lower packet loss rate than the distributed solutions in a network with time-varying topology.

The rest of this chapter is organized as follows. The system model and problem formulation are presented in Section 5.1. Section 5.2 describes the proposed cross-layer routing and resource allocation scheme assisted by dynamic topology estimation. The simulation results and analysis is provided in Section 5.3. A concluding discussion is given in Section 5.4.

5.1   System Model and Problem Formulation

5.1.1   Network Topology

In this chapter, a two-level cluster based topology structure [19] is considered, as depicted in Fig. 5.1. The first connection level is between the outlets (appliances) and the associated derivation box. The second level refers to the connections between derivation boxes. In a typical indoor network, PLC modems are installed only at derivation boxes which coordinate the communication within the cluster and perform data exchange with derivation boxes in other clusters. Therefore, this work focuses on the communication among the derivation boxes only, and all other nodes are carried back to the corresponding derivation boxes as described in [19].
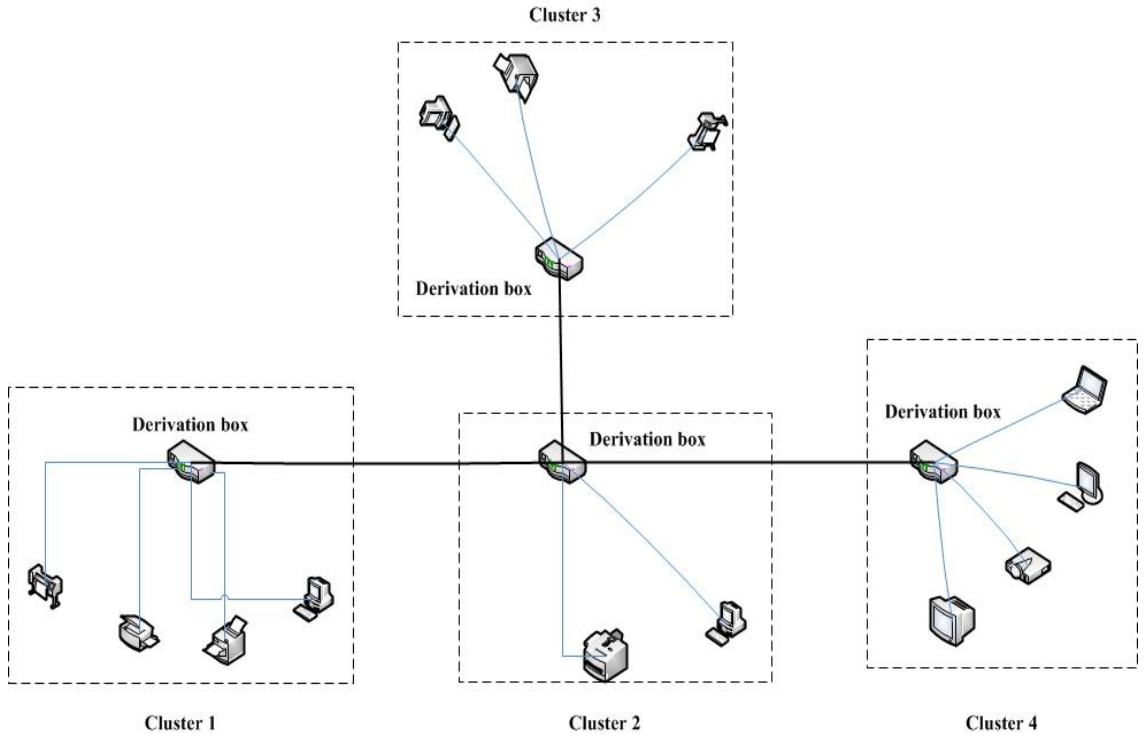
Fig. 5.1 Example cluster based PLC network structure

The topology is represented by a graph $G = (V, E)$, in which each vertex $v \in V$ denotes a node in the network. If two nodes v_i and v_j are connected in the PLC network, there exists an edge $e = (v_i, v_j)$ between them. The locations of the derivation boxes and the power line connecting them are static, however, the connectivity between each pair of nodes is considered to be dynamic. An integer parameter $X_e \in \{0,1\}$ is used to indicate the connectivity of link e, where $X_e = 1$ means e is connected, otherwise it is disconnected. To obtain the instantaneous channel status and connectivity, the dynamic topology estimation scheme proposed in Chapter 4 is utilized. Fig. 5.2 shows a network which represents a typical European low-voltage power distributed network in residential areas [3]. Circles represent derivation boxes (network nodes) of clusters, and the edges are the power line cables connecting them.

As can be seen from the figure, there are some "rings" included in the topology, for example, 5-9-10-6. However, each node in this figure does not represent a single outlet/appliance in a circuit, but refers to a derivation box in a cluster which connects a number of outlets/appliances [19]. Therefore, the "rings" do not represent physical loops in an electrical circuit. Moreover, there are actually ring topologies used for PLC in some countries [50]. Even if in a topology without any "rings", the results of routing schemes in this chapter will not be affected at all, since they search routes according to the knowledge of instantaneous topology as described in section 5.2.1.
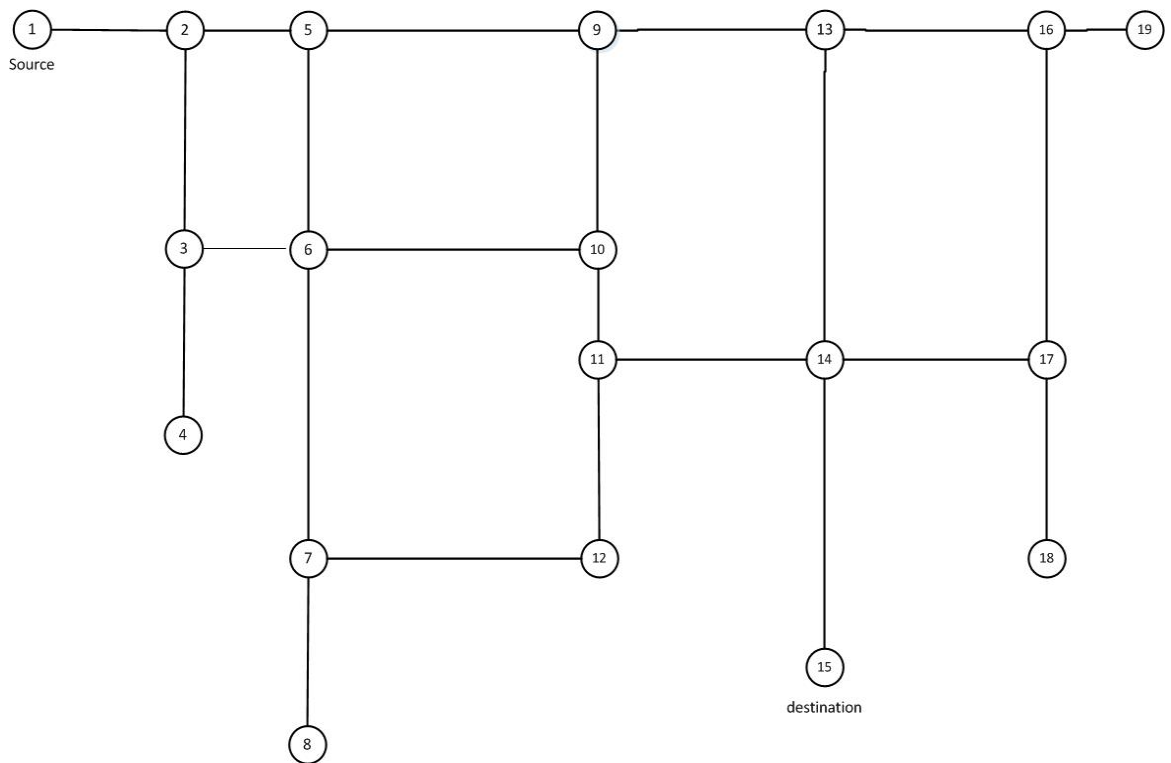

Fig. 5.2 A typical topology of derivation boxes of an indoor PLC network

5.1.2 Channel and Noise Models

As described in Chapter 4, the channel of each link e of the power line network can be represented by a multi-path frequency-selective fading model. The signal traveling along path i is characterized by the weighting factor $g_{e,i}$, the attenuation factor $A_{e,i}(f)$, and the distance of path $d_{e,i}$. The attenuation factor can be represented by [59]:

$$A_e(f) = \sum_{i=1}^{I} e^{-(a_0 + a_1 f^x) d_{e,i}}$$

(5.1)

where a_0, a_1, and x are the attenuation parameters of the power line network. Thus, the frequency response of the top-down PLC channel model is formulated as [59]:

$$H_e(f) = \sum_{i=1}^{I} g_{e,i} \cdot e^{-(a_0 + a_1 f^x) d_{e,i}} e^{-j2\pi f d_{e,i}/v_p}$$

(5.2)

where v_p is the propagation speed of signal on power line. Different from wireless channel which has AWGN background noise, PLC channel is shared by a number of appliances and suffers random load impedance changes. Therefore, the background noise of PLC is considered to be colored which is a superposition of numerous low intensity noise sources whose PSD decrease with the increase of frequency [119]. In this chapter, the colored background noise model in [119] is employed, whose PSD is approximated as [119]:

$$B(f) = B_\infty + B_0 \cdot e^{-f/f_0}$$

(5.3)

where B_∞ is the PSD when $f \to \infty$, B_0 is the difference between the maximum PSD and B_∞, and f_0 refers to the decaying exponential rate.

The occurance of impulsive noise is considered as another factor that has impact on data transmission due to its high amplitudes and strong time variance. The BG model as introduced in Chapter 4 is cosidered as a suitable stastical model to represent the impulsive noise in PLC channels [71]. The frequency domain noise can be generated according to the probability density function which is:

$$p = (1-P) \cdot G(0, \sigma_b^2) + P \cdot G(0, \eta \sigma_b^2) \tag{5.4}$$

where P is the probability of impulsive noise occurrence, η is the ratio of impulsive noise power to background noise power and $G(0, \sigma_b^2)$ represents the Gaussian distribution of the background noise with zero mean and variance σ_b^2.

An OFDM system is considered in this work. Assume there are K users in total at a source node to transmit packets to a destination node. For each link of the transmission route, it is assumed that a total bandwidth of W is divided into N independent subcarriers and shared by the K users. The OFDM signaling is time-slotted and each time slot is of length t_s. Assuming perfect CSI of the network is available, the achievable data rate of user k on subcarrier n of link e can be calculated as:

$$R_{e,k,n} = \frac{W}{N} \log_2 (1 + p_{e,k,n} \cdot \eta_{e,k,n}) \tag{5.4}$$

where $\eta_{e,k,n}$ is the CNR for user k on subcarrier n. Thus, the total achievable data rate of link e can be expressed as:

$$R_e = \sum_{n=1}^{N} \sum_{k=1}^{K} S_{e,k,n} R_{e,k,n} \tag{5.5}$$

where $S_{e,k,n} \in \{0,1\}$ denotes subcarrier allocation for subcarrier n in link e. If subcarrier n is allocated to user k, $S_{e,k,n} = 1$, otherwise $S_{e,k,n} = 0$.

5.1.3 Problem Formulation

In this subsection, a cross-layer routing and resource allocation problem of the investigated system is formulated. The queuing information is used for the PHY layer resource allocation, while the result of resource allocation determines the network layer routing strategy. Define node s and d as the source and destination node respectively. Since the instantaneous topology is obtained by the proposed dynamic topology estimation scheme, $Z_{(s,d)}$, the set of all possible routes from s to d can be obtained. Let P_T denote the maximum total transmit power and P_v denote the maximum transmit power of node v. Without loss of generality, it is assumed that all nodes in the network have the same maximum transmission power constraint and do not employ power adaptation, i.e. each node has a fixed power constraint, and if the power is not used up at one node, the remaining power won't be used by other nodes, which can be easily extended to the case with different node power constraints. It is also assumed that for user k there is a maximum delay tolerance $T_{v,k}$ at node v, and $T_{v,k} = T_k$ is constant across all nodes. The objective of the scheme is to find the route with maximal optimized throughput from the source to the destination in a PLC network, which can be formulated as:

$$\arg \max_{z \in Z_{(s,d)}} R_z \tag{5.6}$$

$$\text{S.t.} \qquad \sum_{k=1}^{K} P_{v,k} \le P_v \qquad \forall v, v \in z \tag{5.7}$$

$$\sum_{v \in z} P_v < P_T \quad P_v \ge 0 \tag{5.8}$$

$$d_{v,k} \le T_k \qquad \forall v, k , \quad v \in z \tag{5.9}$$

5.2 Cross-Layer Routing and Resource Allocation assisted by Dynamic Topology Estimation

5.2.1 Dynamic Topology Estimation assisted Centralized Routing

The initial design objective was single path routing based on deterministic resource allocation along different paths. However, as introduced in the previous chapters, the topology of a PLC network is time varying and the changes of connectivity are random. Different from the previous work which deals with the topology changes by either updating the connection information periodically [28] or attempting repeatedly when transmission fails [27], the stochastic problem is transformed into a deterministic one by utilizing the dynamic topology estimation algorithm. The initial topology before changes is only required to be estimated once with the TFDR based algorithm, and the connectivity of nodes can be instantly updated whenever a topology change is detected. With the estimated topology and the instantaneous connectivity information, all the routes for transmitting signal form the source to the destination $Z_{(s,d)}$ can then be found. For each route $z \in Z_{(s,d)}$, the power and subcarrier are allocated to the users jointly at each node to obtain the maximum throughput of the route. Finally, the route with maximum throughput while satisfying heterogeneous delay requirements can be found. Fig. 5.3 shows the flowchart of the scheme.
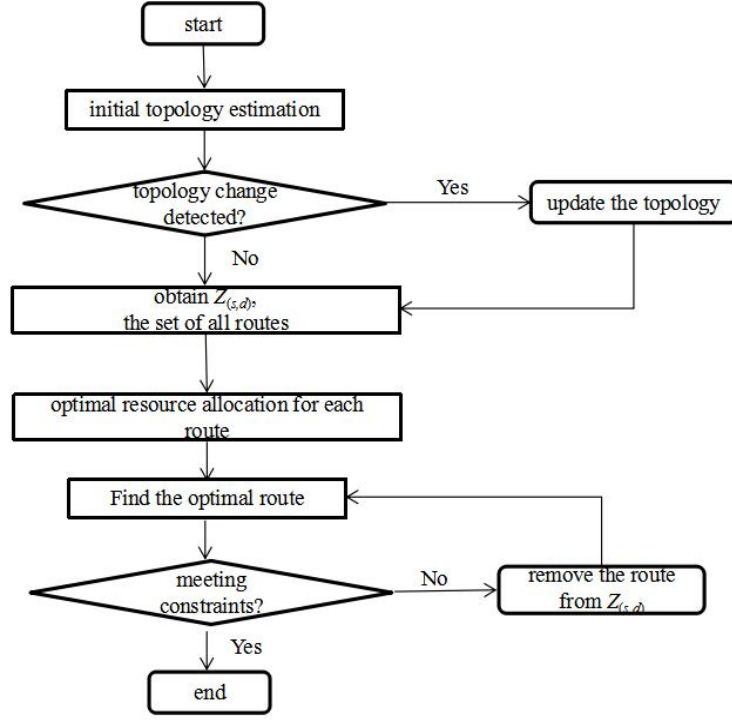
Fig. 5.3 The flowchart of the topology estimation assisted dynamic routing and resource allocation scheme

5.2.2   Optimal Resource Allocation

Since the throughput of a route is determined by the link with the minimal throughput [120], the capacity of route R_z, $z \in Z_{(s,d)}$ is expressed as:

$$R_z = \min_{v(l) \in z} \{R_{v(1)}, R_{v(2),...,} R_{v(L-1)}\}$$

(5.10)

Where L is the number of nodes in route z. For simplicity, we use $R_{v(l)}$ to express the capacity of the link connecting the l-th and $(l+1)$-th node on route z in the rest of the chapter. The optimization problem can be rewritten as:

$$\max \min_{l=1,...L-1} \{\sum_{n=1}^{N} \sum_{k=1}^{K} S_{v(l),k,n} R_{v(l),n,k}\}$$

(5.11)

Subject to:

$$S_{v(l),k,n} \in \{0,1\} \tag{5.12}$$

$$\sum_{i=1}^{K} S_{v(l),k,n} = 1 \tag{5.13}$$

$$\sum_{n=1}^{N}\sum_{k=1}^{K} S_{v(l),k,n} P_{v(l),k,n} \le P_v \tag{5.14}$$

$$P_{v(l),k,n} \ge 0 \tag{5.15}$$

$$d_{v(l),k} \le T_k \quad \forall v(l),k, \quad v(l) \in z \tag{5.16}$$

It can be deduced that (5.11) is maximized only if

$$\sum_{n=1}^{N}\sum_{k=1}^{K} S_{1,k,n} R_{1,k,n} = \sum_{n=1}^{N}\sum_{k=1}^{K} S_{2,k,n} R_{2,k,n} = ... = \sum_{n=1}^{N}\sum_{k=1}^{K} S_{L-1,k,n} R_{L-1,k,n}$$ [120]. Hence, (5.11) can be

rewritten as:

$$\max_{S_{v(l),k,n}, P_{v(l),k,n}, d_{v,k}} \left(\sum_{l=1}^{L-1}\sum_{n=1}^{N}\sum_{k=1}^{K} S_{v(l),k,n} R_{v(l),k,n} \right) \tag{5.17}$$

To solve the optimization problem (5.17), the heterogeneous delay constraint (5.16) needs to be expressed in terms of PHY layer parameters. An M/M/1 queuing model [121] is considered. At node v, packets of heterogeneous users come into buffer according to a Poisson process with rate $\lambda_{v,k}$, which is the average packet arrival rate of user k at node v. Let $\mu_{v,k}$ denote the average service rate of user k at node v, then the average waiting time of packets of user k can be expressed as [121]:

$$d_{v(l),k} = \frac{1}{\mu_{v(l),k} - \lambda_{v(l),k}} - \frac{1}{\mu_{v(l),k}} \tag{5.18}$$

Since the service rate is the reciprocal of the time a packet at the server before departing, $\mu_{v(l),k}$ can be calculated as $F/R_{v(l),k}$. Where F is the fixed packet size in bits,

and $R_{v(l),k}$ is the data rate of queue k at node $v(l)$. The service time can be expressed as

$$\frac{1}{\mu_{v(l),k}} = \frac{F}{R_{v(l),k}} \; .$$

Then (5.18) can be expressed as:

$$d_{v(l),k} = \frac{\dfrac{\lambda_{v(l),k}F}{R_{v(l),k}}}{\dfrac{R_{v(l),k}}{F} - \lambda_{v(l),k}} \tag{5.19}$$

Therefore, an equivalent rate constraint of (5.16) is:

$$R_{v(l),k} \geq \frac{\lambda_{v(l),k}T_k + \sqrt{(\lambda_{v(l),k}T_k)^2 + 4\lambda_{v(l),k}T_k}}{2T_k} F \tag{5.20}$$

which can be rewritten as $R_{v(l),k} \geq G_{v(l),k}$, where

$$G_{v(l),k} = \frac{\lambda_{v(l),k}T_k + \sqrt{(\lambda_{v(l),k}T_k)^2 + 4\lambda_{v(l),k}T_k}}{2T_k} F \; .$$

The Lagrangian of the modified objective function is:

$$L = \sum_{l=1}^{L_z}\sum_{n=1}^{N}\sum_{k=1}^{K} S_{v(l),n,k} R_{v(l),n,k} - \sum_{l=1}^{L_z}\sum_{n=1}^{N}\gamma_{v(l),n}(\sum_{k=1}^{K}S_{v(l),n,k}-1) - \sum_{l=1}^{L_z}\phi_{v(l)}(\sum_{n=1}^{N}\sum_{k=1}^{K}P_{v(l),n,k}-P_v) - \sum_{l=1}^{L_z}\sum_{k=1}^{K}\varepsilon_{v(l),k}(G_{v(l),k}-S_{v(l),k}R_{v(l),k})$$

$$= \sum_{l=1}^{L_z}\sum_{k=1}^{K}(1+\varepsilon_{v(l),k})\sum_{n=1}^{N}S_{v(l),n,k}\log(1+\frac{P_{v(l),n,k}\cdot\eta_{v(l),n,k}}{S_{v(l),n,k}}) - \sum_{l=1}^{L_z}\sum_{n=1}^{N}\gamma_{v(l),n}(\sum_{k=1}^{K}S_{v(l),n,k}-1) - \sum_{l=1}^{L_z}\phi_{v(l)}(\sum_{n=1}^{N}\sum_{k=1}^{K}P_{v(l),n,k}-P_v) - \sum_{l=1}^{L_z}\sum_{k=1}^{K}\varepsilon_{v(l),k}G_{v(l),k} \tag{5.21}$$

where $\gamma_{v(l),n}$, $\varepsilon_{v(l)}$ and $\phi_{v(l)}$ are the Lagrange multipliers. It can be derived that:

$$\frac{\partial L}{\partial S_{v(l),n,k}} = (1+\varepsilon_{v(l),k})\left[\log_2(1+\frac{P_{v(l),n,k}\cdot\eta_{v(l),n,k}}{S_{v(l),n,k}}) - \frac{P_{v(l),n,k}\cdot\eta_{v(l),n,k}}{S_{v(l),n,k}+P\cdot\eta_{v(l),n,k}}\right] \tag{5.22}$$

$$\frac{\partial L}{\partial \widetilde{P}_{v(l),n,k}} = \frac{(1+\varepsilon_{v(l),k})S_{v(l),n,k}\cdot\eta_{v(l),n,k}}{S_{v(l),n,k}+P_{v(l),n,k}\cdot\eta_{v(l),n,k}} - \phi_{v(l)} \tag{5.23}$$

By setting $\dfrac{\partial L}{\partial \widetilde{P}_{v(l),n,k}} = 0$, $\dfrac{\partial L}{\partial S_{v(l),n,k}} = 0$ and relaxing $S_{v(l),n,k}$ as [120] did, subcarrier n is

allocated to user k^* at node $v(l)$ which satisfies:

$$k^* = \arg\max_k (1+\varepsilon_{v(l),k})([\log_2(\frac{(1+\varepsilon_{v(l),k})\cdot\eta_{v(l),n,k}}{\phi_{v(l)}})]^+ - [\frac{(1+\varepsilon_{v(l),k})\cdot\eta_{v(l),n,k}-\phi_{v(l)}}{(1+\varepsilon_{v(l),k})\cdot\eta_{v(l),n,k}}]^+)$$

(5.24)

which indicates that the user with higher urgency factor $\varepsilon_{v(l),k}$ has a higher chance to be allocated with subcarriers.

The corresponding optimal power allocated to subcarrier n of user k on link $e(v(l),$ $v(l+1))$ is:

$$\begin{cases} P_{v(l),n,k^*} = \left[\dfrac{(1+\varepsilon_{v(l),k^*})}{\phi_{v(l)}} - \dfrac{1}{\eta_{v(l),n,k^*}}\right]^+ & \forall s_{v(l),k}=1 \\ \qquad\qquad 0 & \text{otherwise} \end{cases}$$

(5.25)

which can be interpreted as a multi-level water filling strategy. The users with stringent delay requirements are transmitted at a higher power water-level $(1+\varepsilon_{v(l),k})/\phi_{v(l)}$, while the delay-insensitive users ($\varepsilon_{v(l),k}$ is very small) are allocated at the water level $1/\phi_{v(l)}$. Since the frequencies of the subcarriers are close to each other, it would be difficult for the hardware to allocate power to each subcarrier after modulation. One way to realised the power allocation is by assigning different weights to subcarriers according to (5,25) before modulation. The modulation can then be conducated with the weights of subcarriers, and the power amplifer can allocate the subcarriers with desired values.

The Lagrange multiplier can be obtained by solving the system of equations:

$$f_{v(l)}(\varepsilon,\phi) = P_v - \sum_{n=1}^{N}\sum_{k=1}^{K} S_{v(l),n,k^*}[\frac{(1+\varepsilon_{v(l),k^*})}{\phi_{v(l)}} - \frac{1}{\eta_{v(l),n,k^*}}]^+ = 0$$

,

$$g_{v(l),k}(\varepsilon,\phi) = \varepsilon_{v(l),k}(\sum_{n=1}^{N} S_{v(l),n,k}[\log_2(\frac{(1+\varepsilon_{v(l)})\cdot\eta_{v(l),n,k}}{\phi_{v(l)}})]^+ - G_{v(l),k}) = 0$$

(5.26)

To search for the roots of (5.26), the bisection method [122] is used. First of all, the single-variable functions $f_{v(l)}(\phi)$ and $g_{v(l)}(\varepsilon)$ are mono-increasing. The lower bound and upper bound of the feasible search range of ε_k and ϕ can then be derived and expressed as: ε_k^L, ε_k^U and ϕ^L, ϕ^U respectively. The search algorithm for the Lagrange multipliers can be described as:

1. Initialize ϕ and ε_k.

2. While $g_{v(l)}(\varepsilon_k) \neq 0$,

update $\varepsilon_k^L \begin{cases} \varepsilon_k & g_{v(l)}(\varepsilon_k) < 0 \\ \varepsilon_k^L & g_{v(l)}(\varepsilon_k) > 0 \end{cases}$, $\varepsilon_k^U \begin{cases} \varepsilon_k & g_{v(l)}(\varepsilon_k) > 0 \\ \varepsilon_k^U & g_{v(l)}(\varepsilon_k) < 0 \end{cases}$, and $\varepsilon_k = \dfrac{\varepsilon_k^L + \varepsilon_k^U}{2}$.

3. If $f_{v(l)}(\phi) \neq 0$, update $\phi^L \begin{cases} \phi & f_{v(l)}(\phi) < 0 \\ \phi^L & f_{v(l)}(\phi) > 0 \end{cases}$, $\phi^U \begin{cases} \phi & f_{v(l)}(\phi) > 0 \\ \phi^U & f_{v(l)}(\phi) < 0 \end{cases}$, and $\phi = \dfrac{\phi^L + \phi^U}{2}$.

4. Substitute ϕ obtained in step 3 into step 2 and update ε_k.

5. Repeat steps 3 and 4 until $\begin{cases} f_{v(l)}(\phi) = 0 \\ g_{v(l)}(\varepsilon_k) = 0 \end{cases}$, the $\varepsilon_k{}^*$ and ϕ^* is then obtained.

5.3   Simulation Results

This section presents numerical results to demonstrate the performance of the proposed cross-layer routing and resource allocation assisted by dynamic topology estimation (RRA-DTE) for the power line network. Comparisons with other centralized and distributed routing schemes are also provided.

5.3.1   Simulation Setup

For the simulation experiments, an OFDM system with total bandwidth of 20 MHz consisting N=128 subcarriers is considered. The duration of a scheduling slot t_s is assumed to be 2 ms. Three different classes of users with the arrival rates and delay tolerance as $(\lambda, T) = \{(0.3,2),(0.4,4),(0.6,1000)\}$ (packet per time slots, time slots) are considered. Class 1 and Class 2 represent delay-sensitive users, and Class 3 represents delay-insensitive users. In this Chapter, each user refers to one smart appliance connected to the corresponding derivation box, and different users have different impedance and paths to the derivation box [19]. Therefore, the attenuation of transmission of each user is different, but since they are coordinated by the same derivation box, their transmission channels to other nodes are correlated. We assume that each packet contains 64 bits. The topology shown in Fig. 5.2 is used as the initial network, node 1 and node 15 are set to be the source and destination respectively. The power line channel parameters of network are assumed the same as considered in [117]: a_0=0, a_1=7.8×10^{-10}, x=1, v_p=2×10^8 m/s. The number of dominating paths of

the multi-path reflection is set to $I= 5$ and the path factor $g_{e,i}$ is randomly generated over [0.1, 0.4] for each user. The path distance $d_{e,i}$ is also randomly generated by uniform distribution over [60 180]. The PSD of the colored background noise of each link is randomly generated by uniform distribution over [-75+46.7$e^{-1.6f}$, -85+46.7$e^{-1.6f}$] (dBm/Hz), where the unit for f is MHz. In this work we also examed the influence of occurance of impulisive noise to system throughput in Fig. 5.8 and Fig. 5.9. Since similar indoor enviroment is considered, the same set up of parameters of the impulsive noise in chapter 4 are used in this chapter. Fig. 5.4 depicts typical unit power CNR curves of three arbitrary users on one link of the power-line channels, which also demonstrated the multiuser diversity of the system. All the results shown in this section are obtained by averaging the results of 1000 independent trials.
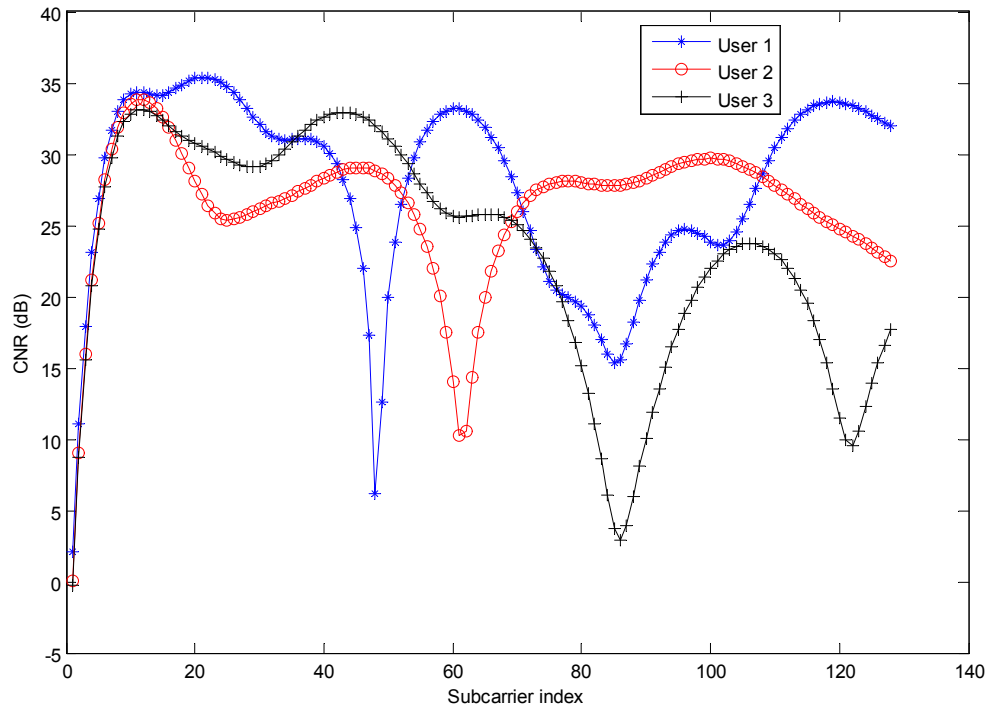

Fig. 5.4 Multiuser diversity of the system demonstrated by CNR curves of three arbitrary users

5.3.2   Numerical Results

Fig. 5.5 illustrates the total system throughput obtained by the proposed RRA-DTE versus the number of users K when the power constraint of node $P_v = 40$ dBm. Three experiments are conducted to show the impact the number of users of different classes. In each experiment, the number one class of user increases while the other two classes has one user each. As can be seen, the throughput increases with the number of users due to multiuser diversity gain. Since Class 1 and Class 2 users require more power to support the stringent delay requirements, the throughput increases the most when the number of the delay insensitive Class 3 users increases.
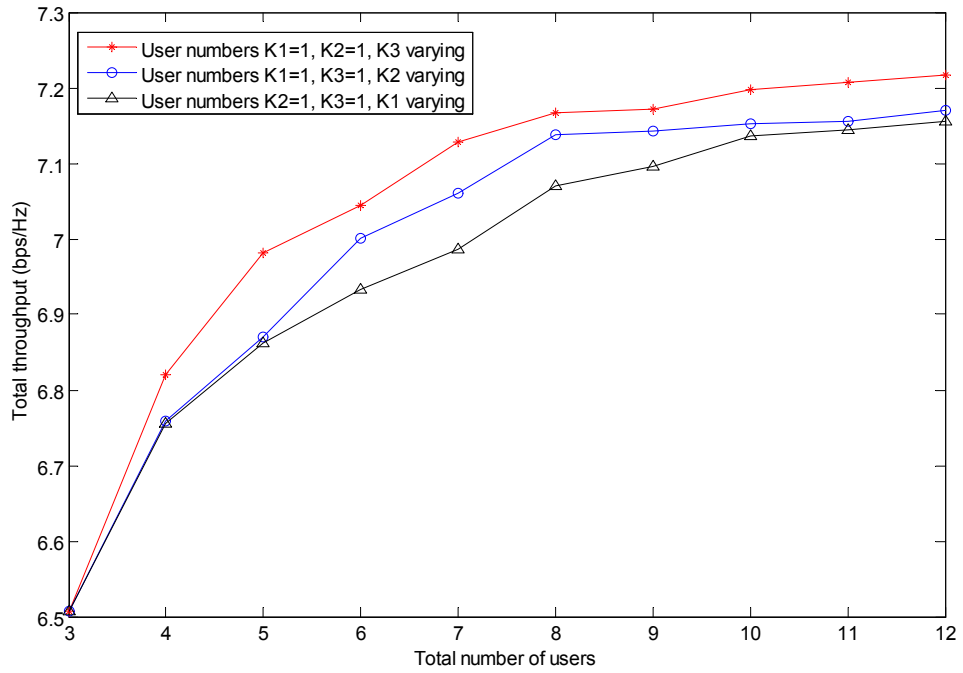

Fig. 5.5 Average total system throughput vs different number of each class of users

In Figs. 5.6 and 5.7, the average system throughput versus node power constraint of different schemes are depicted by considering a system with the number of each class of users: $(K_1, K_2, K_3)= (1, 1, 1)$. Fig. 5.6 shows the comparison between the proposed RRA-DTE scheme and the SPR [29]. Both methods are centralized routing methods, but the SPR does not consider resource allocation. In the following figures, 'SA only' denotes that only the subcarrier allocation is applied and the power allocated to each subcarrier is uniform and equals to P_v/N. On the contrary, 'PA only' indicates that only power allocation is applied and subcarriers in two consecutive slots are simply paired by their corresponding subcarrier indices. As shown in Fig. 5.6, the proposed scheme achieves the best performance. When the transmit power is high, the performance of the SPR with SA is close to optimal, because PA provides only marginal gains at high SNR. Fig. 5.7 compares the proposed scheme with a distributed solution, BBR [108], which is considered to be a reliable algorithm comparing with other distributed algorithms. As shown in the figure, the BBR achieves a much lower throughput even with the proposed resource allocation algorithm. This is because the distributed methods rely on the neighborhood knowledge only, however, the throughput of a route is determined by the link with minimal capacity which is hard to optimize without the overall route information. Both Figs. 5.6 and 5.7 also indicate that the minimal power required to support the delay tolerance is substantially reduced by using the proposed RRA-DTE.
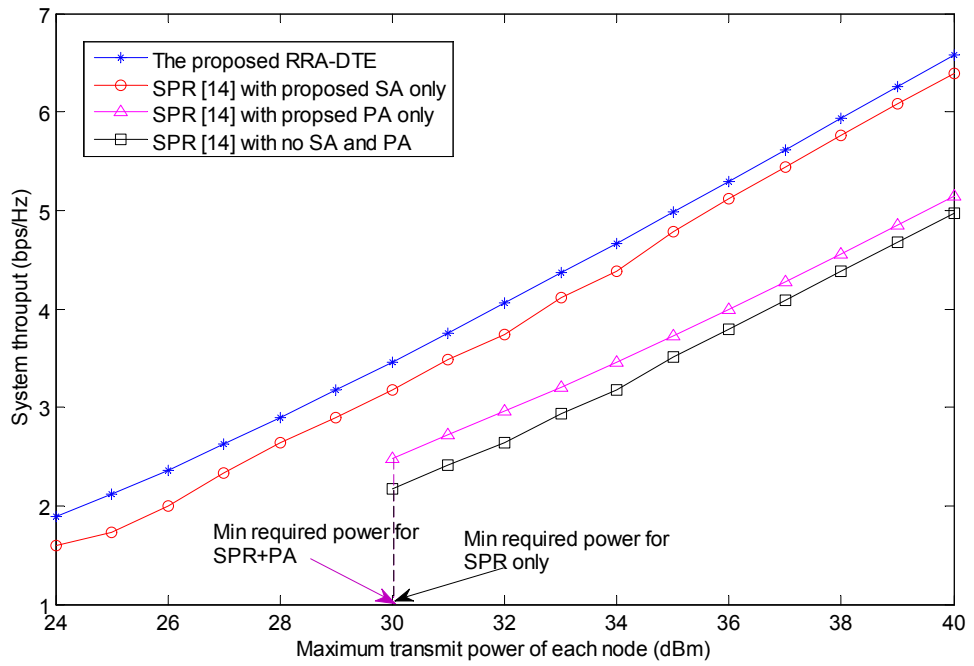
Fig. 5.6 Average system throughput vs node transmit power constraint of different centralized schemes
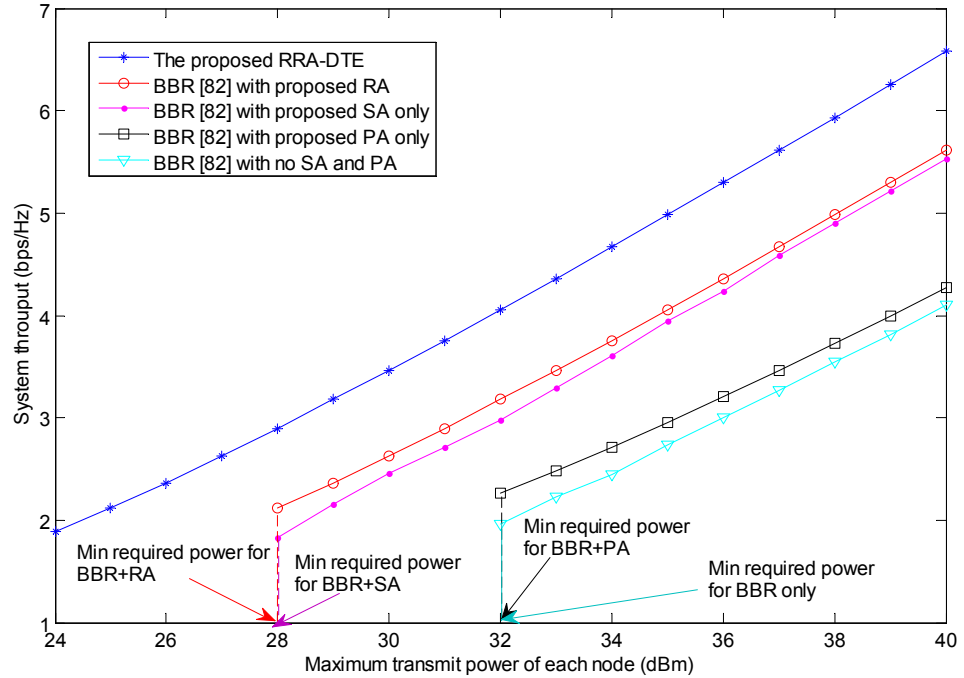

Fig. 5.7 Average system throughput vs node transmit power constraint of the proposed scheme and BBR [108]

Figs. 5.8 and 5.9 show the system throughput versus node power constraint of the centralized and distributed solutions under the occurance of an impulsive noise on the route. As can be seen, the average system throughput obtained by each scheme has decreased greatly comparing to it under the same transmit power in Figs. 5.6 and 5.7. This is because the amplitude of the power of an impulsive noise is much higher than the background noise, and therefore results in a lower CNR in (5.4), i.e. lower throughput is obtained. Due to the similar reason, the minimum required power for each scheme has increased in Figs. 5.8 and 5.9. However, since the same set up of impulsive noise are used which has the same impact to each algorithm, the priority of the solutions in system throughput does not change as shown in both figures. As can be derived from optimazition problem (5.11), the occurance of an impulsive noise does not change the principle of a resource allocation algorithm, and its occurance is also low in practical. Therefore, without lossing generality, we mainly considered background noise in the rest of the simulations.
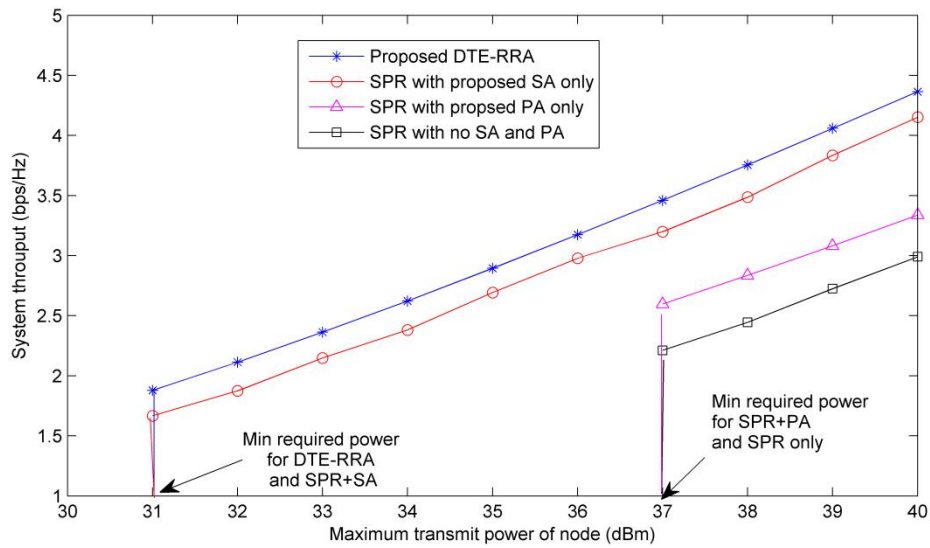
Fig. 5.8 Average system throughput of different centralized schemes under the occurance of an impulsive noise on the route
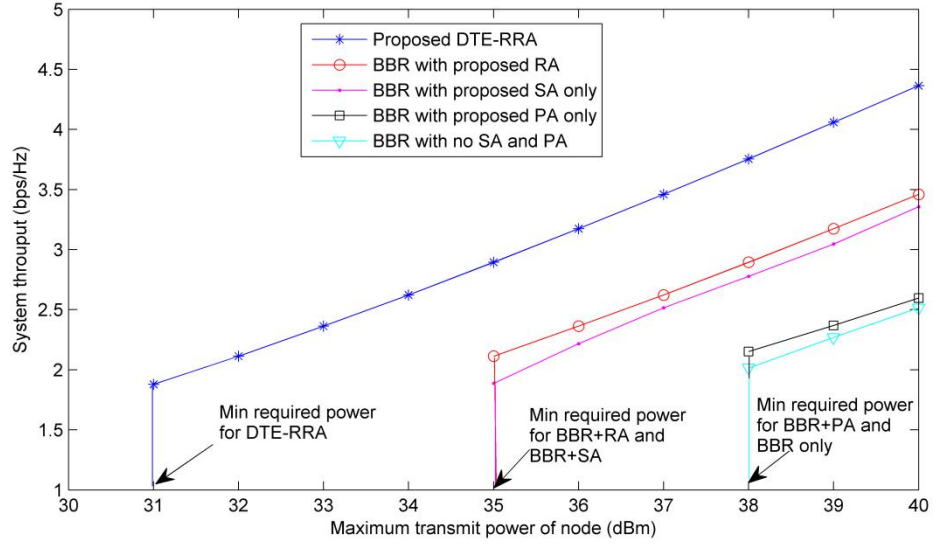
Fig. 5.9 Average system throughput of the proposed scheme and BBR [108] under the occurance of an impulsive noise on the route

Figs. 5.10 and 5.11 show the PLR of the schemes when the node power constraint is smaller than the minimal required power for the delay constraints. PLR is defined as the ratio of the number of packets that could not be delivered to the number of packets sent by the source. As can be seen, the proposed scheme achieves the lowest PLR in the whole range of the power and satisfies the delay constraints with the minimum node power. For instance, the proposed method has the PLR of 0.17 when the node power constrain is 20 dBm which is about 1/4 of the PLR of the BBR without resource allocation. Although the power is not sufficient to support all delay requirements, the urgency factor and water-filling level remain the same. Therefore, the proposed algorithm still achieves the minimal overall PLR.

Fig. 5.10 PLR of the centralized methods when the node power constraint is smaller than the minimal required power for the delay constraints
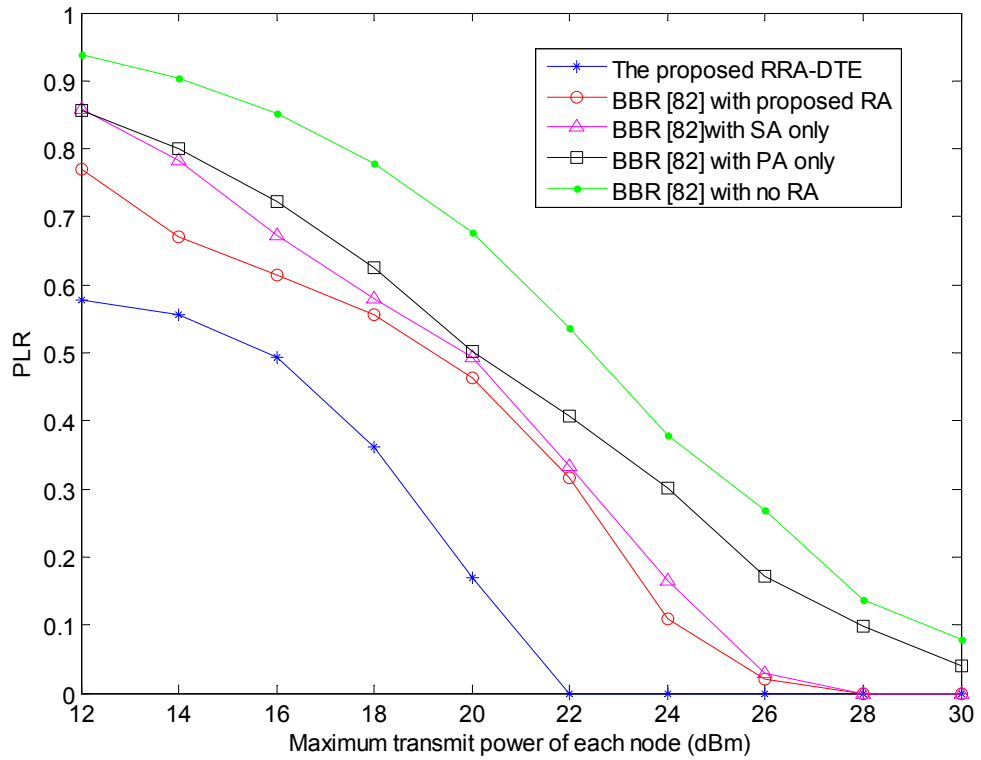
Fig. 5.11 PLR of the proposed method and the BBR methods [108] when the node power constraint is smaller than the minimal required power for the delay constraints
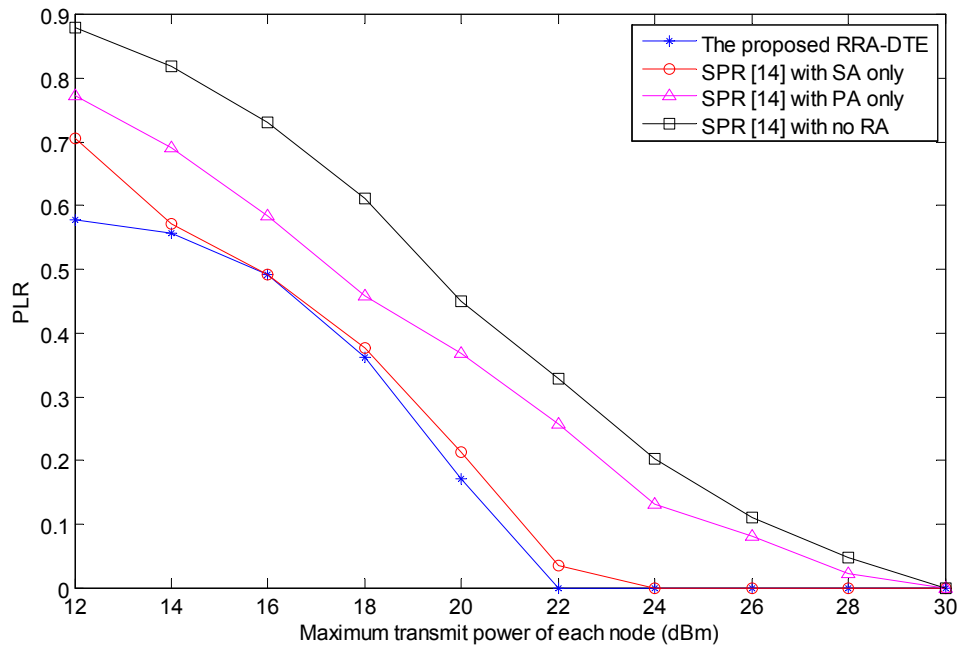
Fig. 5.12 shows the effect of randomly switching off nodes on PLR to demonstrate the performance of the proposed scheme in a dynamic topology. The node power constraint P_v is assumed to be 30 dBm, and the numbers of each class of users are $(K_1, K_2, K_3) = (1, 1, 1)$. Utilizing the topology change detection approach, the topology knowledge is updated instantaneously. As a result, the proposed scheme keeps the PLR at 0 when the number of disconnected nodes is not much. On the contrary, BBR has only the neighborhood knowledge, broken links may appear in target route and therefore forced to pick links with poor channel condition, which causes increase of PLR. For example, when 4 nodes are randomly disconnected, the PLR of the topology estimation based method is still 0 while the BBR based method has a PLR of 0.42. However, when a large number of nodes are disconnected, there may be no route which can support all delay requirements resulting in high PLR for both methods.
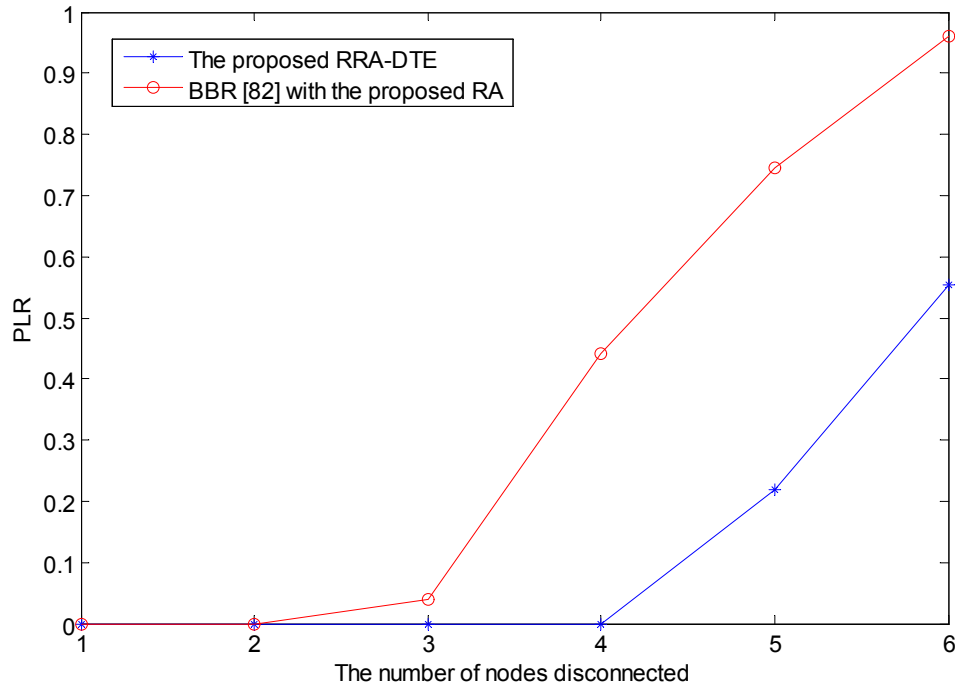
Fig. 5.12 Average PLR due to nodes being randomly disconnected (switched off)

5.4   Summary

In this chapter, a cross-layer routing and resource allocation scheme assisted by dynamic topology estimation has been proposed to optimize the system throughput of an indoor PLC network with heterogeneous delay requirements. The proposed scheme utilizes the estimation scheme developed in chapter 4 to obtain the instantaneous topology and connectivity information of the network. Thus, the network layer routing can be done centrally at the source which is more robust against topology changes comparing to distributed algorithms. With optimal resource allocation, the maximized capacity of each link can be obtained in advance so that the maximized-minimum throughput of a whole route can be obtained easily. Simulation results show that the optimal resource allocation is essential in improving system throughput and reducing PLR. Moreover, with the assistance of the dynamic topology estimation, the proposed scheme substantially outperforms the distributed solution BBR [108] in terms of throughput and PLR. It is also shown that the proposed scheme is much more reliable for a time-varying network than the neighborhood knowledge based distributed schemes.

Chapter 6

Conclusions and Future Work

6.1   Conclusions

In this thesis, efficient and reliable solutions have been investigated for PLC networks, including dynamic topology estimation and cross-layer routing and resource allocation for smart grid applications.

In Chapter 2, the network structure and channel modeling of a PLC network was reviewed. The communication applications of the HV, MV and LV networks were discussed. While the bottom-up and top-down approaches for channel modeling were reviewed. It was found that the random and unpredictable topology changes are crucial research challenges for PLC applications.

In Chapter 3, a detailed topological analysis of LV PLC networks was provided, and a popular random topology generator was introduced. Furthermore, basic

knowledge of time-frequency domain analysis and resource allocation for OFDM based system were studied for a better understanding of the investigated topics.

In Chapter 4, a dynamic topology estimation scheme assisted by impulsive noise source detection was proposed for indoor PLC networks. The scheme estimates signal path lengths with TFDR first, and performs a node-by-node greedy algorithm at the single measurement point to reconstruct the topology according to the estimated path lengths. With the original PLC network topology estimated, impulsive noise source is detected to infer dynamic topology changes in the network. Simulation results show that the proposed TFDR method significantly outperforms the FDR based methods [32] [97] in terms of resolution and accuracy for path length estimation. Furthermore, the proposed node-by-node greedy algorithm has dramatically reduced the complexity of the topology reconstruction compared to the existing algorithm [32]. With the impulsive noise source detection based method, the number of re-estimations is reduced by about 97.2% over conventional re-estimation schemes with fixed re-estimation frequency. With these advantages in complexity and resolution, the proposed scheme is particular for applications of time-varying in-home power line networks.

In Chapter 5, to fulfill the increasing demand for high speed and multi-tasking communication services of PLC, a cross-layer routing and resource allocation scheme assisted by dynamic topology estimation was proposed. The aim of scheme is to optimize the system throughput of indoor PLC network with heterogeneous user delay requirements. Utilizing the dynamic topology estimation presented in Chapter

4, routing is done with a centralized solution which is more robust against topology changes comparing to distributed algorithms. With optimal resource allocation, the maximized capacity of each link is obtained in advance so that the maximized-minimum throughput of a whole route can be calculated. It was found from the simulation results that the optimal resource allocation plays an essential role in improving system throughput and reducing PLR [29]. Moreover, with the assistance of the dynamic topology estimation, the proposed scheme substantially outperforms the distributed solution BBR [108] in terms of throughput and PLR. The low PLR achieved in a time-varying network also proved that the proposed scheme is a more reliable solution for practical PLC applications.

6.2 Future Work

In the research on topological analysis and resource management of PLC systems presented in this thesis, the results are based on simulations of the signal and channel models. The practical measurement has not been conducted, since a micro power grid is expensive and difficult to build. Furthermore, the throughput optimization is only conducted in PLC systems, the smart grid can utilize hybrid communication technologies in different scenarios to enhance system performance. Hence, the future research topics are summarized as the following:

1. A micro power grid will be built so that measurements can be done to analyze the practical channel characteristics, and that the dynamic topology estimation scheme can be verified and refined according to the measurement results.

2. Topology estimation schemes will be developed for a hybrid (both wired and wireless) communication system for smart grid applications, the optimized switching point from one network to another can be determined afterwards.

3. Routing and resource allocation schemes will be extended to a hybrid communication system for smart grid. They can also be utilized for selecting and switching among different networks either to improve system performance or reduce resource cost.

4. The optimization scheme investigated in Chapter 5 will also be applied to other performance metrics such as energy consumption and end-to-end delay. Furthermore, the scheme is going to be extended to a hybrid communication system for smart grid applications.

Bibliography

[1] M. Schwartz, "History of communications- Carrier-wave telephony over power lines: Early history" *IEEE Communications Magazine*, vol. 47, pp. 14–18, Jan. 2009

[2] K. Dostert, *Power Line Communications*. 2001: Prentice Hall

[3] H. Ferreira, L. Lampe, J. Newbury, and T. Swart, Eds, *Power Line Communications*, 2010: Wiley

[4] S. Galli, A. Scaglione, and Z. Wang, "For the Grid and Through the Grid: The Role of Power Line Communications in the Smart Grid," *Proceedings of the IEEE*, vol. 99, pp. 998-1027, Jun. 2011

[5] K. Dostert. "Telecommunications over the Power Distribution Grid- Possibilities and Limitations" in Proc. IEEE International Symposium on Power Line Communications and Its Applications (ISPLC), Essen, Germany, April. 1997

[6] H. Latchman and L. Yonge, "Power line local area networking (Guest Editorial)," *IEEE Communication Magazine*, vol. 41, pp. 32–33, Apr. 2003.

[7] N. Pavlidou, A. Vinck, J. Yazdani, and B. Honary, "Power line communications: State of the art and future trends," *IEEE Communication Magazine*, vol. 41, pp. 34–40, Apr. 2003.

[8] S. Galli, A. Scaglione, and K. Dostert, "Broadband is power: Internet access through the power line network (Guest Editorial)," *IEEE Communication Magazine*, vol. 41, pp. 82–83, May 2003.

[9] E. Biglieri, S. Galli, Y. Lee, H. Poor, and H. Vinck, "Power line communications (Guest Editorial)," *IEEE Journal on Selected Areas in Communications*, vol. 24, pp. 1261–1266, Jul. 2001.

[10] Williams, Jasmin (2007-11-30). "Edison Lights The City". New York Post. Retrieved 2008-03-31

[11] M. Y. Zhai "Transmission Characteristics of Low-Voltage Distribution Networks in China Under the Smart Grids Environment", *IEEE Transactions on Power Delivery*, vol. 26, pp.173 -180, Jan. 2011

[12] B. Heile, "Smart grids for green communications", *IEEE Wireless Communications*, vol. 17, pp. 4-6, Jun. 2010

[13] T. Sauter and M. Lobashov, "End-to-end communication architecture for smart grids", *IEEE Transactions on Industrial Electronics*, vol. 58, pp. 1218-1228, Apr. 2011

[14] C. Hauser , D. Bakken and A. Bose, "A failure to communicate: Next-generation communication requirements, technologies, and architecture for the electric power grid", *IEEE Power Energy Magazine*, vol. 3, pp. 47-55, Mar. 2005

[15] F. Bouhafs, M. Mackay, M. Merabti, "Links to the Future: Communication Requirements and Challenges in the Smart Grid", *IEEE Power Energy Magazine*, vol. 10, pp. 24 - 32, Jan. 2012

[16] R. Hashmat, P. Pagani, A. Zeddam and T. Chonavel, "MIMO communications for inhome PLC networks: measurements and results up to 100 MHz," in *Proc. IEEE International Symposium on Power Line Communications and Its Applications (ISPLC)*, Rio de Janeiro, Brazil, Mar. 2010

[17] D. Clark, "Powerline communications: Finally ready for primetime?" *IEEE Internet Computing*, vol. 2, pp. 10–11, Jan. 1998

[18] S. Galli, A. Scaglione, and Z. Wang, "Power line communications and the smart grid," *in Proc. IEEE International Conference on Smart Grid Communications (SmartGridComm)*, Gaithersburg, MD, pp. 303-308, Oct. 2010.

[19] A. Tonello and F. Versolatto, "Bottom-up statistical PLC channel modeling—Part I: random topology model and efficient transfer function computation," *IEEE Transactions on Power Delivery*, vol.26, pp. 891-898, Apr. 2011

[20] T. Erseghe, S. Tomasin and A. Vigato, "Topology estimation for smart micro grids via powerline communications," *IEEE Transactions on Signal Processing*, vol. 61, pp. 3368-3377, Apr. 2013

[21] N. Saputro, K. Akkaya and S. Uludag, "A survey of routing protocols for smart grid communications", *Computer Networks*, vol. 56, pp. 2742 -2771, Jul. 2012

[22] T. Erseghe and S. Tomasin, "Power flow optimization for smart micro-grids by SDP relaxation on linear networks," *IEEE Transactions on Smart Grid*, vol.4, pp. 751-762, Jun. 2013

[23] C. Paul, *Analysis of Multiconductor Transmission Lines*, *2nd ed.* , 2008: John Wiley and Sons

[24] F. Corripio, J. Arrabal, L. del Rio, and J. Munoz, "Analysis of the cyclic shortterm variation of indoor power line channels," *IEEE Journal on Selected Areas in Communications*, vol. 24, pp. 1327-1338, Jul. 2006.

[25] H. Meng, S. Chen, Y. Guan, C. Law, P. So, E. Gunawan, and T. Lie, "Modeling of Transfer Characteristics for the Broadband Power Line Communication Channel," *IEEE Transactions on Power Delivery*, vol. 19, pp. 1057-1064, Jul. 2004

[26] L. Rugini, P. Banelli, and G. Leus, "Simple equalization of time-varying channels for OFDM," *IEEE Communications Letters*, vol. 9, pp. 619-621, Jul. 2005.

[27] G. Bumiller, L. Lu and Y. Song, "Analytic performance comparison of routing protocols in master-slave PLC networks," in *Proc. IEEE International Symposium on Power Line Communications and Its Applications (ISPLC)*, Vancouver, Canada, pp. 116-120, Apr. 2005

[28] Z. Wang; Y. Wang; J. Wang, "Overlapping clustering routing algorithm based on L-PLC meter reading system," in *Proc. IEEE International Conference on Automation and Logistics (ICAL)*, Shenyang, China, pp. 1350-1355, Aug. 2009

[29] M. Biagi, S. Greco and L. Lampe, "Neighborhood-knowledge based geo-routing in PLC", in *Proc. IEEE International Symposium on Power Line Communications and Its Applications* (*ISPLC*), Beijing, China, pp. 7 -12, Mar. 2012

[30] M. Biagi and L. Lampe, "Location assisted routing techniques for power line communication in smart grids", *in Proc. IEEE International Conference on Smart Grid Communications*, Maryland, US, pp. 274 -278, Oct. 2010

[31] N. Andreadou and F.-N. Pavlidou "Modeling the noise on the OFDM power-line communications system", *IEEE Transactions on Power Delivery*, vol. 25, pp. 150 -157, Dec. 2010

[32] M. Ahmed and L. Lampe, "Power line network topology inference using frequency domain reflectometry," in *Proc. IEEE International Communications Conference(ICC)* , Ottawa, Canada, pp. 3419-3423, Jun. 2012

[33] X. Fang, S. Misra, G. Xue, and D. Yang, "Smart grid - the new and improved power grid: A survey," *IEEE Communications Surveys and Tutorials*, vol. 14, pp. 944 -980, Apr. 2012.

[34] Z. M. Fadlullah, M. M. Fouda, N. Kato, A. Takeuchi, N. Iwasaki, and Y. Nozaki, "Toward intelligent machine-to-machine communications in smart grid," *IEEE Communications Magazine*, vol. 49, pp. 60 -65, Apr. 2011.

[35] A. Ghassemi, S. Bavarian, and L. Lampe, "Cognitive radio for smart grid communications," in *Proc. IEEE International Conference on Smart Grid Communications (SmartGridComm)*, Gaithersburg, USA, Oct. 2010.

[36] D. Niyato, L. Xiao, and P. Wang, "Machine-to-machine communications for home energy management system in smart grid," *IEEE Communications Magazine*, vol. 49, pp. 53 -59, Apr. 2011.

[37] M. Souryal, C. Gentile, D. Griffith, D. Cypher and N. Golmie , "A methodology to evaluate wireless technologies for the smart grid", in *Proc. IEEE International Conference on Smart Grid Communications (SmartGridComm)*,' Gaithersburg, USA, Oct. 2010

[38] I. F. Akyildiz and X. Wang , "A survey on wireless mesh networks", *IEEE Radio Communications*, vol. 43, pp. 23 -30, Sep. 2005

[39] B. Akyol, H. Kirkham, S. Clements and M. Hadley , "A survey of wireless communications for the electric power system" , *Computer Networks,* vol. 50, pp. 877-897, May. 2006

[40] V. Gungor, D. Sahin, T. Kocak, S. Ergut, C. Buccella, C. Cecati and G. Hancke, "Smart grid technologies: Communications technologies and standards", *IEEE Transactions on Industrial Informatics,* vol. 7, pp. 529 -539, Nov. 2011

[41] Y. Peizhong, A. Iwayemi and C. Zhou, "Developing ZigBee deployment guideline under WiFi interference for smart grid applications", *IEEE Transactions on Smart Grid*, vol. 2, pp.110 -120, Mar. 2011

[42] R. P. Lewis, P. Igic and Z. Zhongfu, "Assessment of communication methods for smart electricity metering in the U.K.", *in Proc. IEEE PES/IAS Conference on Sustainable Alternative Energy (SAE)*, Valencia, Spain, Sep. 2009

[43] G. N. Srinivasa Prasanna, A. Lakshmi, S. Sumanth, V. Simha, and G. Bapat, J.abd Koomullil, "Data communication over the smart grid", *in IEEE International Symposium on Power Line Communications and Its Applications (ISPLC)*, Dresden, Germany, pp.273-297, Mar. 2009.

[44] J. Liu, B. Zhao, L. Geng, Z. Yuan, and Y. Wang, "Communication performance of broadband PLC technologies for smart grid", *in IEEE International Symposium on Power Line Communications and Its Applications (ISPLC)*, Udine, Italy, pp. 491-496, April. 2011

[45] C. Xavier. *Power Line Communications in Practice,* 2009: Artech House

[46] U. Kontges, "Integration of a ripple control system for the switching of electric night storage heating in a network control system", *Power Industry Computer Application Conference (PICAC)*, Baltimore, MD, pp.38-44, May 1991

[47] -------, *Solid-state ripple control system, Electronics and Power*, vol.14, 1968

[48] M. Nassar, J. Lin, Y. Mortazavi, A. Dabak, I. Kim, and B. Evans, "Local Utility Power Line Communications in the 3500 kHz Band: Channel Impairments, Noise, and Standards," *IEEE Signal Processing Magazine*, vol. 29, pp. 116-127, Sep. 2012.

[49] S. Galli, "A novel approach to the statistical modeling of wireline channels," *IEEE Transactions on Communications,* vol. 59, pp.1332 - 1345, May. 2011.

[50] P. Amirshahi, F. Canete, K. Dostert, S. Galli, M. Katayama, and M. Kavehrad, *Power Line Communications: Theory and Applications for Narrowband and Broadband Communications over Power Lines*, 2010: Wiley

[51] M. Gotz, M. Rapp, and K. Dostert, "Power line channel characteristics and their effect on communication system design," *IEEE Communication Magazine*, vol. 42, pp. 78–86, Apr. 2004

[52] F. Canete, J. Cortes, L. Diez, and J. Entrambasaguas, "A channel model proposal for indoor power line communications," *IEEE Communications Magazine*, vol. 49, pp. 166-174, Dec. 2011

[53] A. M. Tonello and F. Versolatto, "Bottom-Up Statistical PLC Channel Modeling-Part II: Inferring the Statistics," *IEEE Transactions on Power Delivery*, vol. 25, pp. 2356-2363, Oct. 2010

[54] S. Galli and T. Banwell, "A deterministic frequency-domain model for the indoor power line transfer function," *IEEE Journal on Selected Areas in Communications*, vol. 24, pp. 1304-1316, Jul. 2006

[55] E. G. Bakhoum, "S-Parameters Model for Data Communications Over 3-Phase Transmission Lines," *IEEE Transactions on Smart Grid*, vol. 2, pp. 615-623, Dec. 2011

[56] T. Banwell and S. Galli, "A Novel Approach to the Modeling of the Indoor Power Line Channel Part I: Circuit Analysis and Companion Model," *IEEE Transactions on Power Delivery*, vol. 20, pp. 655-663, Apr. 2005

[57] T. Esmailian, F. R. Kschischang, and P. Glenn Gulak, "In-building power lines as high-speed communication channels: channel characterization and a test channel ensemble," *International Journal of Communication Systems*, vol. 16, pp. 381-400, Jun. 2003

[58] D. Anastasiadou and T. Antonakopoulos, "Multipath Characterization of Indoor Power-Line Networks," *IEEE Transactions on Power Delivery*, vol. 20, pp. 90-99, Jan. 2005

[59] M. Zimmermann and K. Dostert, "A multipath model for the powerline channel," *IEEE Transactions on Communications*, vol. 50, pp. 553-559, Apr. 2002.

[60] S. Guzelgoz, H. B. Celebi, and H. Arslan, "Statistical Characterization of the Paths in Multipath PLC Channels," *IEEE Transactions on Power Delivery*, vol. 26, pp. 181-187, Jan. 2011.

[61] A. M. Tonello, F. Versolatto, B. Bejar, and S. Zazo, "A Fitting Algorithm for Random Modeling the PLC Channel," *IEEE Transactions on Power Delivery*, vol. 27, pp. 1477-1484, Jul. 2012

[62] M. Tlich, A. Zeddam, F. Moulin, and F. Gauthier, "Indoor Power-Line Communications Channel Characterization Up to 100 MHzPart I: One-Parameter Deterministic Model," *IEEE Transactions on Power Delivery*, vol. 23, pp. 1392-1401, Jul. 2008

[63] C. Paul, *Analysis of Multiconductor Transmission Lines*, 2008: John Wiley and Sons

[64] M. Zimmermann and K. Dostert, "Analysis and modeling of impulsive noise in broad-band powerline communications," *IEEE Transactions on Electromagnetic Compatibility*, vol. 44, pp. 249-258, Feb. 2002

[65] M. Babic, M. Hagenau, K. Dostert, and J. Bausch, "Theoretical postulation of plc channel models," *EU OPERA IST Integrated Project*, Technical Report, 2005.

[66] K. Tomsovic, D. Bakken, V. Venkatasubramanian, and A. Bose, "Designing the next generation of real time control, communication, and computations for large power systems," *Proceedings of the IEEE*, vol. 93, May 2005.

[67] L. Di Bert, P. Caldera, D. Schwingshackl and A. M. Tonello, "On noise modeling for power line communications" , in *Proc. IEEE International Symposium on Power Line Communications and Its Applications (ISPLC)*, pp.283 -288, Udine, Italy, Apr. 2011

[68] M. Katayama, T. Yamazato, and H. Okada, "A mathematical model of noise in

narrowband power line communication systems," *IEEE Journal on Selected Areas in Communications*, vol. 24, pp. 1267-1276, Jul. 2006.

[69] D. Benyoucef, "A new statistical model of the noise power density spectrum for powerline communication," in *Proc IEEE International Symposium on Power Line Communications and Its Applications (ISPLC)*, Kyoto, Japan, Mar. 2003.

[70] M. Tlich, H. Chaouche, A. Zeddam, F. Gauthier, "Impulsive Noise Characterization at Source", *IFIP Wireless Days Conference (WD)*, Dubai, United Arab Emirates, Nov. 2008.

[71] R. Pighi, M. Franceschini, G. Ferrari, and R. Raheli, "Fundamental performance limits of communications systems impaired by impulse noise," *IEEE Transactions on Communications*, vol. 57, pp. 171-182, Jan. 2009

[72] K. Wiklundh, P. Stenumgaard, and H. Tullberg, "Channel capacity of Middleton's class A interference channel," *Electronics Letters*, vol. 45, pp. 1227-1229, Nov. 2009

[73] A. Kenarsari-Anhari and L. Lampe, "Performance analysis for BICM transmission over Gaussian mixture noise fading channels," *IEEE Transactions on Communications*, vol. 58, pp. 1962-1972, Jul. 2010

[74] Z. Wang, A. Scaglione and R. J. Thomas , "Generating statistically correct random topologies for testing smart grid communication and control networks" , *IEEE Transaction on Smart Grid* , vol. 1 , pp.28 -39 , May. 2010

[75] L. Cohen, "Time-frequency distributions - a review," *Proceedings of IEEE*, vol. 77, pp. 941–981, Jul. 1989.

[76] G. Cunnuningham, "Analysis, synthesis and implementation of time-frequency distributions using spectrogram decomposition," Ph.D. dissertation, The University of Michigan, Ann Arbor, 1992.

[77] J. Jeong and W. Williams, "Kernel design for reduced interference distributions," *IEEE Transactions on Signal Processing*, vol. 40, pp. 402–412, Feb. 1992.

[78] Y. Shin, "Theory and application of time-frequency analysis to transient phenomena in electric power and other physical systems," Ph.D. dissertation, University of Texas at Austin, 2004

[79] L. Cohen, *Time-Frequency Signal Analysis*. 1995: Prentice Hall

[80] R. W. Chang, "Synthesis of Band-Limited Orthogonal Signals for Multichannel Data Transmission," *Bell System Tech. J.*, vol. 46, pp. 1775－1796, Dec. 1966

[81] N. Zhou, X. Zhu, and Y. Huang, "Genetic algorithm based cross-layer resource allocation for wireless OFDM networks with heterogeneous traffic," in *Proc. 17th European Signal Processing Conference*, Glasgow, UK, Aug. 2009.

[82] A. J. Goldsmith and S. G. Chua, "Variable-rate variable-power MQAM for fading channel," *IEEE Transaction on Communications*, vol. 45, pp. 1218-1230, Oct. 1997

[83] J. Jang and K. B. Lee, "Transmit power adaptation for multiuser OFDM systems," *IEEE Journal on Selected Areas in Communications*, vol. 21, pp. 171-178, Feb. 2003

[84] C. Y. Wong, R. S. Cheng, K. B. Letaief, and R. D. Murch, "Multiuser OFDM with adaptive subcarrier, bit and power allocation," *IEEE Journal on Selected Areas in Communications*, vol. 17, pp. 1747-1758, Oct. 1999

[85] J. Chuang and N. Sollenberger, "Beyond 3G: wideband wireless data access based on OFDM and dynamic packet assignment," *IEEE Communication Magazine*, vol. 38, pp. 78-87, Jul. 2000

[86] I. Kalet, "The Multitone Channel," *IEEE Transaction on Communications*, vol. 37, no. 2, pp. 119–124, Feb. 1989

[87] T. M. Cover and J. A. *Thomas, Elements of Information Theory*. 1991: John Wiley & Sons, Inc.

[88] R. G. Gallager (1963). "Low Density Parity Check Codes", *Monograph, M.I.T. Press. Retrieved,* Aug. 2013

[89] C. Berrou, A. Glavieux and P. Thitimajshima, "Near Shannon limit error correcting coding and decoding: turbo codes", *in Proc. IEEE International Communications Conference*, Geneva, Switzerland, pp. 1064-1070, May. 1993

[90] S. Benedetto and G. Montorsi, "Unveiling turbo codes: Some results on parallel concatenated coding schemes", *IEEE Transactions on Information Theory*, vol.42, pp. 409-429, Mar. 1996

[91] E. K. Hall and S. G. Wilson, "Design and analysis of turbo codes on Rayleigh fading channels", *IEEE Journal on Selected Areas in Communications*, vol.16, pp. 160-174, Feb. 1998

[92] M. Ahmed and L. Lampe, "Power line communications for low-voltage power grid tomography", *IEEE Transactions on Communications*, vol. 61, pp. 5163 -5175, Dec. 2013

[93] X. Ma, F. Yang, W. Ding and J. Song, "Topology reconstruction for power line network based on Bayesian compressed sensing", *in Proc. International Symposium Power Line Communications and its Applications(ISPLC)*, Austin, USA, Mar. 2015

[94] D. Laurenson, and P. Grant, "A review of radio channel sounding techniques", *In Proc. European Signal Processing Conference (EUSIPCO),* Florence, Italy, pp. 1-5, Sep. 2006

[95] F. Talebi and T. Pratt, "Channel Sounding and Parameter Estimation for a Wideband Correlation-Based MIMO Model," *in IEEE Transactions on Vehicular Technology*, vol. 65, pp. 499-508, Feb. 2016.

[96] H. S. Kim, S. H. Lee and Y. H. Lee, "Channel Sounding for Multi-Sector Cooperative Beamforming in TDD-OFDM Wireless Systems," *IEEE International Conference on Communications (ICC)*, Cape Town, South Africa, pp. 1-5, May. 2010

[97] M. Ahmed and L. Lampe, "Parametric and nonparametric methods for power line network topology inference," *in Proc. IEEE International Symposium on Power Line Communications and Its Applications (ISPLC)* , Beijing, China, Mar. 2012

[98] C. P. Nemarich, "Time domain reflectometry liquid level sensors," *IEEE Instrumentation and Measurement Magazine*, vol. 4, pp. 40–44, Dec. 2001

[99] M. Yoshida, K. Nakamura, and H. Ito, "A new method for measurement of group velocity dispersion of optical fibers by using a frequency-shifted feedback fiber laser," *IEEE Photonics Technology Letters*, vol. 13, pp. 227-229, Mar. 2001

[100] Y. Shin, E. Powers, T. Choe, C. Hong, E. Song, J. Yook, and J. Park, "Application of time-frequency domain reflectometry for detection and localization of a fault on a coaxial cable," *IEEE Transactions on Instrumentation and Measurement,* vol. 54, pp. 2493- 2500, Dec. 2005

[101] P. Flandrin, Time-Frequency/ Time-Scale Analysis. *Academic Press*, 1998

[102] H. Meng, Y. L. Guan and S. Chen, "Modeling and analysis of noise effects on broadband power-line communications," *IEEE Transactions on Power Delivery*, vol. 20, pp. 630-637, Apr. 2005

[103] J. Yin, X. Zhu and Y. Huang, "Modeling of amplitude-correlated and occurrence-dependent impulsive noise for power line communication", *in Proc. IEEE International Communications Conference (ICC)*, Sydney, Australia, Jun. 2014

[104] T. Oberg and M. Mettiji, "Robust detection in digital communications," *IEEE Transactions on Communications*, vol. 43, pp. 1872-1876, May. 1995

[105] C. Zhang, X. Zhu, Y. Huang and G. Liu, "High-resolution and low-complexity topology estimation for power line communication networks," in *Proc. IEEE International Conference on Communications (ICC),* London, UK, Jun. 2015.

[106] M. Heissenbüttel, T. Braun, T. Bernoulli, and M. Wälchli, "BLR: Beacon-Less Routing Algorithm for Mobile Ad-Hoc Networks," *Elsevier Journal Computer Communications*, vol. 27, no. 11, pp. 1076-1086, Jul. 2004.

[107] B. M. Blum, T. He, S. Son, and J. A. Stankovic, "IGF: A State-Free Robust Communication Protocol for Wireless Sensor Networks," *CS Department, University of Virginia, Technology Report*, 2003.

[108] L. Demoracski, "Fault-tolerant beacon vector routing for mobile ad hoc networks," *in 19th IEEE International Parallel and Distributed Processing Symposium (IPDPDS)*, Denver, USA, Apr. 2005.

[109] G. Bumiller, *Single Frequency Network Technology for Fast ad hoc Communication Networks over Power Lines,* 2010: WiKu-Verlag

[110] G. Bumiller, L. Lampe, and H. Hrasnica, "Power Line Communications for Large-Scale Control and Automation Systems," *IEEE Communincations Magazine*, vol. 48, pp. 106–113, Apr. 2010.

[111] T. B. Yu, J. X. Yang, and Y. X. Zhao "A Routing Algorithm of Edifice Control System Based on Power Line Signal Carrier," *Power System Technology,* vol. 30, pp. 88-91, May. 2006.

[112] X. S. Liu, Y. Zhou, and J. J. Qi "Method Study of Automatic Routing for Power Line Communication", *in Proc of the CSEE*, vol. 26, pp.76-81, Nov . 2006

[113] Z. Wang , Y. Zhang and Y. Zhao, "A distributed routing algorithm for L-PLC network", *IEEE International Conference on Automation and Logistics (ICAL),* Qingdao, China, pp. 2541-2545, Sep. 2008

[114] S. S. W. Lee , K.-Y. Li , C.-S. Wu , J.-Y. Pan and C.-Y. Chuang   "Optimal bandwidth guaranteed routing and time slot assignmentfor broadband PLC access networks", in *Proc. IEEE International Symposium on Power Line Communications and Its Applications (ISPLC),* Beijing, China, Mar. 2012

[115] N. Papandreou and T. Antonakopoulos   "Resource allocation management for indoor power-line communications system", *IEEE Transactions on Power Delivery,* vol. 22, pp. 893 -903, 2007

[116] A. Chaudhuri, M. R. Bhatnagar, "Optimised resource allocation under impulsive noise in power line communications," *IET Communications,* vol.8, pp. 1104-1108, 2014

[117] Z. Q. Xu, M. Y. Zhai and Y. M. Zhao, "Optimal resource allocation based on resource factor for power-line communication systems", *IEEE Transactions on Power Delivery*, vol. 25, pp.657 -666, 2010

[118] R. Dong, M. Ouzzif, S. Saoudi, "Utility-based joint resource allocation and scheduling for indoor power line communications", in *Proc. IEEE International Symposium on Power Line Communications and Its Applications (ISPLC)*, Rio de Janeiro, Brazil, Mar. 2010

[119] G. Eleonora, G. Lorenzo and V. Daniele, "Homeplug AV system and DLC bit-loading algorithm over OPERA power-line channels with impulsive noise", in *Proc. IEEE International Symposium on Power Line Communications and Its Applications(ISPLC)*, Jeju City, Korea, Apr. 2008

[120] N. Zhou, X. Zhu and Y. Huang, "Optimal asymmetric resource allocation and analysis for OFDM based multi-destination relay systems in the down-link," *IEEE Transactions on Vehicular. Technology,* vol. 60, pp.1307 -1312, 2011

[121] Kleinrock, Leonard, *Queueing Systems,* 1975: John Wiley & Sons

[122] J. Bentley, *Programming Pearls,* 1999: Addison-Wesley